MBE Growth of GaAs and InAs on GaAs(001) Patterned Substrates

by

Chryssoula Chandrinou

Submitted for the degree of
Doctor of Philosophy of the University of London
and the
Diploma of Imperial College

Department of Chemistry
Imperial College
London

2004

ABSTRACT

The growth of ridge structures on GaAs(001) patterned substrates has been investigated using Atomic Force Microscopy and Scanning Electron Microscopy. These techniques provide morphological and topographical information from which the kinetic processes of the adatom diffusion can be postulated.

The research is split into two main sections. The first concerns the growth of GaAs on GaAs (001) patterned substrates, involving variation of substrate temperature, the effective V/III ratio and deposition quantity. The effects of changing these growth parameters on the evolving facet morphology are investigated and direct comparison is made between growth on mesas with vertical and non-vertical sidewalls. In all cases {110} facets were formed and the degree of overgrowth of the ridge bases was found to be dependant on the growth conditions.

The second area concentrates on the growth of InAs on GaAs(001) patterned substrates with vertical sidewalls. Here, the effect of differing growth conditions and initial mesa stripe width was studied, in particular with respect to the formation of quantum dots. Specific emphasis was placed on the alteration of the quantum dot number density and the implications in terms of the In adatom diffusion processes. It was observed that dot density and size varied considerably with respect to the initial mesa widths and the different growth conditions used. For all investigations the dot sizes were larger and the dot densities lower that those reported for InAs/GaAs growth on planar GaAs(001) substrates.

List of Acronyms

AFM	Atomic Force Microscopy
AH	Atomic Hydrogen
CL	Cathodoluminescence
CRT	Cathode Ray Tube
DBR	Distributed Bragg Reflector
EDX	Energy Dispersive X-ray Analysis
IR	Infra-Red
K-cell	Knudsen Cell
LPE	Liquid Phase Epitaxy
MBE	Molecular Beam Epitaxy
MBMS	Modulated Beam Mass Spectrometry
MFM	Magnetic Force Microscopy
ML	Monolayer
MOCVD	Metal-Organic Chemical Vapour Deposition
μm	Micrometre
μ-PL	Micro-Photoluminescence
μ-RHEED	Microprobe-Reflection High Energy Electron Diffraction
nm	Nanometre
PBN	Pyrolitic Boron Nitride
PL	Photoluminescence
QD	Quantum Dot
QMS	Quadrapole Mass Spectrometer
QW	Quantum Well
QWR	Quantum Wire
RHEED	Reflection High Energy Electron Diffraction
RIE	Reactive Ion Etching
SAE	Selective Area Epitaxy
SEM	Scanning (or Secondary) Electron Microscopy
SPE	Swimming Pool Effect
STM	Scanning Tunnelling Microscopy
TEM	Transmission Electron Microscopy

TMP	Turbo Molecular Pump
TSP	Titanium Sublimation Pump
UHV	Ultra High Vacuum
1D	One-dimensional
2D	Two-dimensional
3D	Three-dimensional

TABLE OF CONTENTS

ABSTRACT 1

LIST OF ACRONYMS 2

TABLE OF CONTENTS 4

CHAPTER 1: Introduction 8

1.1. Fundamentals Properties of GaAs 8

1.1.1. GaAs Structure

1.1.2. GaAs(001) Surface Reconstructions

1.1.3. Low Index Planes

1.1.4. Epitaxial Growth Modes

1.2. The Surface Chemistry of MBE Growth on GaAs 13

1.3. Growth on Non-Planar GaAs Surfaces 17

1.4. Growth on Patterned Substrates 20

1.4.1. Introduction

1.4.2. Methods Used to Investigate Growth on Patterned Substrates.

1.4.2.1. μ-RHEED Investigations

1.4.4. Growth of Low Dimensional structures on Patterned Substrates.

1.4.5.Formation of Multi-Layer and Low Dimensional Structures on Patterned Substrates along the <001>.

1.5. Growth of InAs/InGaAs on GaAs(001) 31

1.5.1. Introduction on QDs

1.5.2. Growth on Planar Substrates

1.5.2.1. Initial Work on QDs

1.5.2.2. QD Composition

1.5.2.3. Growth Conditions Control on QDs

1.5.2.4. QD Position/Size Control

1.5.3. Growth on Non-Planar Surfaces

1.6. Aims 38

CHAPTER 2: Experimental **39**

2.1. MBE: Brief Overview **39**

2.1.1. Background Theory

2.2. The MBE Chamber **40**

2.2.1 Fast Entry Load Lock

2.2.2. Preparation Chamber

2.2.3. Sample Manipulation

2.2.4. The Growth Chamber

2.2.5. Baking Procedure

2.2.6. Molecular and Atomic Beam Sources

2.3. In-Situ Monitoring Techniques **47**

2.3.1. Reflection High Energy Electron Diffraction

2.4. Sample Cleaning Techniques **50**

2.4.1. Oxygen Plasma Ashing

2.4.2. Atomic Hydrogen Cleaning

2.5. Post-Growth Analysis **53**

2.5.1. Scanning Electron Microscopy

2.5.2. Atomic Force Microscopy

CHAPTER 3: Wet Chemical Etching **62**

3.1. Introduction **62**

3.2. Background Review **63**

3.3. Present Work **66**

3.4. Sample Preparation **71**

CHAPTER 4: Effect of Mesa Width on Ga Adatom Diffusion Processes **73**

4.1. Introduction **73**

4.2. Experimental Details **74**

4.3. Growth on the 5 μm Mesas **75**

4.4. Growth on the 15 μm Mesas **78**

4.5. Measurements of Facet Angle and Length **81**

4.5.1. Summary.

4.6. Discussion **84**

4.6.1. Swimming Pool Effect

4.6.2. Formation of the {110} Facet

4.6.3. Formation of the Trench and How It Affects Growth for the {110} Facets

4.6.4. Bottom Facet Domination

4.6.5. Comparison With Work Done on 90° Sidewalls

CHAPTER 5: Influence of the Growth Conditions on GaAs Depositions on Mesa Stripes **94**

5.1. Introduction **94**

5.2. Experimental Details **94**

5.3. Growth Using a 0.50 μm/h Ga flux at 570°C **95**

5.3.1. Summary

5.3.2. Discussion

5.4. Growth Using a 0.25 μm/h Ga flux at 480°C **101**

5.4.1. Summary

5.4.2. Discussion

5.5. Effect of As_4 and As_2 **106**

5.5.1. Growth Using a 0.25 μm/h Ga flux at 570°C under As_2

5.5.1.1. Summary

5.5.1.2. Discussion

5.5.2. Growth Using a 0.50 μm/h Ga flux at 570°C under As_2

5.5.2.1. Summary

5.5.2.2. Discussion

5.5.2.3. Comparison Between High/Low Ga Flux for the As_2 Series

5.6. Discussion **115**

CHAPTER 6: Effect of Initial Mesa Width on InAs QD Formation ***117***

6.1. Introduction ***117***

6.2. Experimental Details ***117***

6.3. Effect of Different Mesa Widths on The In Adatom Diffusion ***119***

6.3.1. General Observations For The Formation of QDs

6.3.2. Detailed Characterisation of QD Formation on Mesa Stripes

6.4. Discussion ***129***

CHAPTER 7: Effect of Growth Temperature and Rate on InAs QD Formation ***136***

7.1. Introduction ***136***

7.2. Experimental Details ***136***

7.3. Effect of Temperature ***137***

7.4. Effect of InAs Growth Rate ***140***

7.5. Discussion and Conclusions ***145***

7.5.1. Comparison of the Effect of the Two Different Temperatures on QD Formation

7.5.2. Comparison of the Effect of the Two Different In Fluxes on QD Formation

7.5.3. Conclusions

CHAPTER 8: Conclusions and Future Work ***151***

8.1. Introduction ***151***

8.2. Work on Patterned Substrates ***151***

8.3. InAs/GaAs Growth on Patterned Substrates ***153***

8.4. Modelling Patterned Substrates ***155***

ACKNOWLEDGMENTS ***160***

LIST OF PUBLICATIONS ***161***

REFERENCES ***162***

CHAPTER 1.

Introduction.

1.1. Fundamental Properties of GaAs.

This section presents the basic properties of the GaAs crystal and some concepts regarding the growth of GaAs thin films. The structural properties and surface reconstructions will be outlined. The different modes of epitaxial growth are discussed followed by a brief synopsis of the surface chemistry during MBE growth on GaAs(001).

1.1.1. GaAs Structure.

The GaAs crystal adopts a zinc-blende structure and consists of two interpenetrating Face Centred Cubic (FCC) lattices of Ga and As. It has one type of atom on the FCC sites and the other atoms are placed in half of the tetrahedral holes in the FCC lattice. The structure of the GaAs crystal is shown schematically in figure 1.1.

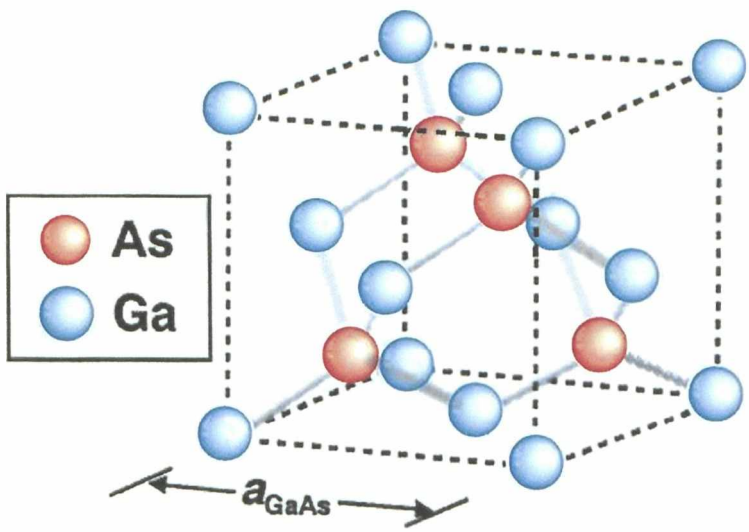


Figure 1.1: Zinc-blende structure of GaAs.

1.1.2. GaAs (001) Surface Reconstructions.

In an ideal surface, the atoms would arrange themselves as in the bulk. However, this is a very rare occurrence and in most cases the surface transforms to reach its minimum energy structure. This can involve relaxation of the atoms from the bulk positions, in which case the surface will have the same symmetry as the bulk lattice, or reconstruction of the surface, which means it will adopt a different (lower) symmetry to that of the bulk structure. The (001) plane adopts a variety of surface reconstructions, the structure of which depends on the particular conditions used to grow the surface. Figure 1.2 highlights the different surface reconstructions that can be formed on the GaAs(001) surface during MBE growth. All the experiments presented in this thesis were performed under As-rich conditions and therefore the GaAs(001) surface was always As-stabilised and As-terminated.

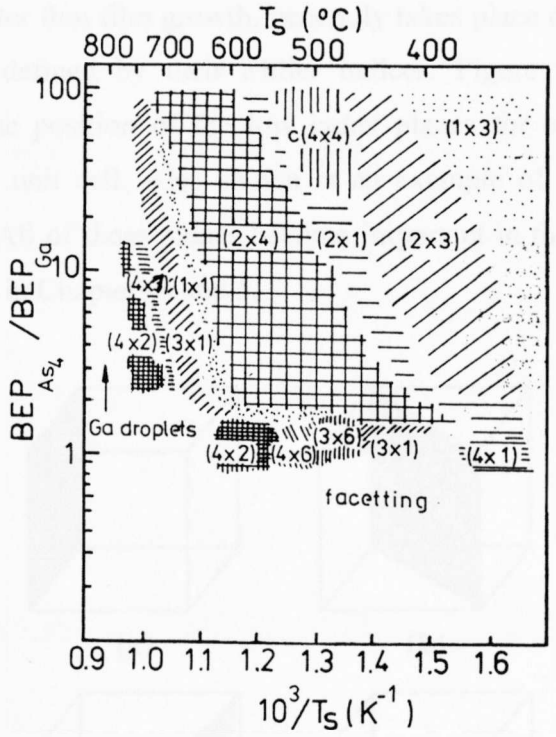


Figure 1.2: Surface reconstructions formed on GaAs(001), misoriented 2° towards (1 $\bar{1}$ 1). Däweritz [1].

The growth conditions used were such that deposition was performed on either the (2×4) or the c(4×4) reconstructed surface. Figure 1.3 shows typical

Reflection High Energy Electron Diffraction (RHEED) patterns for the (2×4) surface obtained along the 2× and 4× directions.

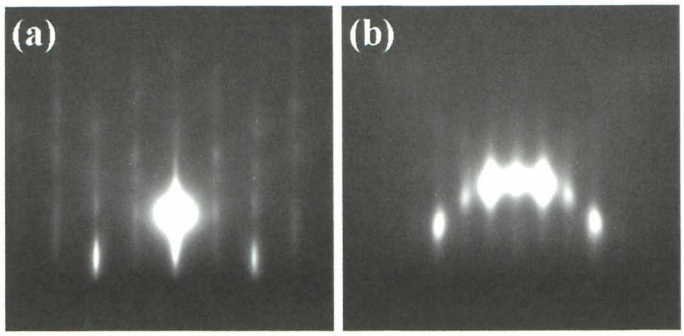


Figure 1.3: RHEED patterns taken from a GaAs(001) (2×4) planar substrate; (a) in the 2×[110] direction and (b) in the 4×[$\bar{1}$10] direction.

1.1.3. Low Index Planes.

Semiconductor thin film growth, generally takes place on low index crystal planes, which are defined by their Miller indices. Figure 1.4 is a schematic representation of the position of the low index planes for a cubic crystal with respect to the bulk unit cell. Also shown is an example of a high index plane namely the {310}. All of these planes become important in the growth studies on patterned substrates in Chapters 4 and 5.

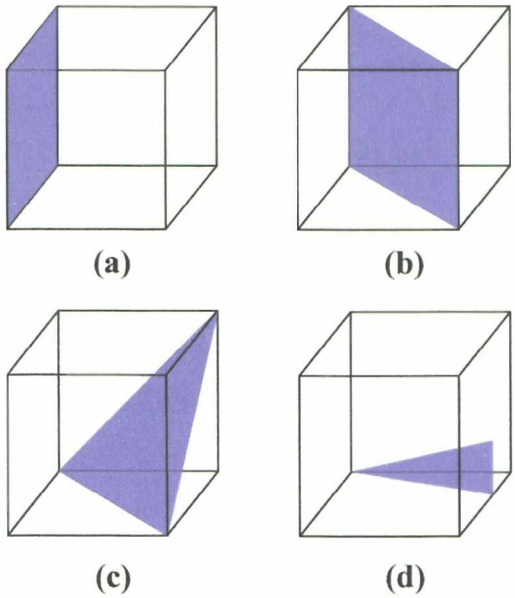


Figure 1.4: The low index planes of III/V semiconductors; (a) {100}, (b), {110}, (c) {111} and (d) {310}.

1.1.4. Epitaxial Growth Modes

Epitaxy is the ordered growth of one crystal upon another with defined coincident planes and directions. If the deposited material is the same as the substrate, the phenomenon is known as *homoepitaxy*, whereas if the substrate and the deposited material are different it is called *heteroepitaxy*. The way the overlayer grows on the substrate (i.e. its morphology) is known as the growth mode, and the different modes are distinguished by the way the deposited atoms arrange themselves on the substrate. There are three main classic modes of epitaxial growth [2]:

(i) Monolayer two-dimensional (2D) growth (Frank Van-der-Merwe),

(ii) Nucleated three-dimensional (3D) growth (Volmer-Weber),

(iii) Monolayer deposition followed by 3D nucleation (Stranski Krastanov).

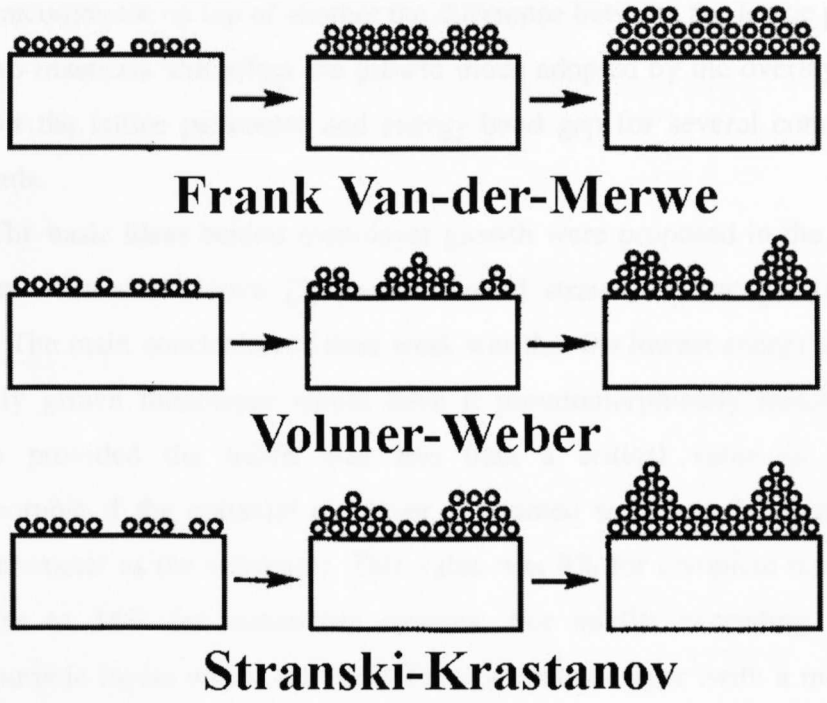


Figure 1.5: Schematic illustration of the three basic modes of thin film growth: monolayer-by-monolayer (Frank Van-der-Merwe), island (Volmer-Weber) and Stranski-Krastanov.

For (i), monolayer (ML) growth occurs when the incoming atoms are more strongly bound to the substrate than to each other (figure 1.5). These atoms nucleate to form small 2D islands, which enlarge with the arrival of more atoms; to eventually form a complete ML. Growth follows this ML-by-ML fashion. Nucleated 3D growth (ii) (Volmer-Weber), occurs when the binding energy of the incoming atoms is stronger than the bond with the substrate. The deposited atoms form small 3D islands, which increase in size as more material is deposited. The islands eventually meet and coalesce to form a continuous film. The third growth mode (S-K) is a combination of the previous two modes; initially the growth of the first few layers occurs in a ML-by-ML mode, but then growth occurs by nucleation of 3D islands on top of the completed ML.

Growth of *homoepitaxial* systems generally occurs by the 2D layer-by-layer mode. For *heteroepitaxial* systems the growth mode is influenced by the structure of the two different components. In particular, for heteroepitaxial growth of one III-V semiconductor on top of another the difference between the lattice parameters of the two materials will affect the growth mode adopted by the overlayer. Figure 1.6 shows the lattice parameter and energy band gap for several common III-V compounds.

The basic ideas behind monolayer growth were proposed in the 1940's by Frank and Van der Merwe [3,4] who studied strained heteroepitaxial growth systems. The main conclusion of their work was that the lowest energy state for an epitaxially grown monolayer would have it pseudomorphically matched to the substrate provided the misfit was less than a critical value (a system is pseudomorphic if the epitaxial overlayer is strained so it has the same in-plane lattice parameter as the substrate). This value was 9% for complete matching and could rise to 14% for metastable systems. For misfits exceeding this value psuedomorphic layers would not form. Once a strained layer (with a misfit below the threshold value) has been deposited on the substrate, further strained layers can be grown on top of this layer and give a pseudomorphic 3D structure.

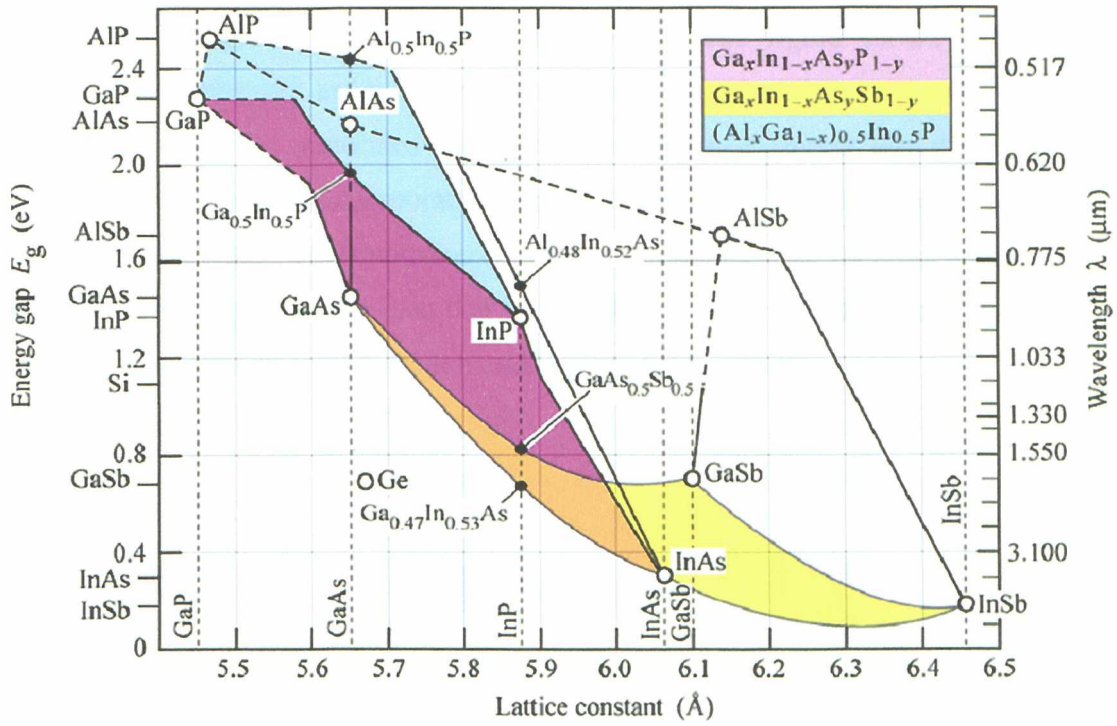


Figure 1.6: Lattice constant as a function of energy band gap at room temperature for various III/V semiconductors and their alloys.

1.2. The Surface Chemistry of MBE Growth on GaAs(001).

There have been extensive studies of the GaAs(001) surface, in terms of its structure and growth parameters required to produce high quality films. GaAs growth by Molecular Beam Epitaxy (MBE) on GaAs(001) substrates has a very complicated chemistry, not least because the cell used to generate the incident arsenic beam produces As_4 molecules, which can then be converted to As_2 molecules. The most important prerequisite for any molecular deposition technique is that the molecular beam should reach the surface collision free. Only surface reactions should be occurring. To successfully study reaction kinetics, Foxon and Joyce [5,6] utilised Modulated Beam Mass Spectroscopy (MBMS) to study the incorporation behaviour of As_2 and As_4 on the GaAs(001) surface.

The As_2 species can either desorb form the surface or associate with another As_2 molecule and then desorb as As_4. Alternatively, and this is the path that leads to growth, the incident As_2 molecules can dissociate on the surface as two As atoms and incorporate to form GaAs (figure 1.7). The figure shows how the incident As_2 molecules are adsorbed in a weakly bound mobile precursor state. During this stage, the molecules have a surface residence time of less than 10^{-5}s. The basic process for As incorporation during film growth is assumed to be simple first order dissociative chemisorption on surface Ga atoms. One As atom sticks for every Ga atom available provided that the Ga flux is lower than half the As_2 flux. The maximum possible incorporation coefficient of As_2 is unity.

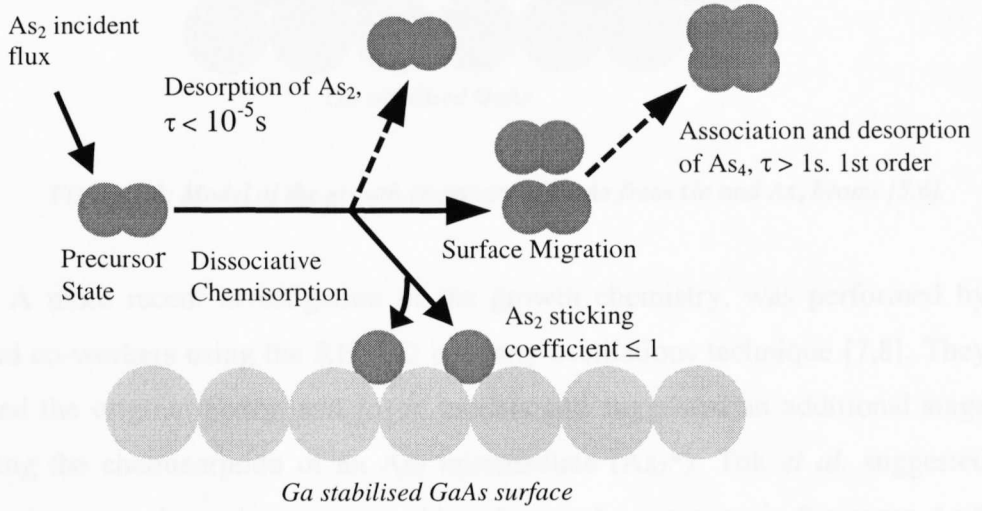


Figure 1.7: Foxon and Joyce model of the growth chemistry of GaAs(001) from Ga and As_2 [5,6]

The reaction mechanism for growth using Ga and As_4, also postulated by Foxon and Joyce, is shown in figure 1.8. The mechanism for the As_4 flux is much more complicated and involves second order reaction kinetics. Here, the As_4 molecules are initially adsorbed into a mobile precursor state. In this case the arsenic sticking coefficient never exceeds 0.5 due to the pair-wise dissociation of As_4 molecules chemisorbed on adjacent surface Ga atoms. The second order reaction kinetics is the important concept, where two As_4 molecules are required

for growth, generating four surface As atoms which are then incorporated into the Ga lattice, while the other four As atoms desorb as an As_4 molecule.

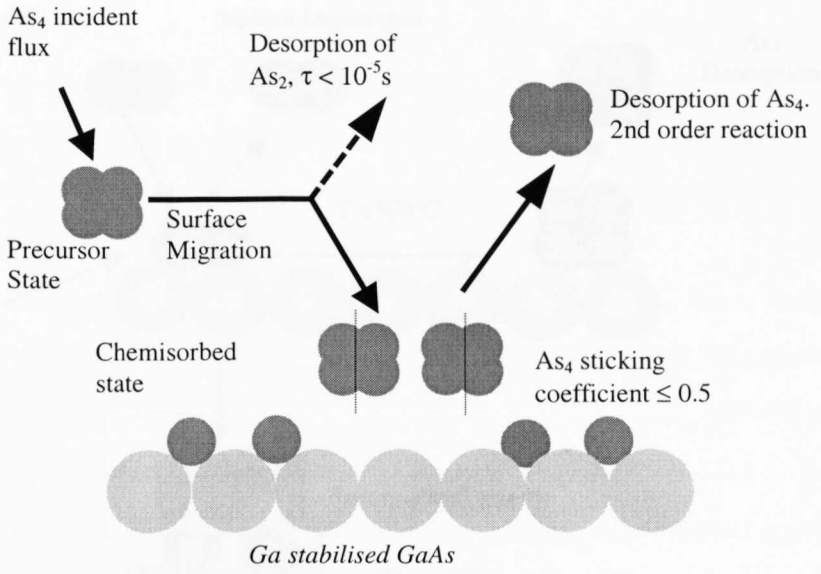


Figure 1.8: Model of the growth chemistry of GaAs from Ga and As_4 beams [5,6].

A more recent investigation of the growth chemistry, was performed by Tok and co-workers using the RHEED intensity oscillations technique [7,8]. They extended the original Foxon and Joyce models and suggested an additional stage involving the chemisorption of an As_2 intermediate (As_2*). Tok *et al.* suggested that the incorporation process using *either* As_2 or As_4 occurs *via* the same As_2* intermediate. The incorporation coefficients of both arsenic species were consistent with the intermediates involved and also with the previous Foxon and Joyce model. Schematic illustrations of the models produced by Tok *et al.* are shown in figures 1.9 and 1.10 for As_2 and As_4 respectively.

For As_2 incorporation, the As_2 molecules are weakly physisorbed into a precursor state, from which they can either desorb back into the gas phase or proceed to the chemisorbed As_2* state before incorporation into the lattice, as atomic As. For As_4 incorporation, growth also occurs via an As_4 precursor state before a pair-wise dissociative interaction occurs between two As_4 species. One As_4 molecule is produced in this reaction, which desorbs to the vapour phase and two molecularly chemisorbed As_2 intermediates are also formed. These

intermediates either desorb or incorporate into the lattice resulting in GaAs formation.

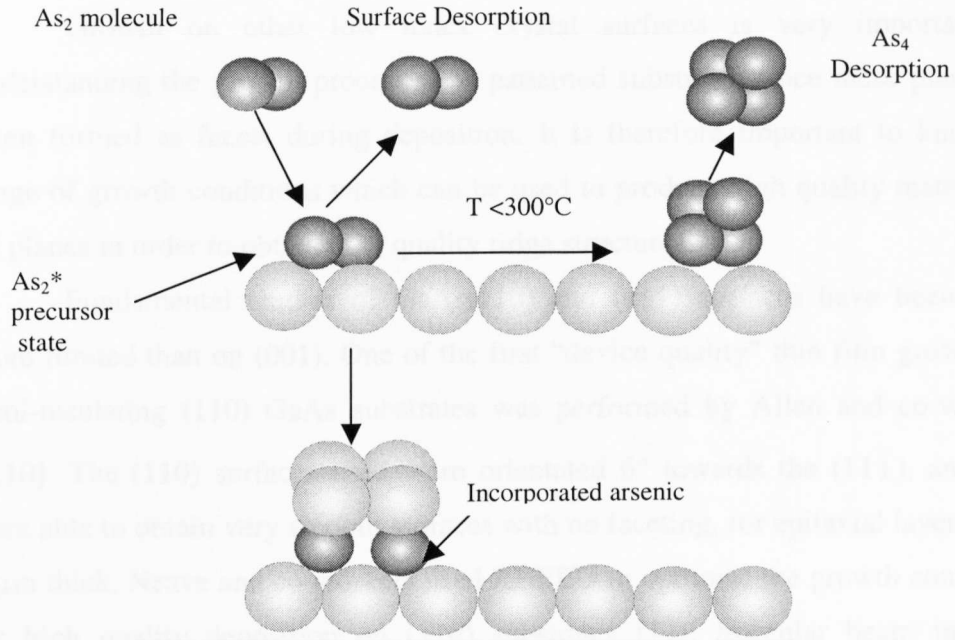


Figure 1.9: Revised model of GaAs (001) growth with Ga and As_2 beams [7,8].

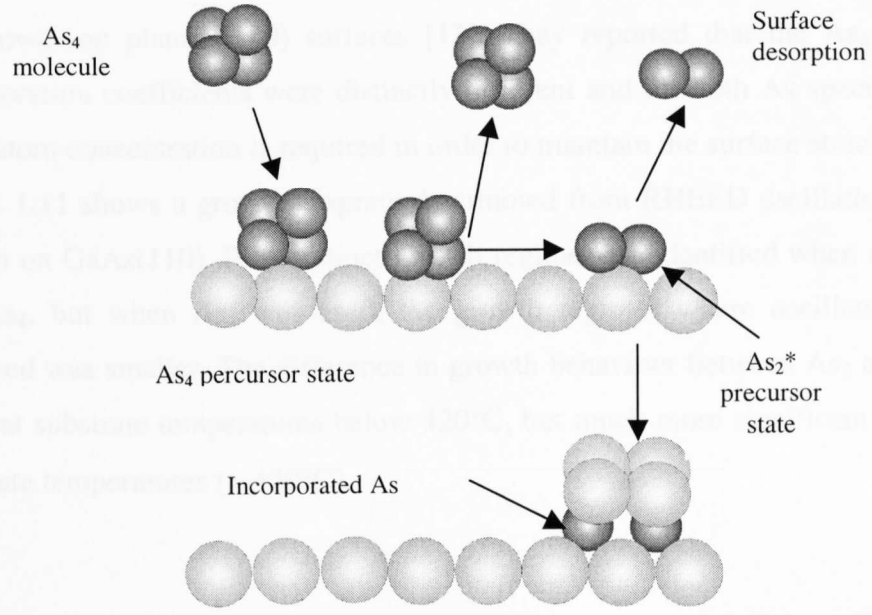


Figure 1.10: Revised model of GaAs (001) growth with Ga and As_4 beams [7,8].

1.3. Growth on Non- Planar GaAs Surfaces.

Growth on other low index crystal surfaces is very important for understanding the growth processes on patterned substrates since these planes are often formed as facets during deposition. It is therefore important to know the range of growth conditions which can be used to produce high quality material on all planes in order to obtain high quality ridge structures.

Fundamental studies of GaAs(110) and (111) surfaces have been much more limited than on (001). One of the first "device quality" thin film growths on semi-insulating (110) GaAs substrates was performed by Allen and co-workers [9,10]. The (110) surfaces used were orientated 6° towards the $(11\bar{1})$, and they were able to obtain very smooth surfaces with no faceting, for epitaxial layers up to 1 μm thick. Neave and co-workers used RHEED to optimise the growth conditions for high quality deposition on (110) substrates [11]. Specular beam intensity oscillations were observed to change for a range growth conditions. Fawcett and co-workers [12] reported that high quality growth on (110) substrates occurs at relatively low temperatures and As-rich conditions.

The influence of the As species was investigated by Holmes and co-workers for growth on planar (110) surfaces [13]. They reported that the As_4 and As_2 incorporation coefficients were distinctly different and for both As species a high As adatom concentration is required in order to maintain the surface stoichiometry. Figure 1.11 shows a growth diagram determined from RHEED oscillations of the growth on GaAs(110). Five distinct growth regimes are identified when using As_2 and As_4, but when As_4 was used, the growth regimes where oscillations were observed was smaller. The difference in growth behaviour between As_2 and As_4 is small at substrate temperatures below 420°C, but much more significant at higher substrate temperatures (> 420°C).

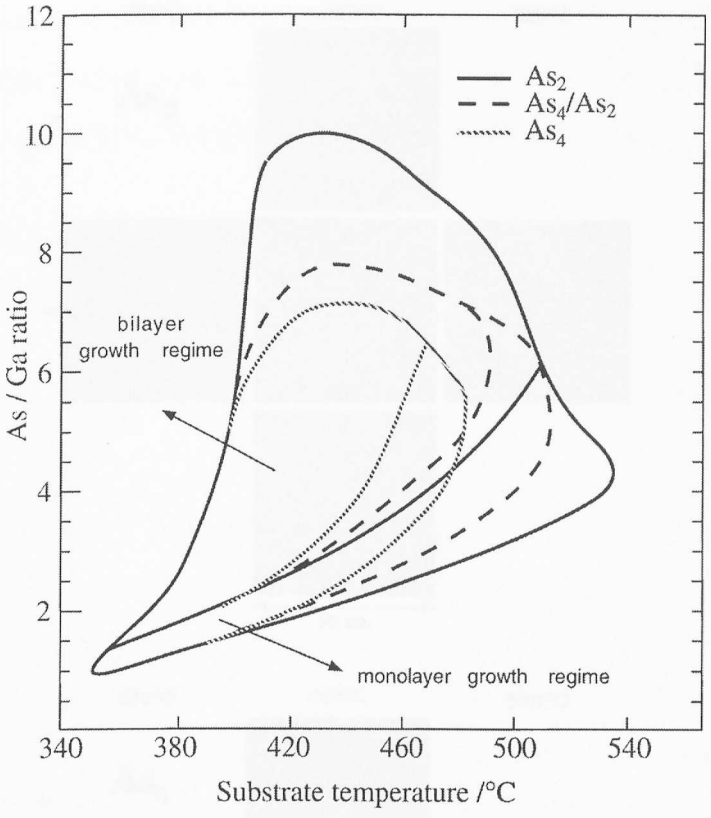


Figure 1.11. Growth diagram determined from RHEED oscillations for GaAs homoepitaxy on GaAs(110) [26]. Growth was carried out using an incident arsenic flux with different As_2/As_4 ratios [14].

Tok and co-workers undertook further investigations on the arsenic (As_2 and As_4) incorporation behaviour for growth on GaAs(110) [15]. They further optimised the growth conditions and produced smooth surfaces and optimal Si doping characteristics. Growth at low temperatures (< 480°C) and high As:Ga flux ratios (30:1) produced smooth *n*-type GaAs(110) layers, whereas at very low V/III ratios, a triangularly faceted surface resulted (Figure 1.12 (c) and (a) respectively).

It was also shown by Holmes *et al.[14]* that the use of As_2 rather than As_4 provided even smoother surfaces. Figure 1.12 shows Nomarski micrographs of a GaAs(110) surface at various substrate temperatures and V/III ratios for two As cracker cell temperatures. It can be seen that the smoothest surfaces were obtained under the highest V/III ratio and at the lowest substrate temperatures for both As_2 and As_4. With As_4; the surface shows a "preference to stack in a triangular orientation". For As_2; the features are smoother and rectangular islands are favoured.

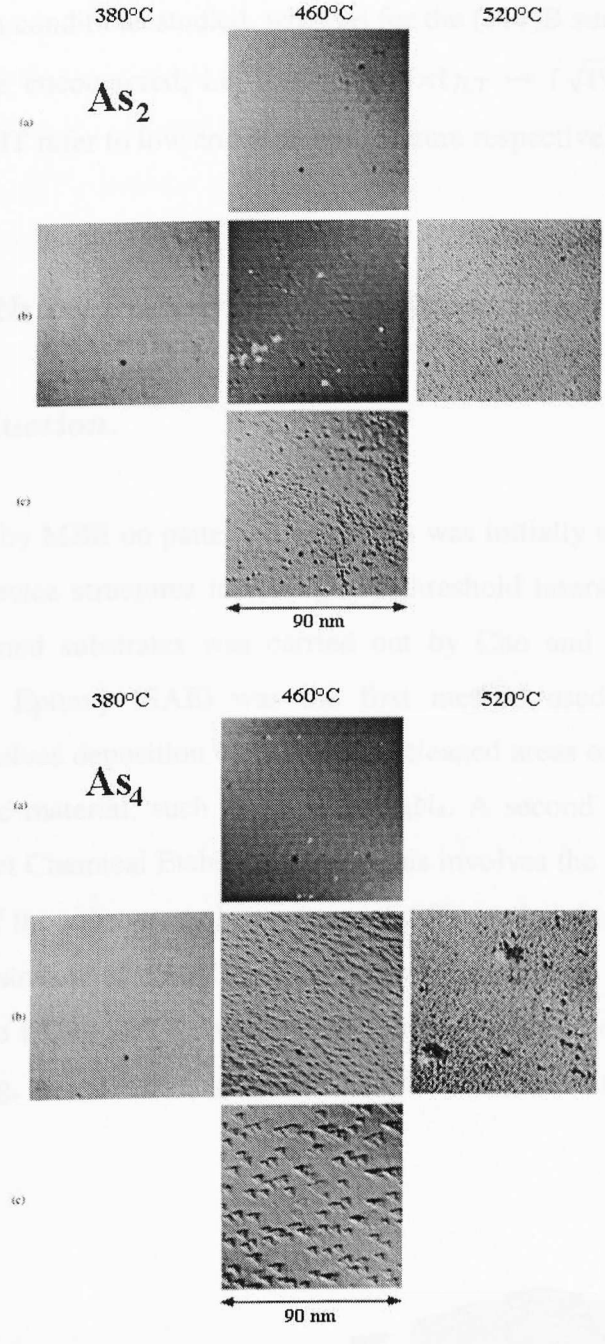


Figure 1.12: Normaski microscopy images of GaAs(110) surfaces after deposition of 1000ML of GaAs at five different growth conditions using As_2 and As_4. Substrate temperatures were 380, 460 and 520°C and the As/Ga atomic flux ratios were (a) 10, (b) 6, and (c) 2. Taken from Holmes et al. [14].

For the (111)A surface, studies have shown that in order to produce smooth (111)A surfaces, high V/III flux ratios and low substrate temperatures are also required [16,17]. RHEED studies by Woolf and co-workers [18], showed that for the (111)A surface, only the (2×2) reconstruction was observed for the complete

range of growth conditions studied, whereas for the (111)B surface three reversible transitions were encountered, i.e. $(2\times2) \leftrightarrow (1\times1)_{LT} \leftrightarrow (\sqrt{19}\times\sqrt{19}) \leftrightarrow (1\times1)_{HT}$ where LT and HT refer to low and high temperature respectively.

1.4. Growth on Patterned Substrates.

1.4.1.Introduction.

Growth by MBE on patterned substrates was initially used in an attempt to produce new device structures including low threshold lasers [19,20]. The initial work on patterned substrates was carried out by Cho and co-workers [21,22]. Selective Area Epitaxy (SAE) was the first method used for patterning the substrate. It involves deposition onto specially cleaned areas of a substrate covered with a dielectric material, such as SiO_2 or Si_3N_4. A second method of substrate patterning is Wet Chemical Etching (WCE). This involves the chemical removal of specific areas of the substrate to leave areas of different heights. Figure 1.13 shows a schematic illustration of these two main forms of patterning. The main difference between the two techniques being physical removal of areas of the substrate with chemical etching, and the coverage of areas of the substrate with dielectric material for SAE.

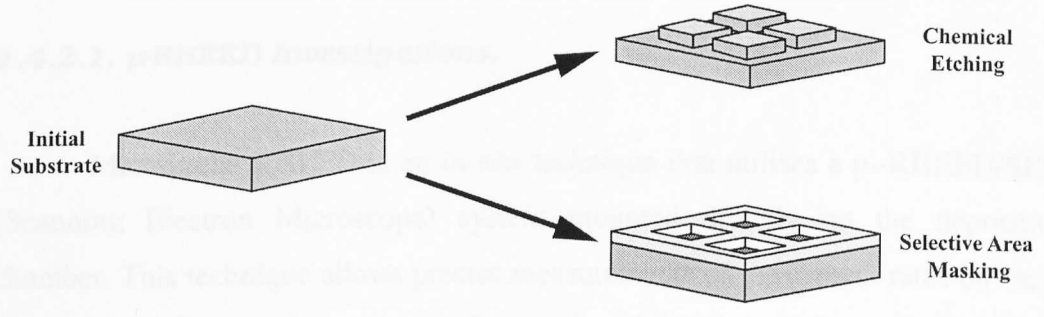


Figure 1.13. Schematic illustration of the two main forms of patterning: Chemical Etching and Selective Area Masking.

The latter method normally produces mesa features and V-grooves. Both methods have been used extensively and have their positive aspects as well as their downsides. However, chemical etching has been more extensively employed for devices because of the reduction of the strain-induced defects that may be formed using SAE. For some device applications, the surfaces have to be very smooth and free of strain defects. However, wet chemical etching can cause damage and contaminate the surface because of the use of hard chemicals in the processing stages if not precisely controlled. It is therefore very important for the substrates to be very thoroughly cleaned prior to growth to remove all surface impurities (primarily carbon).

1.4.2. Methods Used to Investigate Growth on Patterned Substrates.

Several groups have investigated growth on patterned substrates and there are essentially three different methods for studying deposition on these substrates. The first, involves the utilisation of microprobe RHEED (μ-RHEED) for measurements of growth rates in selected areas; the second involves structural determination of multi-layered structures; and the third is the controlled formation of structures by systematic alteration of the growth conditions. These are explained in the following section below.

1.4.2.1. μ-RHEED Investigations.

Microprobe RHEED is an *in-situ* technique that utilises a μ–RHEED/SEM (Scanning Electron Microscope) system mounted directly on the deposition chamber. This technique allows precise measurements of the growth rates on small areas of the substrate, due to the small spot size of the electron beam (focused with the SEM optics) compared with a standard RHEED system. One of the first groups to employ this technique for measurements of the growth rates on GaAs(001) patterned substrates was Hata and co-workers [23]. They investigated growth on mesa grooves oriented along the $[\bar{1}10]$ direction with (111)A sidewalls. When a

particular point on the scan area is observed, the growth rate at this point is measured by its RHEED oscillation period during deposition. Growth rate measurements were taken on the mesa sidewalls, and the upper (001) surface at points close to- and far from- the area of interaction with the sidewalls. Their study revealed that the growth rate on the upper (001) surface near the edge was larger and that the growth rate decreases exponentially as a function of distance from the edge of the mesa. It was suggested that Ga adatom diffusion from the (111)A surfaces causes the increase in the growth rate on the upper (001) surface near the edge. The value measured for the Ga adatom diffusion length, on the (001) surface, was 1 μm (at 560°C). This value was far larger than the one of 10 nm at 560°C, previously measured by Neave and co-workers [24] using conventional RHEED intensity oscillations on vicinal GaAs(001) surfaces. The μ-RHEED results indicated that Ga adatom diffusion over ML steps was a likely occurrence, contrary to the work of Neave *et al.* The difference in the two measurements was that Ga adatoms were able to migrate significantly more freely than expected between adjacent terraces on the vicinal surfaces. Consequently, the capture rate for ML steps appeared to be far less than unity, which was the earlier assumption of Neave *et al.*

Hata and co-workers undertook extensive investigations of (001)-(111)A and (001)-(111)B inter-facet diffusion processes. They determined that the Ga adatom diffusion length along the [110] direction was 1 μm and about eight times larger along the $[\bar{1}10]$ at 560°C [25]. An example of a schematic illustration for these non-planar substrates is shown on figure 1.14.

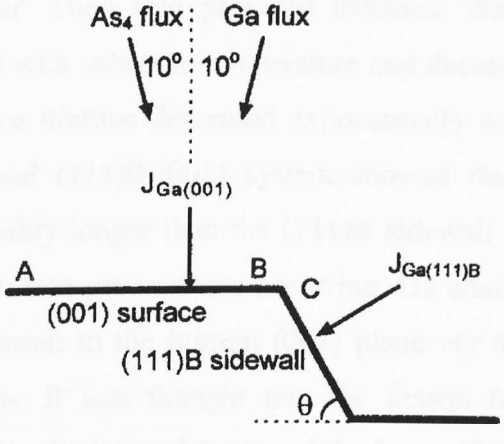


Figure 1.14: Schematic illustration of the (001)–(111)B system. Taken from [26].

Other groups performed similar studies on (111)A and (111)B surfaces and observed comparable results [26-29].

Further research on the As pressure dependence using (111)A or (411)A /(001) system, demonstrated that the As pressure affected the Ga adatom diffusion; the Ga diffusion length was found to decrease exponentially with increasing As pressure. In addition, the *local* V/III ratio was determined to be different to the impinging flux ratio at growth steps [27]. For the (111)B-(001) system the results revealed that for pressures higher than 4×10^{-4} Pa, the growth rate increased on the (001) plane as a function of the distance from the edge as Hata *et al.* reported [23]. However, at pressures greater than 4×10^{-4} Pa, a small decrease in the growth rate on the (001) plane was observed. Therefore at low As pressures, the Ga adatoms migrate from the (111)B facets to the (001) surface. The ratio of the Ga adatom diffusion coefficient on the (111)B facet to that on the (001) plane was calculated to be ~140 [28]. The result at high As pressures, suggested Ga diffusion to the (111)B facets from the (001) ridge top, which is surprising since ridges structures were formed on mesa stripes along these directions [29]. Therefore, at some point during growth, the net adatom flux must have been directed from the sidewalls to the top, otherwise the ridges could not form. It should be noted however, that μ-RHEED measurements are taken during the first few monolayers of growth, whereas more complete ridge formation happens during the later stages of growth.

Nomura *et al.* [30] used $(\bar{1}\,\bar{1}\,\bar{1})$B substrates for the formation of stripes with {100} sidewalls and the {111} plane as an upper surface. The measured Ga diffusion length for the $(\bar{1}\,\bar{1}\,\bar{1})$B surface was ~10 μm at 570°C and at an As pressure of 5.7×10^{-6} mbar. They also provided evidence that the Ga adatom diffusion length increased with substrate temperature and decreasing As flux, and that the Ga adatom surface lifetime decreased exponentially with increasing As_4 flux. Research on the total (111)B-(001) system showed that the Ga adatom diffusion length was probably longer than the (111)B sidewall length, and that a three-plane inter-facet diffusion process was occurring. Ga adatoms could diffuse from the upper (001) sidewall to the bottom (001) plane *via* the sidewall under suitable growth conditions. It was thought that the reason for the three-facet diffusion process was due to the stepped nature of the lower (001) surface, caused by the substrate etching, and acting as an adatom sink.

Special substrates were prepared using Liquid Phase Epitaxy (LPE) [26], to investigate a two-face facet diffusion with patterned substrates with very long (111)B sidewalls. It was discovered that at low As pressures Ga adatoms diffuse from the (111)B sidewalls to the top (001) plane, whereas at high As pressures, the flux direction reversed and Ga adatoms diffused from the top (001) to the (111)B sidewalls. At very high As pressures the direction changed again, concurrent with the change of the initial ($\sqrt{19}\times\sqrt{19}$) sidewall surface reconstruction to a (2×2) reconstructed surface. Further work by Nishinaga *et al.* [26] involved growth on disk–like mesas, prepared on GaAs (111)B substrates, and monitored using *in-situ* μ-RHEED/SEM MBE. GaAs deposition produced {221} facets at the base of the mesas, which quickly expanded in three directions. Upon further deposition, {110} facets formed, creating three-sided pyramidal structures as shown in figure 1.15.

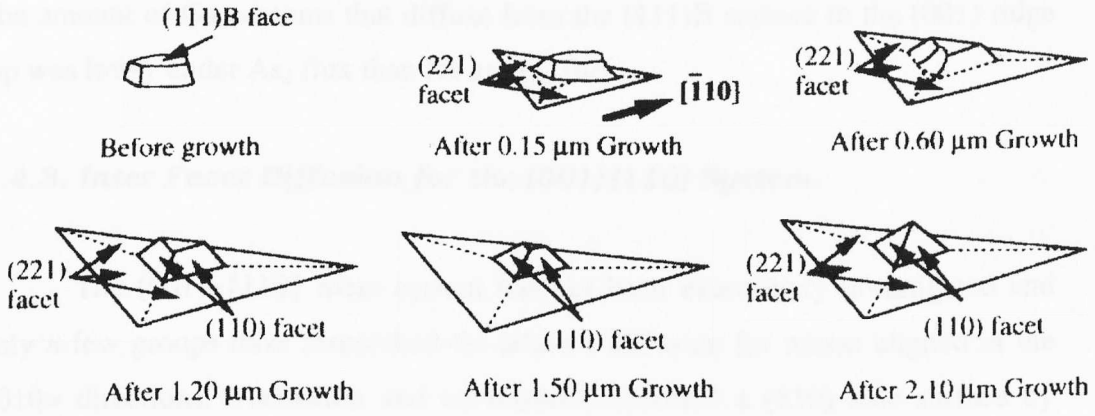


Figure 1.15: Schematic illustrations of the real time observations of the faceting process on the (111)B patterned substrate during growth at 580°C. Taken from [26].

Until this stage of growth, the mesa top did not shrink, suggesting that the amount of Ga diffusing from the sidewalls to the mesa top was low. However, when the {110} planes became the predominant facets, the Ga adatoms began to reduce the size off the (111)B upper surface, eventually closing of the three-sided pyramidal structure. Measurement of the growth rate at various positions allowed the (111)B Ga incorporation lifetime to be estimated at $1/70^{th}$ of that on the {110} and a Ga adatom diffusion coefficient fifty times greater than those measured on the {110} facets. When the temperature was increased to 620°C, in place of the {221} facets, a {111}B facet of triangular shape was formed with three edges touching the foot

of the mesa. The rest of the growth proceeded like the lower temperature samples, with the formation of {110} facets and completion of the pyramidal structures. It was found that the pyramidal structure was completed much more rapidly at the higher growth temperature, due to the longer Ga adatom incorporation lifetime and diffusion length.

Further investigations of the affect of the As species on ridge structures along the <110> direction on the GaAs (001) surface were conducted by Ogura *et al.* [31]. The investigation was focused on the effects of As_4 and As_2 flux during growth on the patterned substrates monitored by μ–RHEED/SEM. As growth proceeded, the mesas formed ridges with (111)B facets, and the size of the top surface was decreased for both As_2 and As_4 fluxes. However, SEM observations showed that shrinkage of the mesa top was faster with As_4 than with As_2. Using the model, it was found that employing As_2 resulted in a smaller Ga diffusion length. The amount of Ga adatoms that diffuse from the (111)B surface to the (001) ridge top was lower under As_2 flux than for an As_4 flux.

1.4.3. Inter Facet Diffusion for the (001)-{110} System.

The (001)–{110} mesa system has not been extensively investigated and only a few groups have researched Ga adatom diffusion for mesas aligned in the <010> directions. Yamashiki and co-workers, obtained a (110) side surface by cleaving the (001) surface along the $<\bar{1}10>$ orientation [32]. The length of the (110) side surface was ~630 μm, which was expected to be considerably longer than the Ga adatom diffusion length on the (110) surface. The measurements were taken using μ-RHEED. They suggested that the inter-surface diffusion occurs from the (110) sidewalls to the (001) top surface at lower As pressures while at higher As pressures it occurs from the (001) top surface to the (110). This was quite different than the belief that the surface As population decreased with increasing substrate temperature. However, these measurements were conducted on an "ideal" (110) sidewall meaning that it did not involve any additional processing and the sidewalls were sufficiently long not to involve three-way inter-facet diffusion.

Measurements of the Ga diffusion length on patterned substrates under different growth conditions were performed by Lopez *et al.* [33]. Mesa stripes of 100 μm width and 1 μm depth oriented along the [001] direction were produced

with sidewalls making a 100° external angle with the (100) bottom plane. The growth rate was measured using *in-situ* μ-RHEED. Under all conditions, an increase in the growth rate near the edge of the (100) mesa top was observed, due to the flow of Ga adatoms from the sidewalls to the top of the mesa stripe. Furthermore, the Ga diffusion length was observed to increase with increasing temperature and decreasing As_4 pressure. At 570°C, and an As pressure of 1.2×10^{-3} Pa, the Ga diffusion length for the (110) plane was measured to be 1.8 μm which increased to 12 μm at 620°C. This was in disagreement with the results produced by Yamashiki and Nishinaga, but it was thought that the increase of the Ga diffusion length with decreasing arsenic pressure was more likely to occur on the {110} due to the less favourable condition for Ga incorporation into the {110} planes at lower As surface concentrations.

1.4.4. Growth of Low Dimensional Structures on Patterned Substrates.

The use of mesa structures as a media for improving carrier confinement has been extensively studied with research directed towards the formation of Quantum Wires (QWRs) and Quantum Dots (QDs). Several key investigations in this field are discussed here. Temkin *et al.* [34], grew InGaAs/InP Quantum Well (QW) layers, which was one of the first attempts to form low dimensional quantum confined structures. QWRs and QDs with transverse dimensions of ~300Å were fabricated from the patterning of an InP/InGaAs/InP QW with small mesa stripes and circles using Reactive Ion Etching (RIE). Low temperature cathodoluminescence (CL) and photoluminescence (PL) demonstrated the exciton shifts of 8-14 meV expected from low dimensional confinement. Lopez and co-workers also investigated QWR fabrication, using MBE to grow GaAs/AlAs on mesa stripes oriented along the [001] direction [35,36]. Koshiba *et al.*, and Kodoya *et al.* [37,38] reported the formation of QWs on top of mesa and reverse mesa stripes along the [110] direction, with (111)B sidewalls on a GaAs(001) surface structures and they indicate quantum confinement has been achieved due to the measured blue shift of ~60 meV. Ando and Fukui [39] produced some of the best quality QWR structures. High temperature growth and high V/III ratios were used for the fabrication of AlGaAs ridges. A model was proposed for the inter-facet

interactions responsible for the facet formation. Although relatively simple, this model highlights the key surface processes for inter-facet diffusion from the newly formed facet to the upper surface.

Another area of patterned substrate research has concentrated on the formation of QWR structures by deposition in V-grooved substrates. Early work by Kapon *et al.* [40] concentrated on the growth of GaAs/AlGaAs on rounded grooves and used TEM to demonstrate controllable lateral variations in physical properties which depended on the superlattice period. Subsequent work by the same group [41] demonstrated stimulated emission from a *"quasi one-dimensional"* QWR in 1989.

1.4.5. Formation of Multi-layer and Low-Dimensional Structures on Patterned Substrates Along the <001> Directions.

Although most studies on patterned substrates have been concentrated on mesa patterns defined along the <110> directions, there have been a few groups that investigated the growth behaviour on patterns along the <001> directions for the formation of multi-layers and low-dimensional structures.

Lopez and co-workers [35] investigated growth of GaAs/AlAs on mesa stripes along the [001] direction. The patterns comprised of different width (1–10 μm) mesa stripes with ~1 μm depth. SEM observations showed that the stripes along [001] produce smooth (110) and $(1\bar{1}0)$ facets. At lower substrate temperatures (580°C) and higher As pressures (>1.5×10^{-5} Torr), the formation of additional (310) and $(3\bar{1}0)$ facets were also observed between the top (001) surface and the (110) and $(1\bar{1}0)$ facets respectively. These planes are highlighted in the SEM image shown in figure 1.16. A method for fabricating of QWRs was also demonstrated by Lopez *et al.*, which involves reducing the top (001) surface of the mesa to ~50 nm followed by growth of a GaAs/AlAs QW [35].

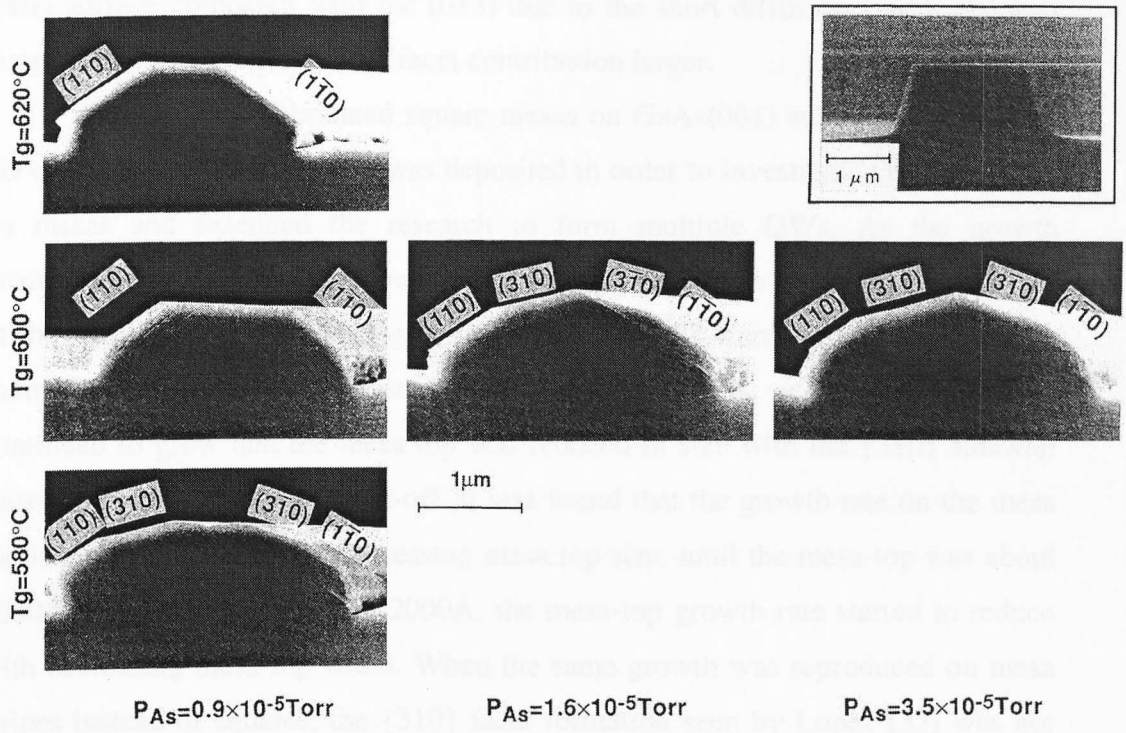


Figure 1.16: Cross sectional SEM images of a ~2 μm ridge taken along the [0 $\bar{1}$ 1] direction at different three different growth temperatures (T_g) and at different As pressures (P_{As}) [35].

Liu *et al.* [42] used similar methods for GaAs and AlAs multi-layer structures on ridges oriented along the [001] direction. The structures were examined by Transition Electron Microscopy (TEM) and SEM. Throughout the reported growths, the most stable facets formed were the {110} planes and that with increasing GaAs/AlAs deposition the (001) top plane reduced in size before it pinched off, forming a GaAs QWR. Moreover, an enhanced Ga and Al migration length was observed on the {110} side facets and the Al diffusion length was determined to be 8 nm at 570°C and for an incident As pressure of 1.3×10^{-3} Pa (V/III = 9).

Investigation of multi-layer GaAs/AlGaAs growth on stripes along the [$\bar{1}$10], [110], and [100] directions with various sidewall angles on GaAs (001) substrates was performed by Takebe and co-workers [43]. For the [100] direction stripes with angles greater than 45° (011) and (031) extra facets were formed. For angles between 19° and 45° the (011) facet disappeared and (013) facet developed, while Lopez [35] observed that both facets seem to co-exist at low temperatures and high As pressures. This has been explained by the faster growth rate on the

(001) surface compared with the (013) due to the short diffusion length at lower temperature – making the (013) facet contribution larger.

Konkar *et al.* fabricated square mesas on GaAs(001) substrates to achieve 3D confinement [44]. AlGaAs was deposited in order to investigate QW formation on mesas and extended the research to form multiple QWs. As the growth proceeded, {110} sidewalls were initially formed, leading to a reduction in the size of the mesa-top. Upon further growth {310} sidewalls were formed, producing a rhombus mesa-top. During further growth, both {310} and {110} sidewalls continued to grow and the mesa top was reduced in size with the {310} sidewall causing the (001) to be pinched-off. It was found that the growth rate on the mesa top initially increased with decreasing mesa top size, until the mesa-top was about 2000Å. When it was less than 2000Å, the mesa-top growth rate started to reduce with decreasing mesa top width. When the same growth was reproduced on mesa stripes instead of squares, the {310} facet formation seen by Lopez [35] was not observed, at high temperatures and low As pressures. The reason for the lack of {310} facets on the mesa stripes could be the inter-facet interaction since Ga might diffuse from the sidewalls towards the mesa top interfering in the regions close to the corners, something that does not happen for the stripes.

Similar work on square mesas was performed by Kasai *et al.* [45,46]. Fabrication of square mesas along the <100> was utilised in order to obtain 3D confined GaAs/AlAs structures. The square mesas were 2.8-4.2 μm^2 in size and the post-growth structures were examined by SEM, AFM and μ-PL. The structures consisted of alternating AlAs/GaAs/AlAs QW layers of 10 nm, 5 nm, and 10 nm thickness respectively, and GaAs buffer and capping layers. SEM images showed the presence of {110} facets and that the lateral size of the mesa top decreased in proportion to the initial pattern size. The squares appeared to be elongated along the [110] direction, possibly due to the different lateral growth rates along the [110] and $[1\bar{1}0]$ [25]. However, during the entire growth sequence, the mesa top remained square and the facets were clean with sharp corners. Low temperature PL and μ-PL experiments exhibited sharp luminescent lines.

Williams and co-workers investigated the growth conditions to produce high quality ridge structures on <100> direction mesa stripes [47]. In all growths, for both stripe and square based mesas, {110} facets were formed. For low V/III ratios, the appearance of triangular faceting on the {110} facets was present but for

higher V/III ratios, the {110} facets produced were smooth. In addition, it was observed that the lower the Ga flux, in this case at a higher V/III ratio, the smoother the resulting mesa structures. Further studies by Williams *et al.* [48], demonstrated an increase in the *"Swimming Pool Effect"* (SPE) with increasing V/III ratio and/or reducing the substrate temperature, as a consequence of changes in the Ga diffusion length. The term SPE here is used to define the formation of raised areas at the edges of the ridges, due to material build-up. It was concluded that the smaller the SPE, the larger the Ga migration length and vice versa. For larger GaAs deposition quantities, the mesa top reduced and eventually lead to the formation of sharp, triangular ridge structures. Geometric models were also suggested which could be used to predict facet evolution for a given deposition quantity.

The same group grew pyramidal structures on patterned mesas for use in an optical micro-cavity structure [49]. The structures utilised ~1 μm square mesas, oriented along the <100> direction. It was found that the phase of light emitted from the pyramidal structure was mode dependant. Further research using digitised charge coupled device images showed high reflectivities for the {110} facets (>80%) [50].

Liu *et al.* investigated the growth of $In_xGa_{1-x}As$/GaAs QWRs on ridges along the [001] direction [51]. The ridges were of different sizes varying from 1.1 μm to 12 μm in width. The multi-layered structures consisted of a GaAs/AlAs buffer layer an $In_{0.22}Ga_{0.78}As$/GaAs QW, a reference GaAs/AlAs QW and a GaAs cap layer. CL measurements showed peaks from the GaAs/AlAs QW, which forms at the edge of the ridge top where the QW layer is thicker due to the preferential migration of Ga from the {110} facets. In addition, the In content of the $In_xGa_{1-x}As$/GaAs QW increased with decreasing ridge width (from flat substrate to 2.9 μm), due to In migration from the initial sidewalls to the (001) top region. For mesa widths of 2.9 μm-0.05 μm the x decreases considerably. Konkar *et al.* [44] also investigated the growth of $In_xGa_{1-x}As$ on GaAs(001) patterned substrates and discovered that if the mesa top is sufficiently small, ~(75 nm), then QD formation is suppressed for monolayer coverages $\geq$ 5 ML. This is in direct contrast to the belief that the 2D layer-by-layer growth of InAs stops at coverages above ~2 ML due to the formation of quantum dots [52,53].

1.5. Growth of InAs/InGaAs on GaAs(001).

1.5.1. Introduction on QDs.

QDs are small 3D islands of a narrow band gap semiconductor (e.g. $In_xGa_{1-x}As$), enclosed in a wide band-gap semiconductor matrix (e.g. GaAs). Provided the bands of these 3D islands and of the host are appropriately aligned, the valence and conduction bands produce a confining potential for the holes in the valence band and the electrons in the conduction band respectively. If these islands are small enough, they will behave as large "artificial atoms" with discrete energy levels. Thus, the recombination spectrum of a single QD consists of a single sharp line, with a practically non–measurable temperature broadening.

1.5.2. Growth on Planar Substrates.

1.5.2.1. Initial Work on QDs.

Numerous studies concentrated on understanding the formation mechanisms of QDs on planar GaAs substrates formed by the Stranski-Krastanow (SK) growth mode (discussed in section 1.3) *i.e.* after the epitaxial growth of a thin layer, the 2D wetting layer, the accumulated strain is relieved by the formation of nanometer scale islands. Some of the first high quality dots were easily fabricated [54-58]. One of the first reports for the presence of InAs quantum dots was in the work of Guha and co-workers [54] for the growth of $In_xGa_{1-x}As$ on GaAs(001) planar substrates. They observed that for values of $x > 0.25$, 3D growth occurs leading to the formation of the QD islands. These islands grew defect free for sizes up to ~250 Å width and 80 Å height.

Another early work was performed by Snyder *et al.*, in which $In_xGa_{1-x}As$ was grown on GaAs(001) substrates, the growth monitored by combination of RHEED and STM [55]. During the first stages of growth the RHEED pattern lost the (2×4) reconstruction and spots appeared, meaning that ripples started to appear on the surface. Upon further deposition the surface started to become 3D and the

film was broken up into large almost circular islands with a relaxed surface lattice constant to release the strain.

Leonard *et al.* [56] in a similar investigation on planar GaAs(001) wafers, grew a structure which contained a 60Å thick InGaAs QW below the $In_xGa_{1-x}As$ dot layer as a reference for PL experiments. TEM was used to characterise the samples, and showed the formation of InAs circular islands, whose size distribution and density depended strongly on the substrate temperature and x value. Experiments performed at different substrate temperatures revealed that at high temperatures (>550°C) the dot formation was inhibited due to In re-evaporation, and the deposition of more ML's without dot formation was possible. Moreover, when the x value was decreased to x = 0.33 low temperatures, resulted in a thick 2D wetting layer due to the very small In diffusion length preventing In migration and island formation. Low temperature PL spectra showed that apart from the QW peak, there was a strong luminescence line at ~1000 nm from the InAs dot layer.

Investigations of the deposition of InAs on planar (001) substrates were also undertaken by Moison and co-workers [58]. As the InAs deposition started, RHEED showed the initial (2×4) reconstruction changed to (3×1) streaks which are typical of a 2D growth but upon further deposition the streaks started weakening in the $[\bar{1}10]$ direction. At 1.75 ML coverage spots were observed on the RHEED pattern, which are consistent with the appearance of 3D islands. The dot width was measured to be 240Å and the height 30Å. As the growth proceeded, the dot density remained constant, but a dramatic increase in the QD size was observed before coalescence occurred at ~3 ML. Above 3 ML deposition, the dot size distribution increased with a high density of large dots present. Moreover, the coalescence of two or more dots into larger islands was apparent. Interestingly, when coalescence occurred, a sudden increase in the inter-dot distance was also observed.

1.5.2.2. QD Composition.

Many studies of QD formation on planar GaAs(001) substrates have been focused in obtaining compositional information. Rosenhauer *et al.* used HR-TEM to study the composition of $In_xGa_{1-x}As$ islands on GaAs(001) [59]. Two samples

were examined, with a nominal In compositions of x = 60% (sample A) and 100% In content (sample B). It was found that the In content for sample A was 24% and for sample B it was 45%. In addition, the In content in the QDs was non-homogeneous since more In was found at the top of the islands. Lin *et al.* investigated the structural anisotropy of InAs and $In_xGa_{1-x}As$ QDs [60]. They reported that for "pure" InAs, *i.e.* $x = 1$, the QD size was uniform and the shape appeared round whereas for $In_xGa_{1-x}As$ with $x = 0.8$ the QDs are extended along the $[1\bar{1}0]$ and for $x = 0.5$, elliptical islands form, aligned in the $[\bar{1}10]$.

1.5.2.3. Growth Conditions Control on QDs.

Several investigations have been undertaken on planar substrates with the aim to better understand the formation of QDs and be able to control their size and density. The majority of these concentrate on the variation of various parameters.

Shiramine *et al.* [61] investigated the effect of growth temperature on In adatom migration on planar GaAs(001) substrates and concluded that the island size increased and the island density decreased with increasing substrate temperature. Similar results were found by Tilmann *et al.*, Madhukar *et al.*, Kamiya *et al.*, and Joyce *et al.*,[62-65]. Joyce and co-workers, optimised the growth of the QDs by varying the growth conditions [66]. It was found that the number density dropped by an order of magnitude when the In growth rate was lowered from 0.13 to 0.003 ML/s. Experiments performed by Bennet *et al.* by varying the substrate temperature on seeded/non-seeded InAs/GaAs dots showed that low growth rate produces significantly large QDs [67]. In addition, Joyce and co-workers [66], suggested that for coverages above 2.5 ML and low growth rates (<0.01 ML/s), there are two types of quantum dots present; the regular elastically relaxed with narrow distributions and large irregular ones, which increase in size and density at high coverages acting as sinks for additional deposited material. This was previously observed by Leonard *et al.* who investigated the critical layer thickness for QD formation [68]. They used RHEED to measure the time taken for the 2D→3D growth mode transition and therefore to be able to calculate the amount of

InAs deposited to form $In_xGa_{1-x}As$ QDs; for x = 1 the QDs formed after 2 ML deposition, and for x = 0.33 the QDs formed after deposition of 12 ML [56].

Solomon *et al.* investigated the effects of substrate temperature and ML coverage on $In_xGa_{1-x}As$ QDs [69,70]. For the InAs growth they reported that coalescence occurred at ~4 ML for a substrate temperature of 388°C and when the substrate temperature increased, the QD size also increased. When x= 0.5 was used, island formation occurred after the deposition of 5 ML compared to the less than 2 ML for x=1. Further investigations included the effect of the V/III flux ratio and growth rate. When the V/III ratio was reduced, the 3D island density increased, while the QD diameter remained the same. As In growth rate decreased from 0.19 to 0.09 μm/h, the QD density was also found to increase from 49 to 57%.

Riel *et al* varied the arsenic pressure during InAs growth on GaAs(001) planar substrates and showed that as the As pressure increases, the QD density increases while the average dot width and height decrease monotonically [71]. Other groups have confirmed these findings [72]. An example of the values of the QDs by varying the As and the InAs coverage by Riel *et al.* and Yamaguchi *et al.* is shown on figure 1.17.

Kitabayashi and Waho carried out a similar set of experiments and used AFM to check the morphology of the InAs QDs grown at different conditions [73]. At lower growth temperatures (<400°C), the island size was reduced and the density increased. When the V/III ratio was reduced from 7.0 to 3.6, the island size became larger and more uniform due to the enhanced In diffusion length caused by the decrease in As pressure. However, as the V/III ratio decreased further, the QDs became smaller again. In contrast, while examining the affect of growth conditions on the QD formation on planar (001) GaAs substrates, Madhukar *et al.[63]* described that at low growth temperatures (420°C) the QD density *decreases* with increasing arsenic pressure, due to the slower dissociation rate of arsenic molecules at these lower temperatures.

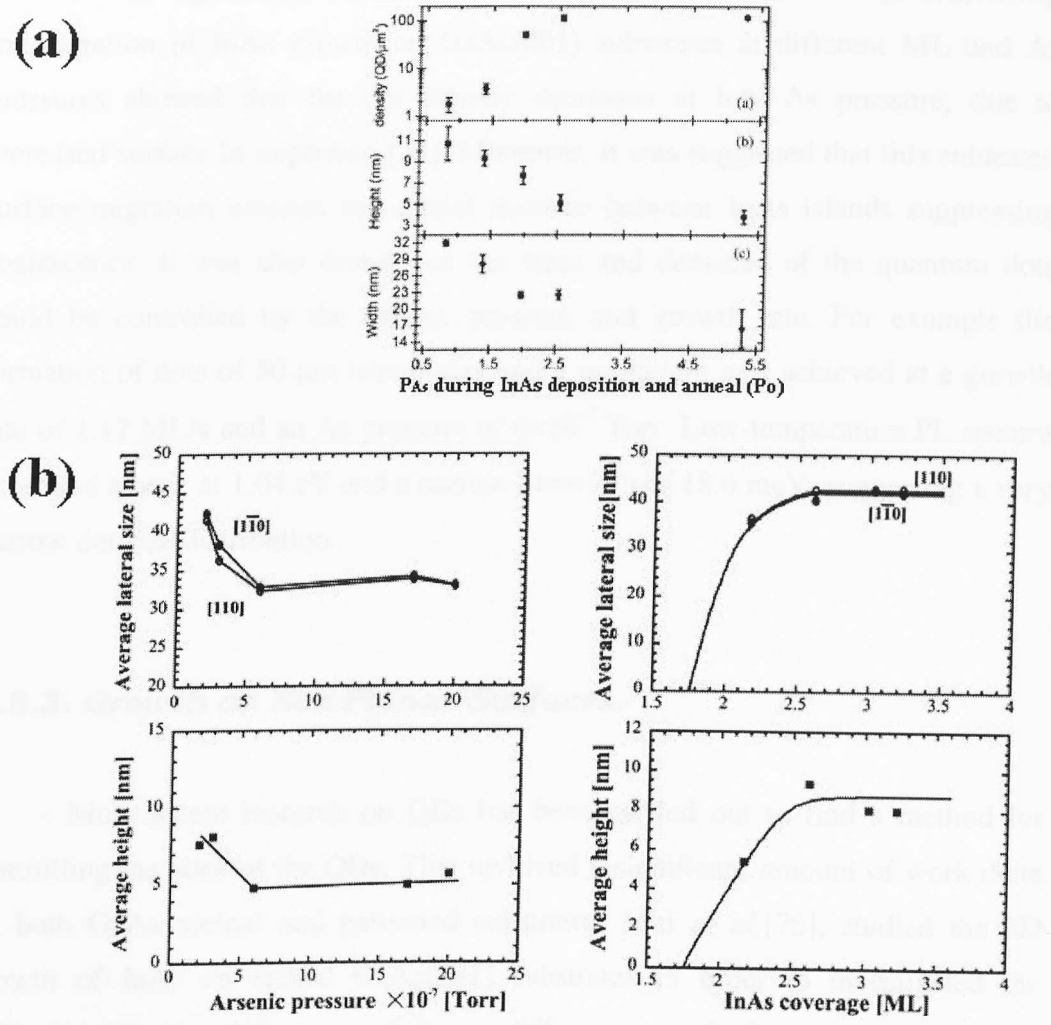


Figure 1.17: (a) Graph showing the QDs density and lateral dimension dependence on As pressure as observed by Riel et al. [71] and (b) the average height and QDs size dependence on the As pressure and the In As coverage as observed by Yamaguchi et al [72].

1.5.2.4. QD Position/Size Control.

Quantum dots are expected to play an important role in the future fabrication of high performance optoelectronic devices. As a consequence, over the past few years; there has been a vast quantity of investigation into the optimisation and characterisation of QDs grown on GaAs (001) substrates. A key step will be to ensure that all the dots are of similar size and shape, so thus emit light at a similar wavelength [74]. The structural uniformity of these QD samples was difficult to

achieve but significant advances were made in this direction [64,68,72,75]. Investigation of InAs growth on GaAs(001) substrates at different ML and As pressures showed that the dot density decreases at low As pressure, due to increased surface In migration [72]. Moreover, it was suggested that this enhanced surface migration extends the spatial distance between InAs islands suppressing coalescence. It was also found that the sizes and densities of the quantum dots could be controlled by the arsenic pressure and growth rate. For example the formation of dots of 30 nm lateral size and 5 nm height was achieved at a growth rate of 1.17 ML/s and an As pressure of 6×10^{-7} Torr. Low-temperature PL spectra exhibited a peak at 1.04 eV and a narrow linewidth of 18.6 meV, suggesting a very narrow dot size distribution.

1.5.3. Growth on Non-Planar Surfaces.

More recent research on QDs has been carried out to find a method for controlling the sites of the QDs. This involved a significant amount of work done on both GaAs vicinal and patterned substrates. Mui *et al.*[76], studied the 3D growth of InAs on etched GaAs(001) substrates in order to investigated the different migration behaviour of In on different crystal planes as a method to control the InAs dot formation. Etched ridges along the [011] and [01$\bar{1}$] directions on (100) substrates were used. For the first orientation the sidewalls were of the (311)B type, and the islands formed were oriented along the ridges at the bottom of the one side. In the [01$\bar{1}$] direction, the islands were situated on the (100) plane along the edges of the sidewalls with more islands along one side of the ridge. The adatoms migrated away from the (533)A type sidewalls, to the adjacent (100) planes. Both samples were not rotated during InAs deposition. When substrate rotation was used, the InAs islands appeared in equal numbers on both sides of the ridges.

Kitamura *et al.* investigated the growth by MOCVD of InAs QDs on GaAs(001) vicinal substrates [77]. A GaAs epilayer with multi-atomic step structures along straight lines were grown on a vicinal GaAs substrate 2° mis-orientated along the [010], [110], and [$\bar{1}$10] directions, and then the InGaAs islands

were grown selectively on the multiatomic step edges using strain effects. Ikoma *et al.* also investigated QD formation on GaAs(001) vicinal surfaces [78]. The substrates were misoriented by 1° toward the [110] direction and InAs was deposited at 450°C with In growth rate of 0.1ML/s. Dots were observed by STM to be aligned along the $[1\bar{1}0]$ whereas the on-axis samples were seen to be distributed more randomly. It was found that 85% of the islands were located near the steps of the terraces. Similar findings were reported by Mano *et al.* [79] and Leon *et al.* [80] where QDs were preferentially aligned on step edges. It was also reported "when step nucleation dominates, polydispersity is greatly reduced". Ishikawa *et al.*, studied the site control and the InAs island sizes using *in-situ* electron beam lithography and self organising molecular beam epitaxial growth [81,82]. Initially, pre-patterned square mesas were constructed on the surface by conventional techniques. InAs coverages of 1.4-1.6 ML were deposited on the patterned samples at 460°C. The In adatoms diffused to the mesa edges where there were a high concentration of atomic steps and QDs were formed. The In adatom diffusion length was estimated to be several tens of μm. The QD concentration was found to be highly dependent on the mesa size. For a 50 μm square mesa only a few dots were found and for a 30 μm square mesa, hardly any. In other experiments, fine holes were formed on GaAs(001) substrates into which, InAs monolayers were deposited. In this case, dots were formed only in the holes after the deposition of 1.8 ML of InAs and it was found that QD density changed with the hole depth. If a hole depth of 5-6 ML was used, a single dot could be formed in its base.

Other work concentrated on patterned substrates includes investigations by Xie *et al.* [83,84], Jeppesen *et al.*[85], Lobo *et al.*[86], Nakamura *et al.*[87], Tsui, Zhang, and Shiralagi [88-90]. SAE and faceted epitaxial growth was used to produce mesa stripes along the [100] direction [89]. The oxide layer, which is used in SAE, prohibits growth of GaAs and InAs on these regions. Using this method only the top (001) facet is available for growth. The mesa stripes were of~1 μm width but were reduced to ~200 nm when the mesa height was ~0.4 μm. The dot densities formed on the wider mesas were not uniform and more dots were concentrated near the edges of the mesas. For the narrower facets, the InAs island densities were quite uniform and surprisingly, the dot density was higher than for the wider facets due to enhanced In diffusion to the top of the mesa. Another surprising fact is that coalescence occurs at >1.7 ML for their patterned mesas,

whereas on planar substrates it normally occurs >3 ML. Further work by the group included stripes on both the [110] and [001] directions. More dots appeared on the stripes along the [001] rather than the [110] directions under the same conditions and more dots appeared on the stripes than on the flat region. Moreover, by reducing the mesa width below 200 nm they were able to obtain well-aligned arrays of three, two –and for widths <100 nm –single array of dots, as shown in figure 1.18.

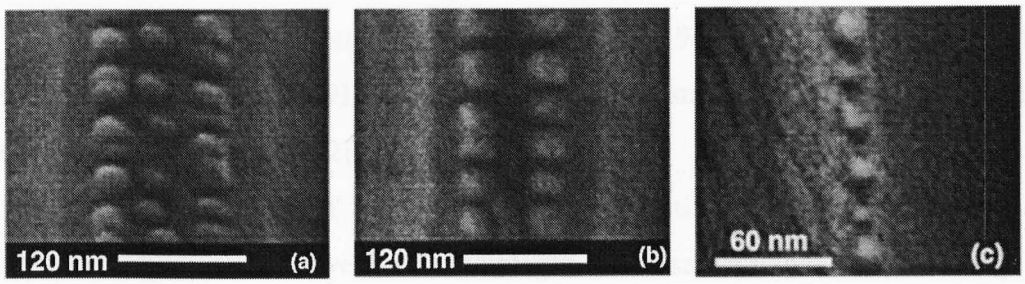


Figure 1.8. SEM images (top view) of InAs QD formation on [001] oriented GaAs mesa stripes with different top facet widths, exhibiting (a) three rows, (b) two rows and (c) one row of aligned QDs [89].

1.6. Aims.

This thesis is divided into two main themes. The first involves GaAs homoepitaxial growth on GaAs(001) mesa patterned substrates, aligned along the <100> directions, in order to investigate the kinetic processes involved in the Ga adatom diffusion. This is achieved with the use of patterned substrates consisting of various width mesa stripes in the two orthogonal <100> directions. A variety of growth conditions and deposition quantities were employed to investigate both facet evolution and morphology.

The second theme concentrates on the investigation of InAs heteroepitaxial growth on partially completed ridge structures. Again these were also defined in the <100> directions. These investigations were an attempt to understand In adatom diffusion and QD formation on mesa stripes. This study involves the optimisation of the growth conditions to obtain uniform size distributions and density control of the InAs quantum dots.

CHAPTER 2.

Experimental

2.1. MBE: Brief Overview.

MBE was first established in the late 1960s for use of producing semiconductor materials [91]. The design and understanding of MBE systems has been reviewed by Joyce [92].

Several deposition techniques can be utilised for the growth on semiconductors and all have their advantages and disadvantages. An advantage of SSMBE (Solid Source MBE) – as opposed to metalorganic vapour phase epitaxy (MOVPE) and chemical beam epitaxy (CBE) – is that it does not utilise metalorganic compounds in the growth chamber and thus avoids any carbon contamination of dopant effusion cells, cracking cells, as well as hot parts of the growth chamber.

In an MBE system, growth using patterned substrates has some additional benefits; (i) it is an *in–situ* technique and so the quantum structures obtained are defect–free and contamination can be minimised, (ii) better confinement can be achieved – *i.e.* two degrees of carrier confinement can be obtained – in a single growth step [93,94].

The general principles of MBE will be discussed below as well as the equipment used for these studies and *in-situ* cleaning and analysis. The *ex-situ* cleaning and analysis techniques will also be discussed in detail.

2.1.1. Background Theory.

The first form of epitaxial deposition was Liquid Phase Epitaxy (LPE) [95]. MBE followed shortly after and became most popular for atomically smooth heterostructure interfaces [96,97].

Solid Source Molecular Beam Epitaxy (SSMBE) is based on a self-organising growth mechanism by a process involving the reaction of one or more thermal molecular beams with a crystalline surface under ultra-high vacuum (UHV) conditions. UHV is needed for the beam to be collision-free until it reaches the sample; in addition, it means that the beam impurity level is very low. The atomic or molecular beams are generated by Knudsen effusion cells (K-Cell). These are evaporation sources with an accurately controlled temperature region inside the cell, from which the beam exits through a very small aperture towards the substrate. The aperture is so small that the vapour pressure inside the cell is maintained at its equilibrium value, so that the small escape rate due to effusion is determined solely by the temperature. The MBE system often contains a variety of analytical tools. RHEED is the most common and it is used both to monitor the crystallographic order of the substrate and the deposit as fabrication proceeds, and to determine the deposit thickness by exploiting the RHEED specular beam intensity oscillations.

2.2. The MBE Chamber.

The SSMBE growth takes place in a UHV stainless steel chamber, ion pumped, with a normal operating base pressure of ~5 $x10^{-10}$ mbar after bake-out, or ~$2x10^{-9}$ unbaked. The four main parts of the machine are: the fast entry load lock, the preparation chamber, the growth chamber and an atomic hydrogen cleaning chamber (figure 2.1). All the parts are individually pumped by either an ion-getter or a turbomolecular pump. A titanium sublimation pump and two liquid nitrogen cooled cryopanels are additionally used to pump the growth chamber. The samples are introduced to the chamber through the load lock and transported on a trolley and pulley system through the preparation chamber and then into the growth chamber.

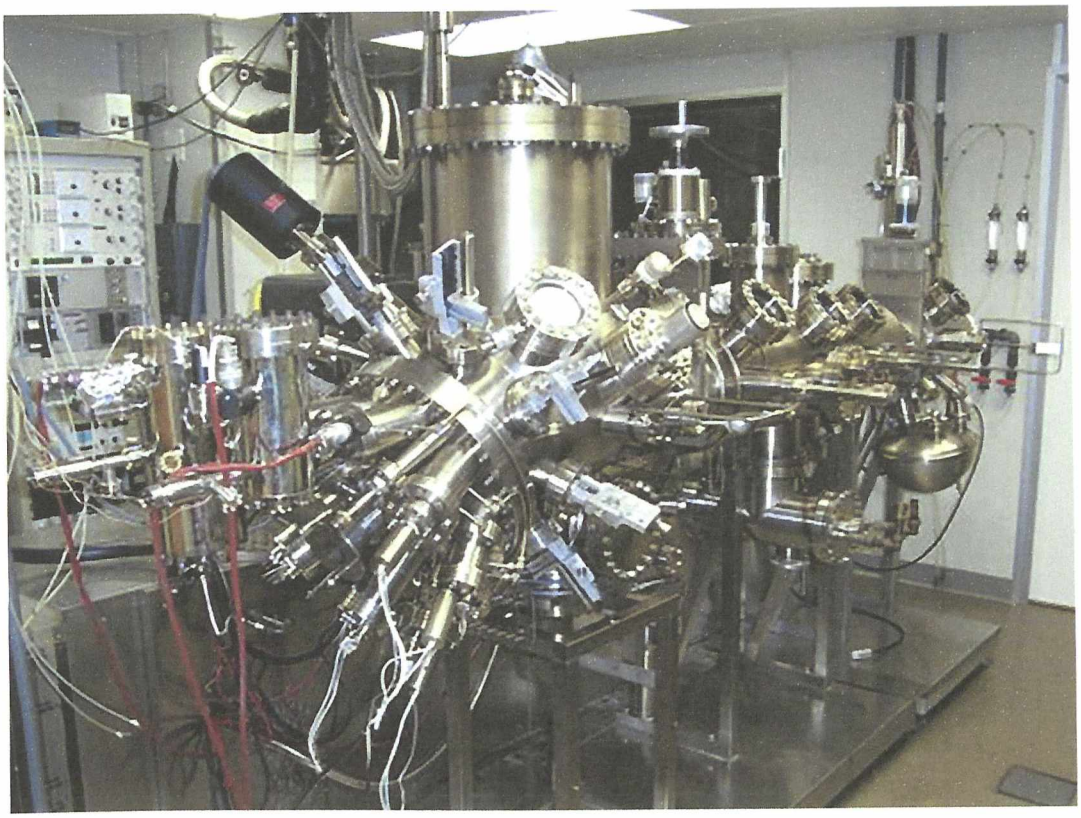


Figure 2.1: V80H MBE machine.

2.2.1. Fast entry Load Lock.

The fast entry load lock is connected to the preparation chamber and ensures rapid exchange of samples, without the danger of breaking UHV (Figure 2.2). The pressure in the load lock is normally held at ~10^{-8} mbar by a turbomolecular pump (TMP), backed by a rotary pump. The introduction and removal of up to 10 samples is possible from the load lock and in order to exchange samples, the TMP is valved off and dry N_2 is introduced to bring the load lock to atmospheric pressure.

The procedure for pumping the load lock from atmosphere involves a series of steps. Firstly the pressure is reduced to ~40 mbar with a venturi pump. The pressure is further reduced to ~10^{-3} mbar by the adsorption pumps.

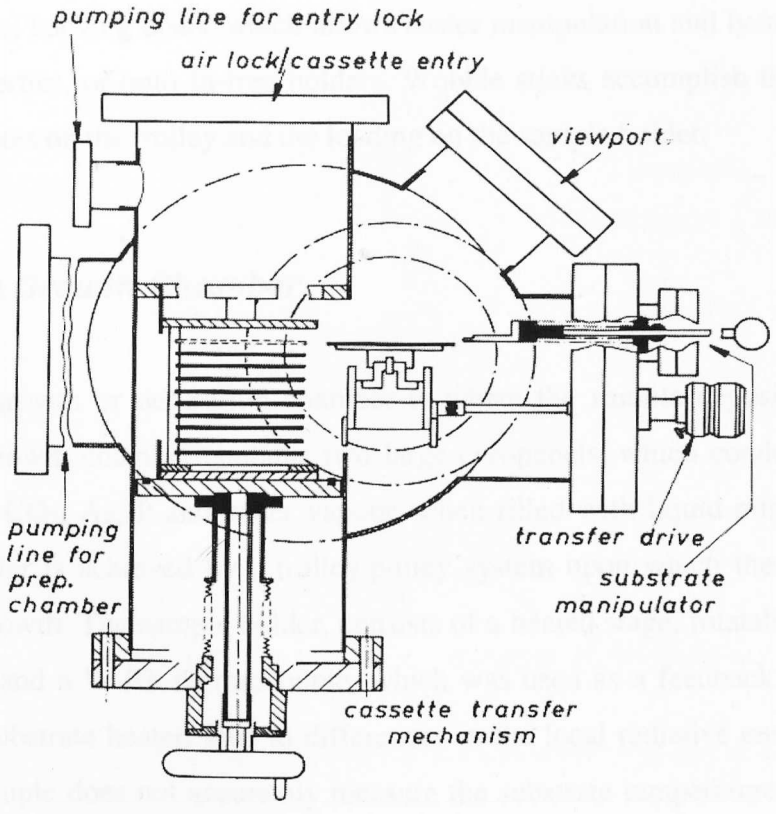


Figure 2.2: Fast entry load-lock. Trolley and pulley system also shown. Taken from Oxford Instruments Plasma Technology.

2.2.2. Preparation Chamber.

The preparation chamber acts as a buffer between the load lock and the growth chamber; it is used also for outgassing and storing the clean samples prior transfer to the growth chamber. Up to 10 separately mounted samples can be stored undamaged. The base pressure of the preparation chamber is sustained at $\sim 5 \times 10^{-10}$ mbar (or less) with an ion-getter pump.

2.2.3. Sample Manipulation.

The substrate manipulation is done with a trolley-pulley system (figure 2.2), which enables substrates to be transferred from the preparation chamber to the growth chamber and *vice-versa*. Semiconductor substrates are brittle and need careful handling and support during loading and growth. They are either In-bonded

onto Mo metal backing disks, which allows easier manipulation and better thermal heating properties, or onto In-free holders. Wobble sticks accomplish the transfer of the substrates on the trolley and the loading on the sample holder.

2.2.4. The Growth Chamber.

The growth or deposition chamber is where the sample deposition takes place. The growth chamber contains two large cryopanels, which condense gases such as CO, CO_2, As, P and water vapour, when filled with liquid nitrogen. The sample transfer is achieved by a trolley-pulley system upon which the sample is placed for growth. The sample holder, consists of a heated stage, rotatable through 360 degrees and a W-Rh thermocouple, which was used as a feedback system to control the substrate heater. Due to differences in the local radiative environment, the thermocouple does not accurately measure the substrate temperature, therefore an IR (or optical) pyrometer is always used in order to accurately define the substrate temperature. The rotation speed of the sample holder is between 5-60 rpm. There is also a tilting mechanism, which enables the substrate to be positioned normal to the K-cells –the standard growth position. The background pressure is monitored by Quadrapole Mass Spectrometer (QMS) and the sample surfaces are examined by RHEED. The latter is discussed in a greater detail in section 2.3.1. The QMS is used for leak detection, monitoring residuals gases and detecting any materials desorbing from the samples when they are being heated.

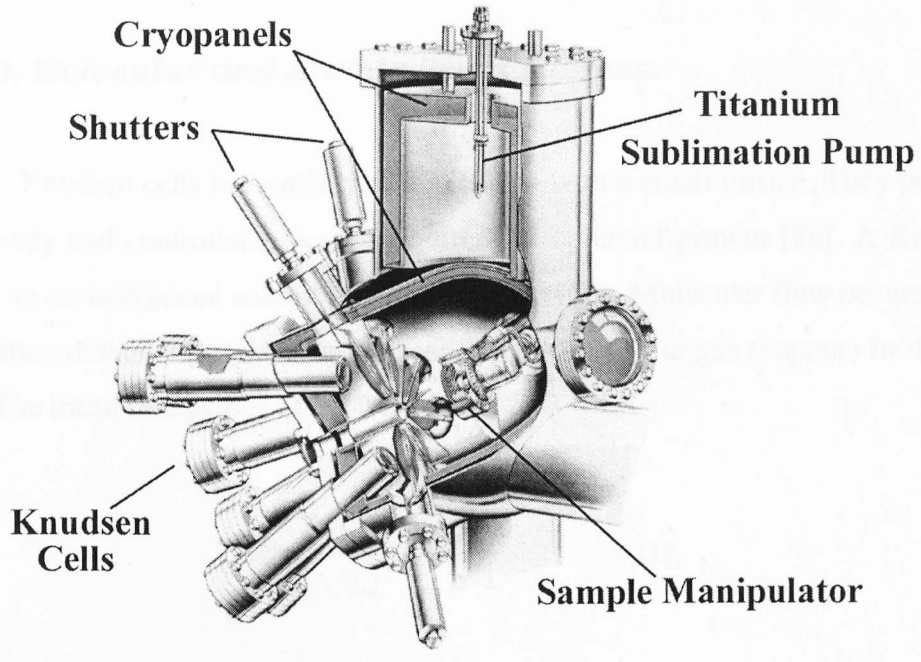


Figure 2.3: Schematic representation of the V80 deposition chamber. (Courtesy of VG Semicon)

2.2.5. Baking Procedure.

In order to reload sources and to carry out essential maintenance, the system is brought to air. The optimum vacuum for growth ($<10^{-10}$mbar) is not easily acquired after the machine has been exposed to air for sometime since residual gases and water vapour are present inside the apparatus. In order remove these contaminants the system is baked. This procedure involves a series of steps. First, the system is pumped down to 10^{-8}mbar for leak checking and initial testing. Then the system is baked to ~50°C and temperature is increased, being careful the pressure does not rise dramatically due to desorption of gases, up to a maximum value of 160°C and at a pressure in the 10^{-8}mbar range. During the bake out process, the cells are always kept 30-50° higher than the system temperature to ensure that all the impurities desorb from the source materials and keep the sources free from impurities. After the bake-out has finished, and when the machine is still warm, all the essential components of the MBE system (cells, heaters, ion gauges) are thoroughly outgassed up to 300°C to make sure all residual gases are removed.

2.2.6. Molecular and Atomic Beam sources.

Knudsen cells are isothermal enclosures with a small orifice. They produce the steady and controllable beams required for epitaxial growth [98]. A Knudsen cell is an an-isothermal enclosure with a small orifice. Molecular flow occurs when the orifice diameter is less than the mean free path of the gas (vapour) in the cell [98]. The mean free path is given by:

$$\lambda = \left(\frac{1}{\sqrt{2d^2}}\right)\left(\frac{kT}{p}\right) \qquad (1)$$

where d is the molecular diameter, p is the pressure and k is the Boltzmann's constant.
In SI units:

$$\lambda = 3.11x10^{-24}\frac{T}{pd^2} \qquad (2)$$

The flux from the cell is given by:

$$J = \frac{pA}{\sqrt{2\pi mkT}} \qquad (3)$$

where p is the pressure in the cell, A is the area or orifice, m is the molecular weight and k is Boltzmann's constant.

A typical cell (group III) construction used for the III-V compounds is shown in figure 2.4. It consists of a hollow cylindrical heater arrangement, usually formed from a Ta wire or foil supported on ceramic insulators. These are surrounded by a Ta radiation shield on the outside and a Ta liner on the inside and the ends are sealed by Ta rings. The material to be evaporated is placed in a cylindrical Pyrolitic Boron Nitride (PBN) crucible, which is the placed in the heated tube. The temperature of the cell is monitored by a W-Rh thermocouple,

mounted directly beneath the crucible. This provides a reproducible measurement for the actual cell temperature, although for precise growth, the cell flux can be accurately represented by the growth of calibration samples at various temperatures.

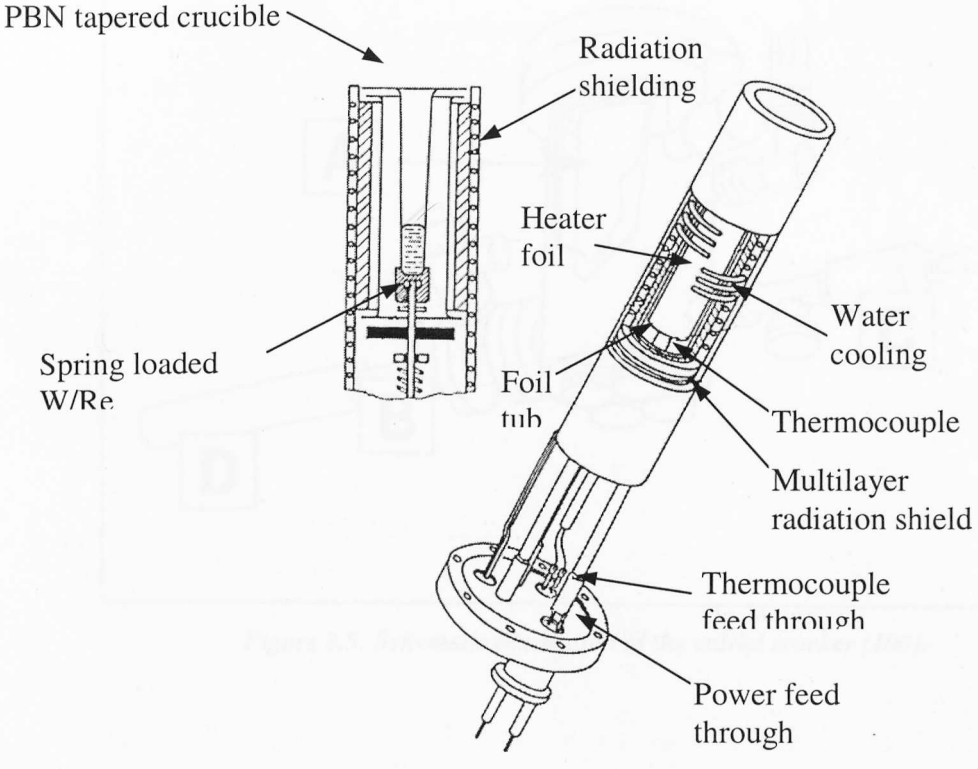


Figure 2.4: Schematic of a Knudsen Cell [99].

The source materials used in our research are arsenic, aluminium, gallium, and indium. All source materials are solid at room temperature. However, Ga has to be kept above 60°C and Al above 700°C once it has been melted. The Al and Ga are kept in a molten state because as they cool to room temperature they may crack the crucible due to expansion (Ga) or contraction (Al).

Arsenic is obtained from valved cracked sources. A schematic of the As valved cracking effusion cell is shown in figure 2.5. Arsenic is loaded into the large capacity (1kg) crucible (A) and heated. A needle valve in the conductance tube (B) regulates the amount of evaporation of As which enters the growth chamber. The valve position is controlled with either a manual micrometer (C) or with an

automated valve positioner. The cracking zone (D) temperature is controlled so as to produce beams of cracked (As_2) or uncracked material (As_4). When the valve closes the evaporant is prevented from entering the growth chamber (*i.e.* giving precise flux control), unlike closing the shutter, which only diverts the beam.

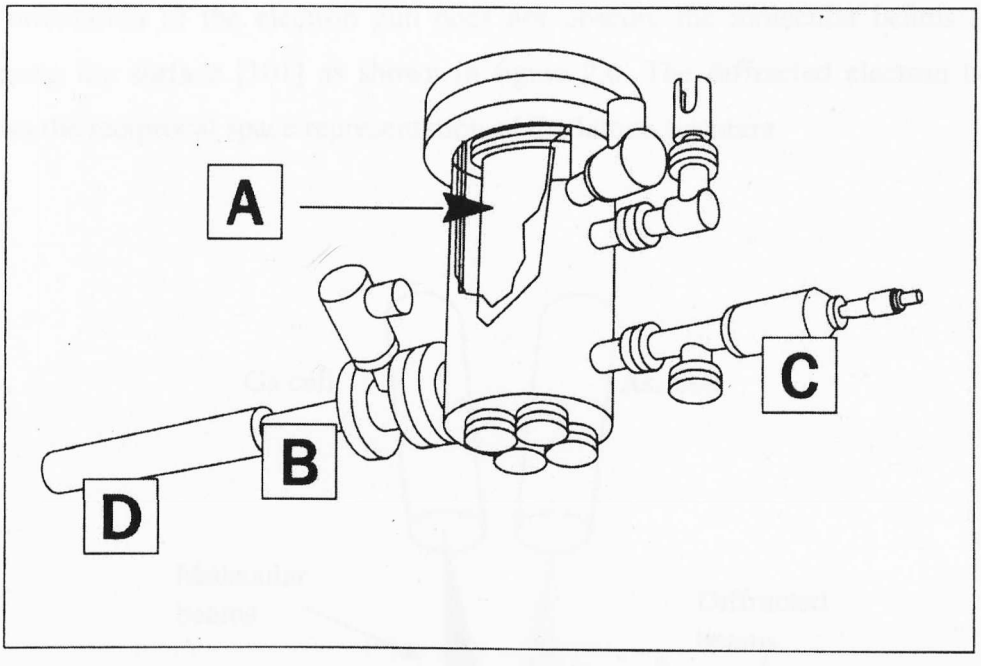


Figure 2.5: Schematic illustration of the valved cracker [100].

2.3. In-Situ Monitoring Techniques

The V80 is also equipped with a quadruple mass spectrometer to measure the impurities in the background and to identify any possible leaks in the chamber, an Auger Electron Spectroscopy analyser and RHEED.

2.3.1. Reflection High Energy Electron Diffraction (RHEED).

A RHEED system is used for calibrating the cell fluxes, monitoring growth rates and for surface structure determination. Since all the growth process take place at the surface of the substrate, it is very important to understand the structure of the surface in order to understand the factors (kinetic, dynamic) that affect growth. Generally, semiconductor surfaces either relax by bond rotation or

reconstruction [98]. Surface crystal structure can be monitored by electron diffraction techniques. The most appropriate technique is RHEED because the electron beam is at grazing angle of incidence whereas the molecular beams are almost normal to the surface. This means that the orientation of the RHEED experiment is such that monitoring is allowed to take place whilst growing because the orientation of the electron gun does not obscure the molecular beams from reaching the surface [101] as shown in figure 2.6. The diffracted electron beam shows the reciprocal space representation of the lattice structure.

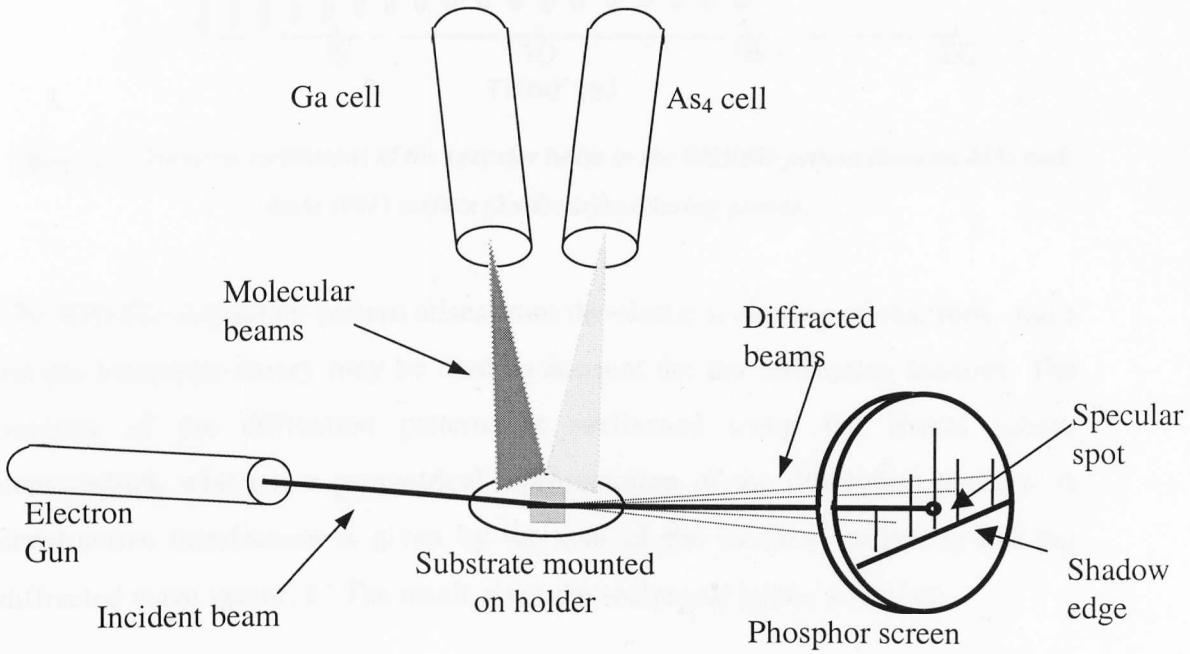


Figure 2.6: An illustration of a typical RHEED experiment

The intensity of RHEED diffracted beams can oscillate as material is deposited upon a flat surface, due to changes in the reflectivity of the surface. [102,103]. These oscillations can only be observed when the depositing material grows in a ML by ML fashion rather than nucleation or small island growth. An example of RHEED oscillations is shown in Figure 2.7.

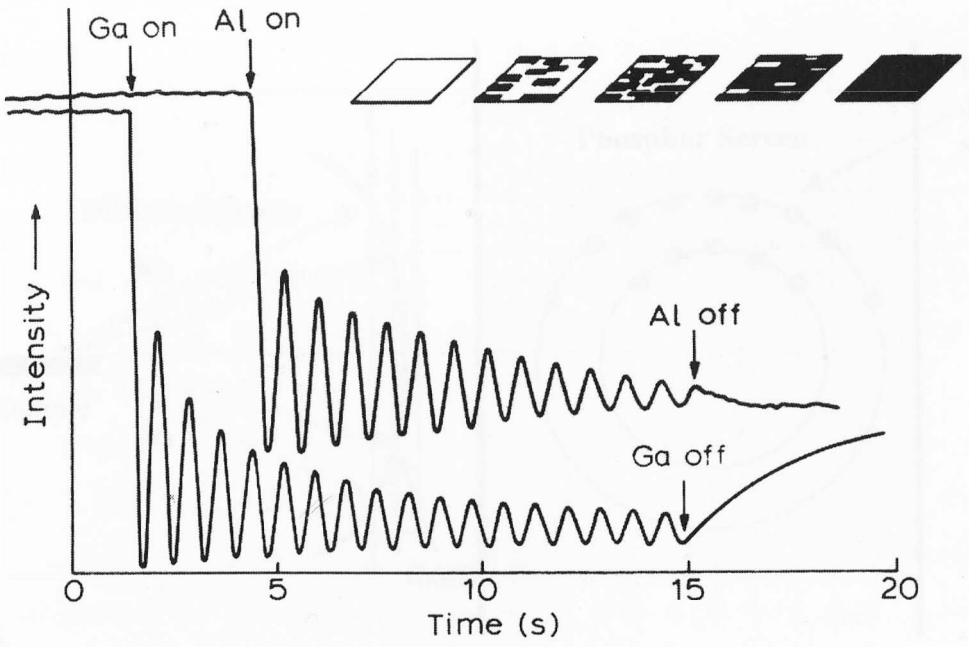


Figure 2.7: Intensity oscillations of the specular beam in the RHEED pattern from an AlAs and GaAs (001) surface (2×4) surface during growth.

The RHEED diffraction pattern arises from the elastic scattering of electrons, and a simple kinematic theory may be used to account for the diffraction features. The analysis of the diffraction patterns is performed using the Ewald sphere construction, which is a geometrical representation of the diffraction process. A constructive interference is given by the sum of the incident vector, k_o and the diffracted wave vector, k'. The result gives the reciprocal lattice vector G:

$$G_{hkl} = k'-k_o \qquad (4)$$

The Ewald sphere of radius of the incident vector k_o is constructed as the incident vector k_o is the radius which passes through the origin of the reciprocal lattice. Any G_{hkl} ending on Ewald sphere will give rise to a diffracted beam meaning that if a point on the reciprocal space lies within the surface of the Ewald sphere, Bragg's law will be satisfied and diffraction will occur [101,104]. The Ewald sphere is very large compared to the spacing of the reciprocal net rods and cuts those rods at grazing angles. This leads to streaking of the diffraction spots perpendicular to the surface [101] (Figure 2.8).

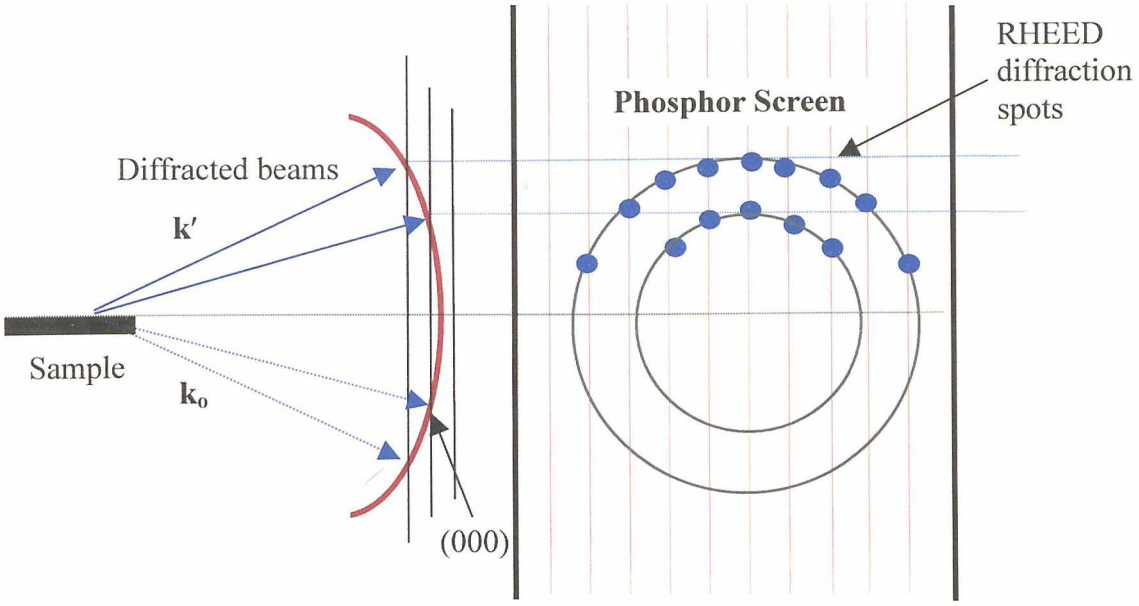


Figure 2.8: Interaction of RHEED beam and infinitely long reciprocal space rods to create RHEED pattern.

2.4. Sample Cleaning Techniques.

To achieve high quality growth on patterned substrates, the sample surfaces need to be extremely clean, therefore surface contaminants, which can cause poor quality growth and defects on the samples, must be kept to a minimum. This is more difficult, when the substrates are chemically processed, such as the ones used here.

When the samples undergo wet chemical etching and processing the level of possible surface contaminants is significantly higher and the risk of poor quality growth is greater. Therefore, a lot of care has been taken with the samples to keep surface contamination to the lowest acceptable levels. After etching, samples were thoroughly cleaned with a variety of solvents and in addition two other cleaning techniques are used *prior* to growth to obtain high quality surfaces. These are *ex-situ* Oxygen Plasma Ashing and *in-situ* Atomic Hydrogen (AH) cleaning. Both were found to improve post-growth sample morphology in our experiments.

2.4.1. Oxygen Plasma Ashing.

Directly before the patterned samples were introduced to the MBE chamber for growth, the samples are oxygen plasma ashed in a Cambridge Fluid Systems MR200-3 Multi-mode Resonant Cavity Reactor. It is fitted with a stainless steel Faraday cage and Quartz reactor into which the sample was placed on top of a 3-inch doped-Si wafer. The samples were oxygen ashed on high power for 45s at a gas flow rate of 2500 cc/min.

Oxygen and microwaves generate an active plasma, which reacts with carbon to form CO, CO_2 etc. Figure 2.9, shows two grown samples, grown simultaneously and mounted side-by-side on the same platen. The two sections both originate from the same patterned wafer. The right hand side Nomarski Micrograph Differential Interference Contrast image is from the sample that was oxygen ashed prior to deposition and the left hand side image is an untreated sample.

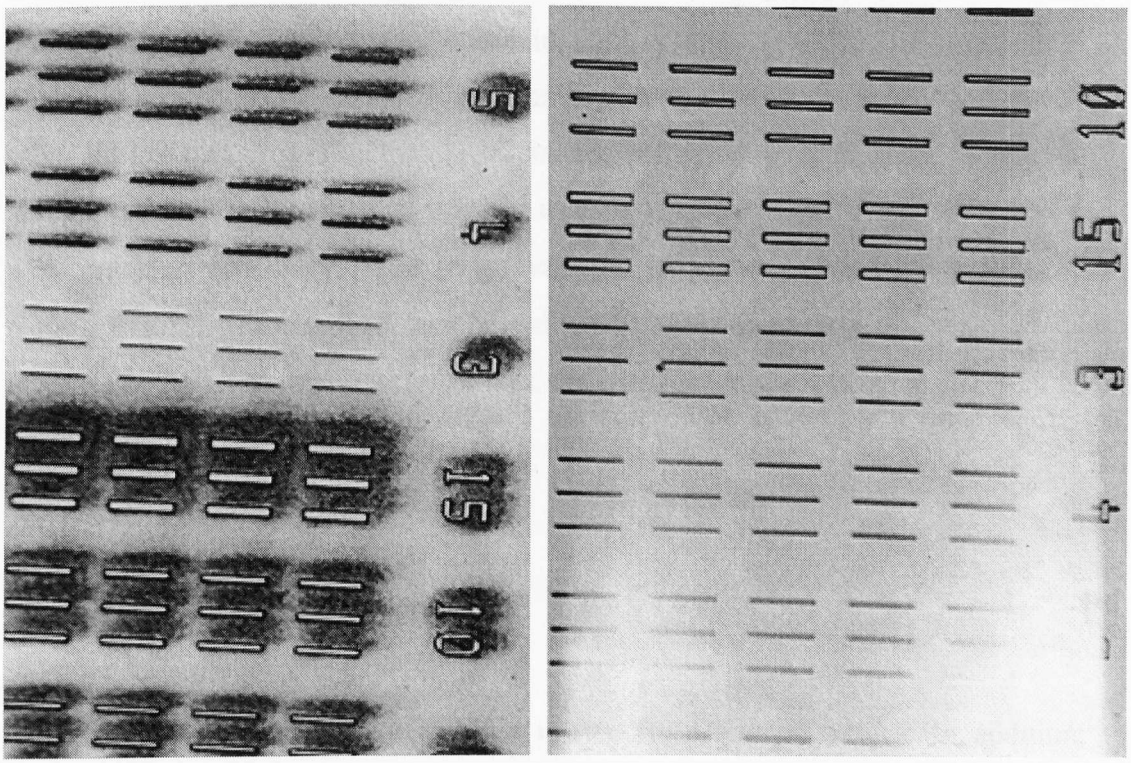


Figure 2.9: Normaski optical micrographs of the difference in growth quality by oxygen ashing. LHS image is a non-oxygen ashed section of the sample, and the one on the RHS is the oxygen ashed section of the same sample. The images are at 1000×magnification.

2.4.2. Atomic Hydrogen Cleaning (AH)

In-situ Atomic Hydrogen Cleaning (AH) is used as a final cleaning treatment prior to growth.

Figure 2.10 shows a schematic representation of the Applied EPI atomic hydrogen source. The tungsten filament in the source operates at ~2100°C to thermally crack the H_2 into ~7% atomic species.

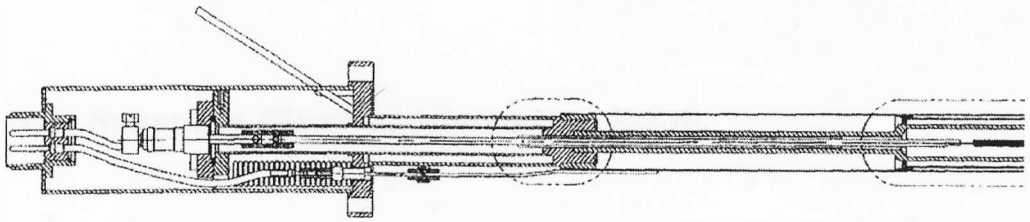


Figure 2.10: Schematic Representation of the Applied EPI atomic hydrogen source.(Applied Epi)

It utilizes an atomic hydrogen beam which hits the surface, reacts with the contaminants and leaves the substrate in H_2O or CH– groups. The substrate is heated to around 400°C and with H_2 chamber pressure between $5x10^{-5}$ and $8x10^{-5}$ mbar during cleaning. The sample is cleaned for about ½ h in order to remove surface oxide. The hydrogen is cracked using a tungsten filament at 2100°C with ~7% cracking efficiency. Prior to growth, this gives an ordered (2×4) RHEED pattern at 30°C. The sample is then heated to 620°C for inspection.

For AH cleaning GaAs substrates, the reactions taking place are [105]:

$$As_2O_x + 2xH^* \rightarrow xH_2O\uparrow + As_2\uparrow \quad \text{for As oxides}$$

$$\left.\begin{aligned} Ga_2O_3 + 4H^* &\rightarrow 2H_2O\uparrow + Ga_2O\uparrow \\ Ga_2O_3 + 4H^* &\rightarrow H_2O\uparrow + 2GaOH\uparrow \end{aligned}\right\} \quad \text{for Ga oxides}$$

These reactions lead to a surface that is free from surface oxides. In addition, surface damage due to cleaning is minimised, and is significantly reduced compared to thermal cleaning.

2.5. Post-Growth Surface Analysis.

The two main techniques used during these investigations were Scanning Atomic Force Microscopy (AFM), where most quantitative information were obtained, and Electron Microscopy (SEM). These two sample assessment techniques are some of the few *ex-situ* techniques that could relate the surface morphology to the conditions used and accurately determine the quality of the surfaces.

2.5.1. Scanning Electron Microscopy (SEM).

The first commercial SEM was made by Cambridge Scientific Instruments in 1965 [106]. SEM is carried out by rastering a narrow electron beam over the sample surface and detecting the yield of either secondary or backscattered electrons as a function of the position of the primary beam [107]. Image contrast is affected by the sample orientation, composition and material type (e.g. Au on C). For a single material sample, the parts of the sample facing the detector generally appear brighter than those with surfaces pointing in other directions. The basic components of SEM are an electron gun, a lens system and an electron detector. An electron gun (filament) produces electrons (generally by thermionic emission) and accelerates them by a large electric field to energies between 0.3 keV and 30 keV. The beam of the electrons is de-magnified by 2 or 3 condenser lenses until it reaches the specimen, with a diameter of 2-10 nm (usually depending on the acceleration potential, filament type and gun type), figure 2.11 [108]. The beam is then scanned across the specimen while a detector counts the number of electrons emitted from each point. At the same time the spot of a cathode ray tube (CRT) is scanned across the screen, while its brightness is modified by the amplified current from the detector. The electron beam and CRT spot are scanned in an analogous manner to a TV receiver.

In SEM, the image is formed from electrons emitted from the surface of the specimen. The principal types of electrons used in image formation in the SEM are secondary and backscattered electrons. Secondary electrons have a low energy (~5–50eV) and originate from the surface region of the sample. Backscattered

electrons come from deeper and carry information on the composition of the sample (heavy elements are more efficient scatterers and can appear brighter in the image).

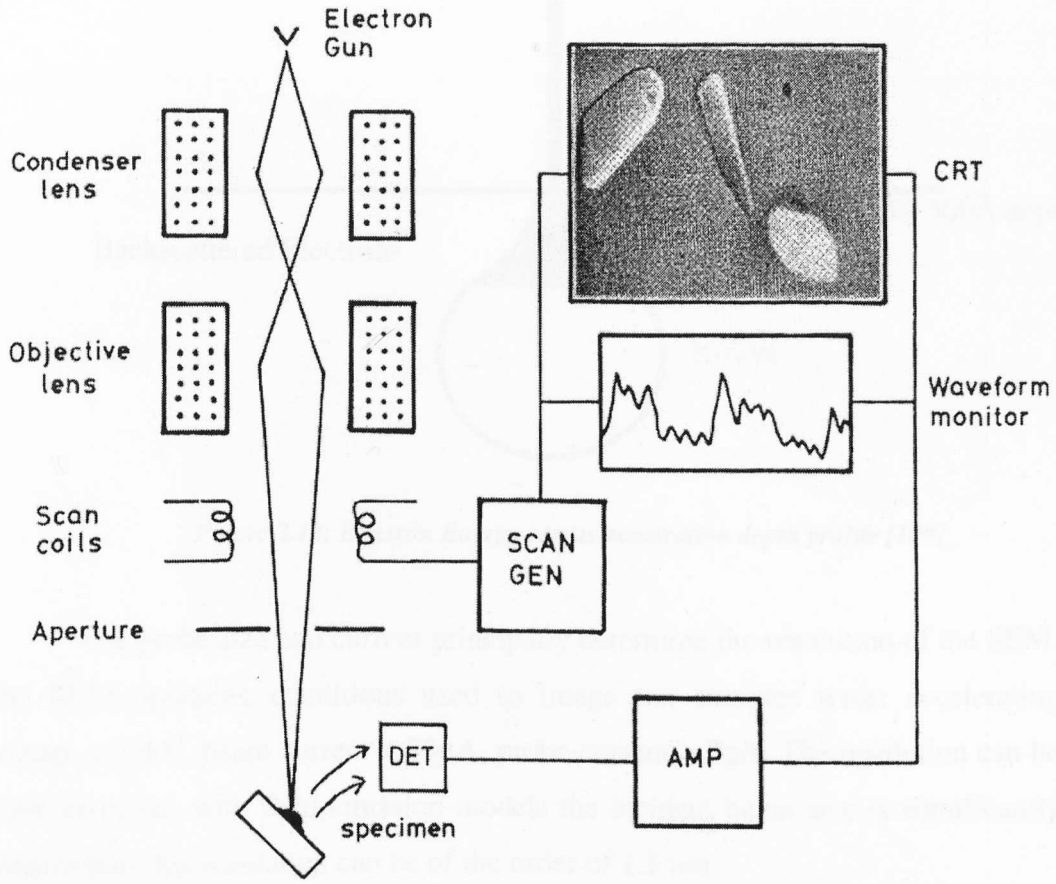


Figure 2.11: Schematic of the main SEM components [108]

The majority of electrons are brought to a stop in the specimen, but a few are backscattered and leave. The volume within which approximately 95% of the electrons are brought to a halt is termed an interaction volume, figure 2.12. The electrons that escape from the specimen surface with energies less than 500V are the secondary electrons. Principally, these are the electrons to which energy has been transferred within a short distance of the surface. They are abundant and the most commonly used signal in SEM.

When the electrons with energy of several kV strike a solid specimen, X–rays characteristic of the atoms in the specimen are produced. Such X-ray emission forms the basis of elemental analysis systems. The impinging electron interacts with an atom in the specimen to eject a core level electron. The atom then

relaxes by movement of an outer shell electron to the vacant core level with concomitant emission of an X-ray.

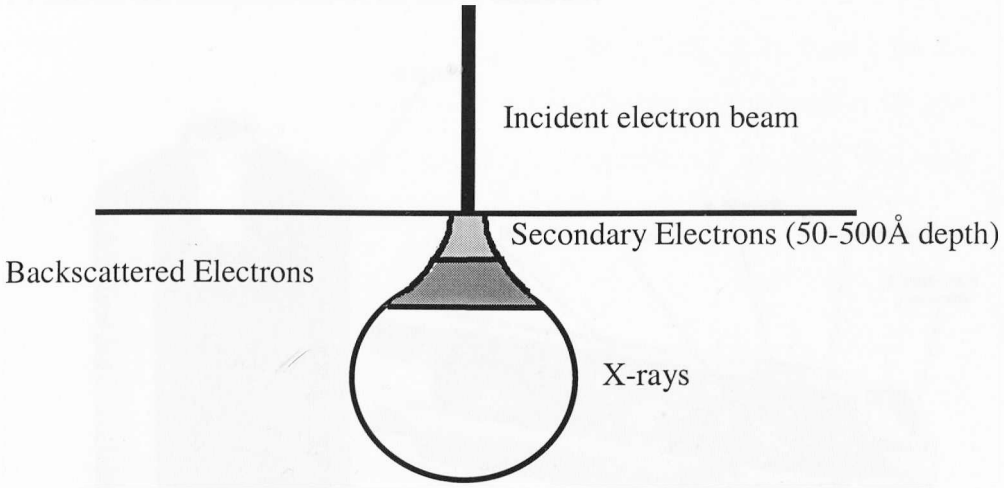


Figure 2.12: Electron Energy versus penetration depth profile [109]

The probe size and current principally determine the resolution of the SEM. The SEM operating conditions used to image our samples were: accelerating voltage = 25kV, beam current = 80μA, probe current = 7pA. The resolution can be 5 nm or better, with field emission models the incident beam size is significantly smaller thus this resolution can be of the order of 1.5 nm.

The filaments most commonly used are made of tungsten, which is bent into a hairpin and resistively heated to thermionically emit electrons. The next generation of filament is made from Lanthanum Hexaboride (LaB_6) which produces increased brightness in the images. The SEM used in these studies has a lanthanum hexaboride (LaB_6) filament which gives better brightness, more stability and improved resolution (~3.5 nm at 30kV).

The energy of the X-ray is characteristic of the core shells of the atom (figure 2.12). Measurement of the energy of emitted X-rays thus enables the atoms present in a sample to be identified (Energy Dispersive X-ray Analysis, EDX).

EDX was also used in some cases where extra clarification was needed. In this technique X-ray photons are produced at the specimen surface as a result of recombination of electrons during primary beam irradiation. The X-ray photons emitted are characteristic, in both wavelength and energy, of the elements present in the irradiated area. EDX provides fast and quantitative elemental analysis of the

specimen under examination. This may also be used to show the special distribution of detected elements by employing a mode known as X-ray Mapping, where the presence of an element at a location is shown by dots within the map. Figure 2.13 shows the components of an EDX detector.

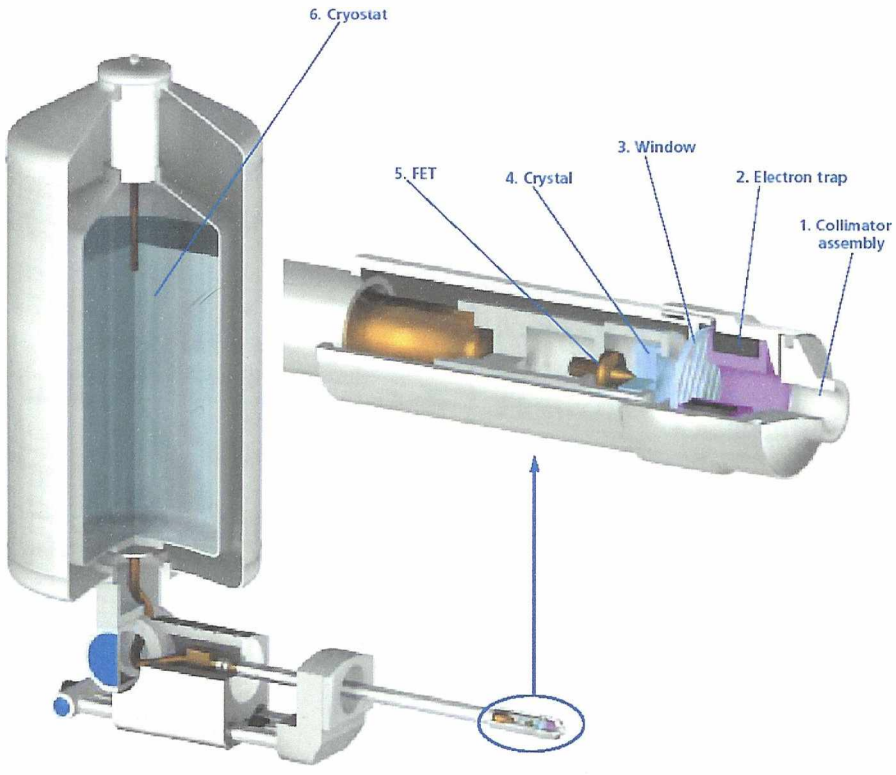


Figure 2.13: Cut-away diagram showing the construction of a typical EDX detector (Courtesy of Oxford Instruments)

The detector comprises of five components: (i) the collimator assembly which provides a limiting aperture through which X-rays must pass to reach the detector, (ii) the electron trap which is a pair of permanent magnets that strongly deflect any passing electrons in order to avoid background artefacts. (iii) The window, which provides a barrier to maintain vacuum within the detector whilst being as transparent as possible to low energy X-rays. (iv) A crystal, which is a semiconductor device that through the process of ionisation converts an X-ray of particular energy into electric charge of proportional size. (v) A Field Emitting Transistor (FET) which is positioned just behind the detecting crystal. This is the first stage of the charge liberated in the crystal by an incident X-ray that then gets converted into a voltage output.

2.5.2. Atomic Force Microscopy (AFM).

AFM was invented by Binnig *et al.*, in 1986 [110]. It is based on the principle of detecting forces between a sharp tip and atoms in the surface (Figure 2.14). The Atomic Force Microscope (AFM) is capable of imaging the local surface topography with atomic resolution under UHV only.

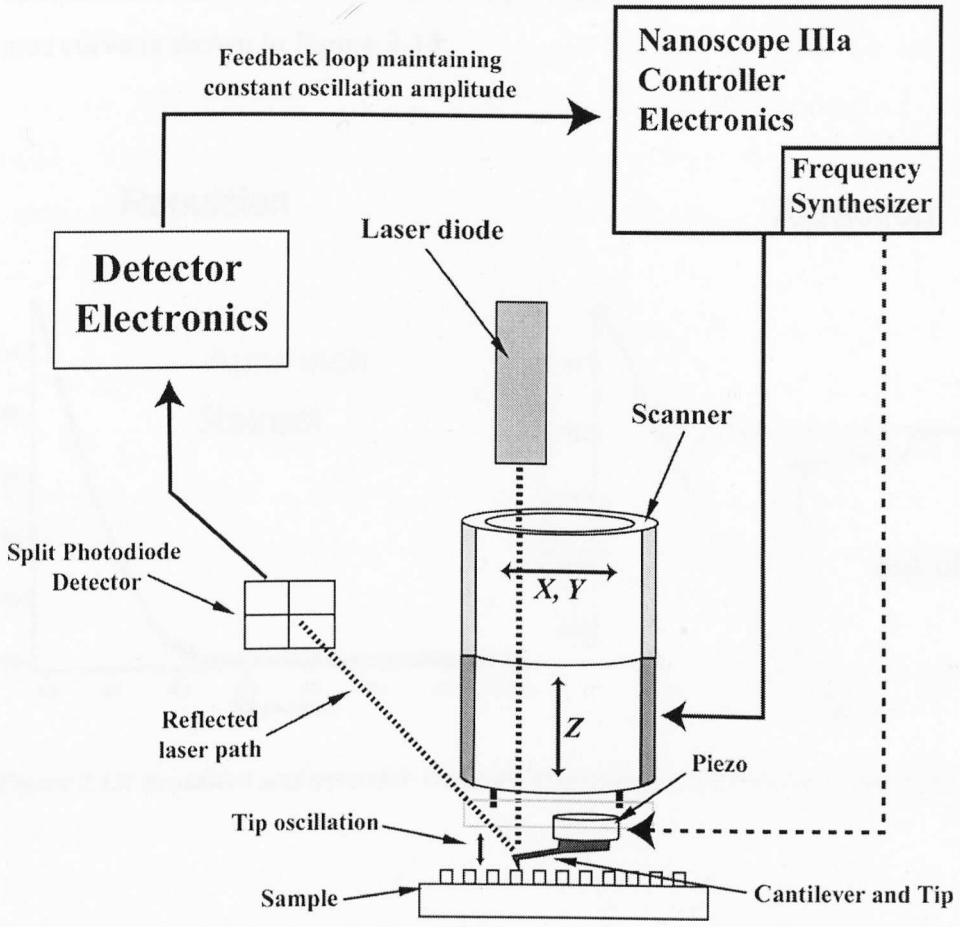


Figure 2.14: Experimental set up of an AFM in tapping mode [111].

All the atomic force microscopes have 5 essential components: A sharp tip mounted on a soft cantilever spring, a mechanism for detecting the cantilever's deflection. A feedback system to monitor and control the deflection (and hence the interaction force). A mechanical scanning system (usually piezoelectric) that moves the sample with respect to the tip (or vice-versa) in a raster pattern. A

display system that converts the measured data into an image. The scanning, feedback and display systems are very similar to those used for STM. The background theory involves the inter-atomic force between point-like objects or atoms which can be described by the Lennard-Jones potential [112]:

$$U(r) = 4\varepsilon\left[\left(\frac{r_0}{r}\right)^{12} - \left(\frac{r_0}{r}\right)^{6}\right] \qquad (5)$$

Where ε is the depth of the potential well, r is inter-atomic distance between atoms, and r_o is the distance between atoms in equilibrium, respectively. A typical force distance curve is shown in Figure 2.15.

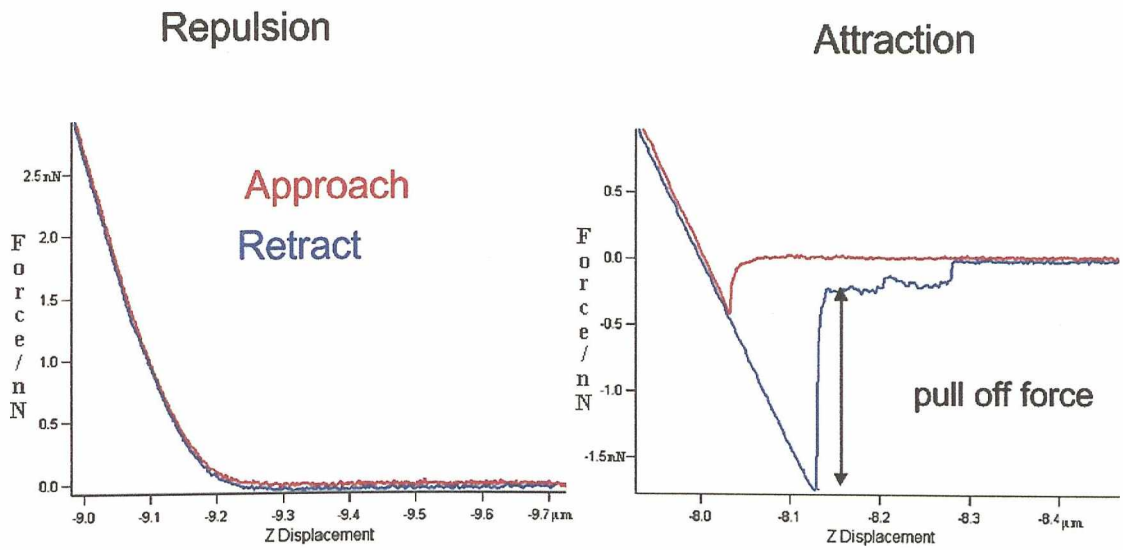


Figure 2.15: Repulsion and attraction Force-Distance Curves taken from N. Elsner [113]

The modes of operation of an AFM fall under two general categories:

Contact mode – it is the most commonly used mode of the AFM operation, where the tip is within a few Å of the surface. In this mode, the AFM stylus is in constant contact with the sample surface and deflects in response to topographical features. Contact mode has much better resolution than non-contact mode and it is easier to measure changes of the repulsive than of an attractive force. Most disadvantages result from the capillary forces present between tip and

sample, due to liquid contamination. This can be avoided with correct AFM set-up (*i.e.* higher spring constant–stiffer tip). Other attractive forces can also contribute to large frictional forces between the tip and the sample. Frictional forces are typically much more destructive to the stylus and sample than normal forces and can create false images. This can be reduced by operating under liquid-but this is not suitable for all samples.

The probe–sample interaction can be measured in static (dc) or dynamic (ac) modes. Under the static mode category, there are two sub-categories: the constant force and the constant height. In the constant force mode, the cantilever deflection is held constant while recording the height of the sample relative to the tip. A feedback loop is used to maintain a small constant force on the sample. In the constant height mode, the height of the sample is kept constant and the variations of the lever deflection are recorded. As a result of the development of very sensitive methods for detection of cantilever deflection, the latter is the most common method.

The dynamic modes include the "tapping mode™" that relies on direct contact forces. The probe oscillates at relative large amplitudes–typically 10-100 nm –so that it lightly taps on the surface at the bottom of each oscillation cycle. The vibration amplitude is much greater than the thickness of contamination layers so the cantilever has sufficient energy to prevent it becoming trapped in the fluid layer. Furthermore, because the tip is only briefly in contact with the sample, frictional damage and directions are minimised.

Non-contact mode. In the non-contact mode, the sample- tip separations is 10 to 100 nm. Forces such as van der Waals, electrostatic, magnetic or capillary forces can be sensed and give information about surface topography, distributions of changes magnetic domain wall structure or liquid film distribution. However, these forces are typically 2-4 orders of magnitude smaller than in the contact mode. The cantilever is typically oscillated at a very small amplitude of around 1 nm. This technique, however, has a lot of limitations, due to the extremely short range of van der Waals force and from capillary forces.

Cantilevers and Tips

Cantilevers play a critical role in force microscopy and have to be made reproducibly for consistent measurements. The ideal sample-tip interaction is shown in figure 2.16.

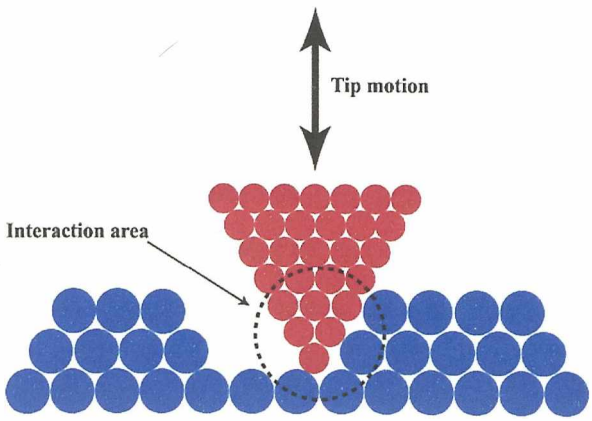


Figure 2.16: An ideal sample-tip interaction in AFM measurements.

However, it is extremely difficult to obtain such consistency. The samples analysed for these studies have patterned sidewalls or features of near 90° or 73° angles. For the AFM to scan such angles accurately the tip profile is of extreme importance. The use of conventional AFM tips gave a false angular measurement of the stripes sidewalls, since the tips were short and wide and their shape was convoluted the images obtained. This kind of result is shown on figure 2.17. Using High Aspect Ratio (HAR) tips solved this problem, making it possible to achieve far less tip convoluted images due to the sharper and longer profile of the tip used. The ones used for the experiments are sharp high aspect ratio tips made out of a single silicon crystal, which results in a high lateral stiffness and rigidity [111].

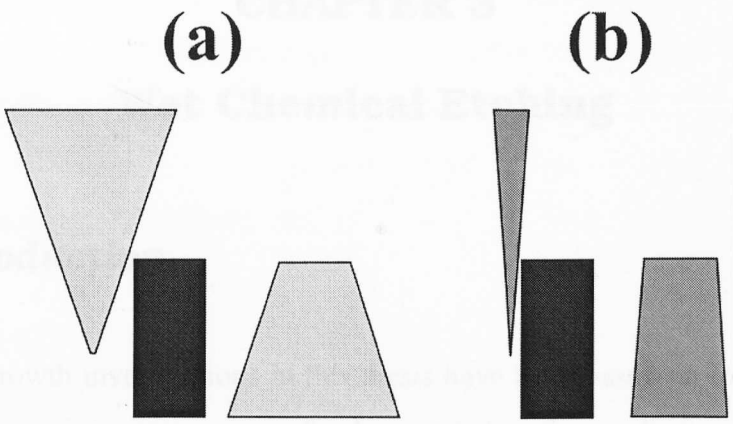


Figure 2.17: shows the measured mesa structure in dark grey with the use of (a) conventional tip and (b) high aspect ratio tip.

For the InAs QDs chapter, the contact mode was used since the features to be measured were ~5 nm tall and 80 nm wide. Non-HAR tips provided by "Nanosensors" were used which proved to be quite reliable since the contact mode provides increased resolution. However, their measurement proved to be a difficult and strenuous job since the area scanned for the QDs was on top of the ~90° angled mesa stripes and special care was taken to ensure the correct position of the tip.

CHAPTER 3

Wet Chemical Etching

3.1. Introduction.

The growth investigations in this thesis have been based on mesa stripes as opposed to mesa squares, since fundamental kinetic studies are simplified. However, the mask used to create these features did include mesa squares if needed to be used for further studies. The mask consisted of squares and stripes in both the <100> and <110> directions. All of the work presented in this thesis is directed towards the study of mesa stripes oriented along the <100> directions and thus allowing access to the {110} planes, as new facets [48].

The stripes were etched to produce {001} planes as the upper sidewall section. Therefore, the mesa top and two adjacent planes had initially the same crystallographic orientation, avoiding dissimilar crystal plane interactions. Consequently, since there are no other planes available on the top of the mesa stripe, all the facets formed after growth resulted from the growth conditions employed and therefore the most favourable facets formed during growth could be investigated.

The sidewalls of the stripes produced from the same etching process in the two orthogonal <110> directions were completely different. Either {111}A or {111}B sidewalls were formed depending on the specific mesa alignment. This suggests that the facets formed on these mesas would be driven by different factors in the two orthogonal directions, a fact that complicates the kinetic processes involved.

Fabricating mesas is a multi-stage process, which involves standard photolithography and two-stage wet chemical etching. The chemical etch was based on a phosphoric acid/hydrogen peroxide/water system followed by resist stripping and solvent cleaning. A Karl Suss model MJB3 mask aligner was used for this work operating at a wavelength of 405 nm. It should be noted that the mask itself had a limited precision. The specification was that the squares and stripes are defined on a 0.03125 μm^2 grid, which had no defects greater than 5 μm. Each step

of the process was monitored using alpha step in order to allow adjustments to refine the size of the patterned substrates. The final etched patterns were assessed using both SEM and AFM to ensure their quality.

3.2. Background Review.

For the fabrication of [110] sidewalls on the <100> etched samples, an investigation was undertaken in order to observe the effect of changing the 90° sidewall angle of the stripes and the squares of the growth of GaAs substrates. The recipe used was previously exploited by Orla McCarthy [114] to produce defined mesas in GaAs substrates. The majority of etches used for GaAs are based on the process of oxidising the surface and the dissolving the oxide. The oxidisers used are usually hydrogen peroxide or halogens ions, but other strong oxidising agents such as $K_2Cr_2O_7$ can also be used. The oxide can be dissolved in either basic or acidic solutions and sometimes organic solvents can also be used, such as methanol. Therefore, there are many possible etching systems that can be employed, some examples of which are listed below.

Some common etch systems used for GaAs:

H_2SO_4: H_2O_2: H_2O
H_3PO_4 :H_2O_2: H_2O
NH_4OH: H_2O_2: H_2O
NaOH: H_2O_2: H_2O
HF: HNO_3: C_2H_5OH
HCl: CH_3COOH: $K_2Cr_2O_7$
Br_2: CH_3OH
KI: I_2: H_2O
$AgNO_3$: CrO_3: H_2O

Several factors must be considered when choosing an etchant. Firstly, the masking material should be compatible with the etchant. Out of those listed above, the acid/peroxide system, sulphuric acid system is one of the most widely used. However, a disadvantage of using that system is that the reactions are strongly exothermic and can cause decomposition of the peroxide during mixing which

makes it difficult to obtain highly reproducible etch rates. The most appealing etching system is the phosphoric acid demonstrated by Mori and Watanabe [115]. This system has a lot of advantages such as that it can be used to obtain a variety of characteristics. The solution has a long lifetime and does not attack photoresist. A summary of the results obtained for the phosphoric acid system using different ratios is shown in Table 3.1.

Further investigation for several etches for a range of sidewall angles which produced some interesting results. Etching along the [01$\bar{1}$] direction on GaAs (001) produced mesa channels [40]. The etchant used was H_2SO_4: H_2O_2: H_2O at a 1:8:40 ratio. The sample was then cleaned and etched again for 45s in H_2SO_4: H_2O_2: H_2O at a 4:1:1 ratio and for 4 min in HCl. The resulting structure had slightly rounded profiles because of the 4:1:1 solution. The structure after growth with GaAs/AlGaAs produced a range of sidewall facets in (411), (111), (811), ($7\bar{1}\,\bar{1}$). Similar work was carried out on V–grooved GaAs (001) substrates [116]. The etchant used was NH_4: H_2O_2: H_2O at 1:1:5 ratio at 2°C. The grooves were etched along the [$\bar{1}$10] direction and (111) A facets appeared due to an anisotropic affect.

A more detailed review on the chemical etching characteristics of (001) GaAs substrates was provided by Adachi *et al.* [117]. They have investigated the different etching solutions on the GaAs (001) substrates patterned along the (110) and ($\bar{1}$10) direction. The solutions used were: H_3PO_4: H_2O_2:H_2O (1:1:1), for 2 min, H_3PO_4: CH_3COOH: H_2O_2 (1:1:1) for 3 min, H_3PO_4: CH_3OH: H_2O_2 (1:1:1) for 2 min, and H_3PO_4: C_2H_5OH: H_2O_2 (1:1:1) for 2 min. For both the [110] and [$\bar{1}$10] directions the H_3PO_4 system exhibited clear crystal habits. For the [001] the SEM analysis indicated reverse-mesa and ordinary mesa shape structures, with sidewalls angles of 115° and 55° respectively from the (110) planes. However, in the [$\bar{1}$10] direction the structures only ordinary mesas were observed forming at 55° from the (110) planes. In total the H_3PO_4 system provided high quality etched surfaces with well-defined profiles and shinny flat bottoms [118].

Etch	Region	H_3PO_4:H_2O_2:H_2O	Etch Rate	Edge Profile			Comments
		(volume ratios)	(μm/min)	parallel	perp.	45°	Trenching, surface quality etc.
A	b	8:1:1	1.0	75° 60°	54°	88° 45°	Shiny surface, slightly milky in dark field. Viscous solution needs agitation, bubble effect seen in corners. Deep trenches formed. Nonlinear etch rate.
B	b/a	8:1:8	1.1	82° 54°	50°	45°	Very milky in bright field. V. rough surface, large scale roughness. Viscous solution needs agitation.
C	a	1:1:8	0.5	45°	40°	30°	Good surface quality, with smooth edge walls. Flat bottomed holes obtained. Significant mask undercut ratio, possibly greater than 1. Cannot obtain vertical sidewalls.
D	d	1:8:80	0.25	not examined	54°		Very bad surface quality (one sample appeared black after etching).
E	d	1:8:40	0.52	78° 55°	54°		Brownish tinge in bright field, milky in dark field. Flat bottomed holes obtained. Undercut ratio ~ 0.9. Repeatable etch rate.
F	d	1:8:20	0.75	63° 50°	54°		Milky in bright and dark field. V. rough sidewalls and jagged edges. Vertical walls.
G	c/d	1:8:8	1.9	not examined	54°		OK surface quality. Trenching and corner effects. V. rough sidewalls.
H	c/d	1:25:24	0.95	65° 54°	54°		V. rough surface, milky. Strong trenching. Less mask undercut than other samples (0.7).
I	c	1:40:8	0.82	58° 55°	54°		Shiny appearance. V. Strong trenching effects.

Table 3.1 : Summary of GaAs etches and results [114].

3.3. Present Work.

The substrates used were "*epi-ready*" SI double polished GaAs (001) ±0.1° manufactured by American Xtal Technology (AXT). All of the work done in this thesis has been achieved with SI double polished wafers, but further research showed that the etching system worked equally well for the n^+ or p^- type doped wafers. The mask used for the photolithography is shown in figure 3.1, and it is divided in four identical quarters.

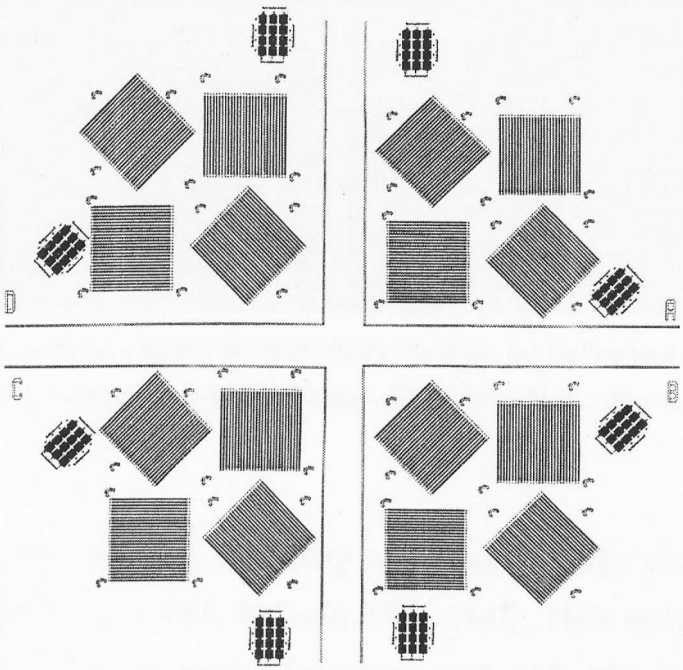


Figure 3.1: Mask used on the GaAs (001) substrates

Three of the quarters were used for growth experiments and one was kept as a reference sample. The reference sample was used to provide information regarding the cleanliness and the quality of the etching prior to growth, when examined by either SEM or AFM. Each quarter consists of squares and stripes of various sizes (5–15 μm,) and positioned on the <110> direction parallel to the major flat, and <100> direction at 45° to the major and minor flat.

In order to obtain two types of initial mesa sidewalls for the two main sections of this research, two differing etch ratios were used. Mesa stripes with 90°

sidewalls were obtained by a two stage phosphoric etch. The first phase in a 1:8:40 produced sidewalls and allowed control over the depth of the mesas; the second, a rapid polish etch in a 8:1:1 ratio, reduced any surface roughness arising from the first etch, and sharpened the vertical part of the sidewall. Figure 3.2 shows SEM images of (8×8)×4 squares without (a) and with (b) the 8:1:1 phosphoric polish etch. It demonstrates the difference in smoothness and also shows the undercut ratio difference from the first etch revealing the rapid nature of the etch.

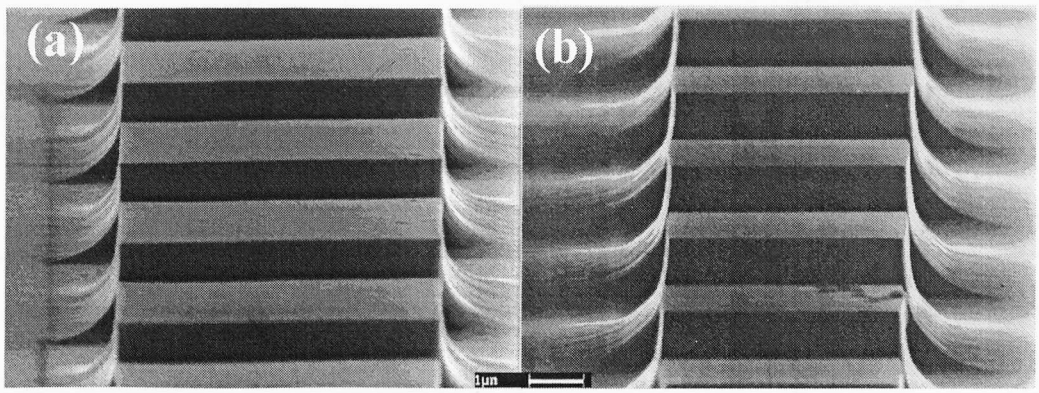


Figure 3.2: (8×8)×4 squares etched along the (001) direction. (a) The etchant is H_2PO_4 : H_2O_2 : H_2O in a ratio of 1:8:40 and (b), with a polishing etch H_2PO_4 : H_2O_2 : H_2O in a ratio of 8:1:1

For the 73° sidewalls, a variety of different etches were investigated including the HCl : CH_3COOH : $K_2Cr_2O_7$, NH_4 : H_2O_2 : H_2O, and H_3PO_4 : H_2O_2 : H_2O. Table 3.2 provides information for various ratios and etches investigated. The best by far was the phosphoric etch in a 1:1:10 ratio, which produced smooth sidewalls with an angle of 73°. Figure 3.3 shows a SEM image of an 8 μm "as-etched" mesa produced with the phosphoric etch. The wafers were spin coated with Shipley 1813 photoresist at 4000 rpm for 3 s and 5000 rpm for 30 s, which produced a uniform layer of photoresist. The coated wafer was then placed in a Petri dish, covered in foil, and put in an oven at 120°C for 30 min and were subsequently left to cool down at room temperature. The photoresist, developer and stripper chemicals were all provided by Shipley. The sample was then placed in the MJB3 Karl Suss aligner and was exposed through the mask to UV light.

Ratio	Etch Time	Etch Depth	Quality
$HCl : CH_3COOH : K_2Cr_2O_7$ System			
1:1:1	1:20 min	~1.8 μm	Quite directional etch Both <100> and <110> badly etched with wobbly edges. Angle produced ~50°
1:1:2	7:20 min	~1.0 μm	Quite slow etch, particularly bad for the squares and wobbly edges. Angle produced ~50°
$NH_4 : H_2O_2 : H_2O$ System			
1:1:8	1:15 min	~1.6 μm	Wobbly stripes <100> more than <110>. Angle produced ~50°
1:1:200	16 min	~0.85 μm	Very slow etch, wobbly stripes on all directions, with a 50°-55° angle.
$H_3PO_4 : H_2O_2 : H_2O$ System			
1:1:10	3:15 min	1.2 μm-1.4 μm	Good quality well defined stripes, with minimum wobble, better for <100> than <110>, good quality squares. Angle produced 66°-73°.

Table 3.2: Various etches investigated and the results obtained

The mesa alignment needed to be relatively precise and therefore, the markers on the mask were accurately aligned with the major and the minor flats of the substrate markers on the wafer. After detailed investigation it was found that the best exposure time for the particular photoresist thickness defined by the two-stage spinning procedure, was 7 s. The wafers were rapidly developed in a 3:1 ratio of developer/high purity de-ionised water, taking approximately 1 ½ min. In order to avoid a *clouding effect* that was observed during some initial etch trials, the

developer solutions were rapidly stirred during wafer development. The *clouding effect* was thought to have been caused by the presence of undissolved floating layers of photoresist, removed from the wafer but still present in the solution, which caused uneven resist development. The wafers were then rinsed with DI (de-ionised) water and blown dry with N_2. The samples were then placed in carefully cleaned PTFE dishes and etched using the 1:1:10 phosphoric etch using mild agitation. The etch rate was ~0.4μm/min and the etch depth around 1.3/1.4 μm. The wafers were rinsed with DI water for ~3 min and blown dry with nitrogen. All samples were then cleaned with a resist stripper in an ultra-sonic bath for 5 min, rinsed in DI water, placed in boiled acetone for another 5 min and finally rinsed with IPA (isopropyl alcohol), and also DI water and dried with N_2. The wafers were examined with optical microscopy and Alpha-step measurements to check the quality and the etch depth of the mesas. After the post processing cleaning procedure described above, the substrates were O_2 ashed and then loaded into the MBE chamber for AH cleaning and finally outgassed thoroughly before growth.

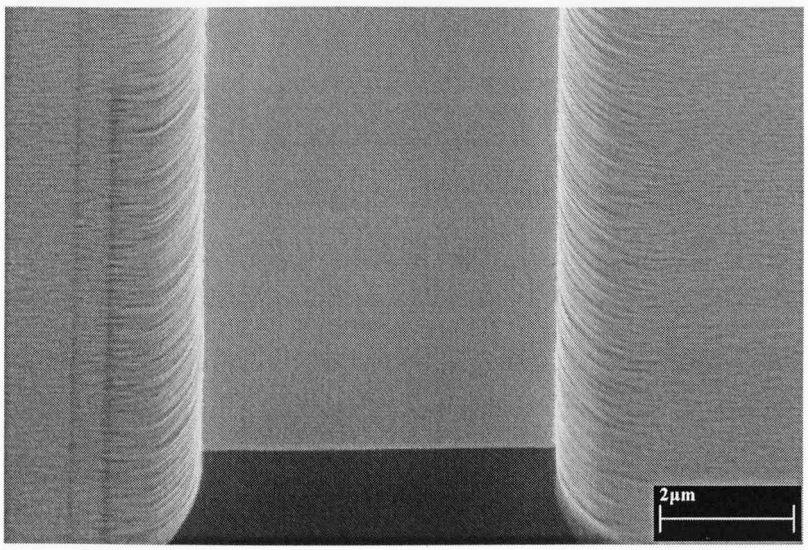


Figure 3.3: Shows an AFM image of an 8 μm stripe produced by the 1:1:10 ratio of the phosphoric etch.

For the ~90° sidewalls, as mentioned above, the etch used was a two stage phosphoric etch. The exposure and developing procedures are identical with previous etch. For the first stage the H_3PO_4 : H_2O_2 : H_2O ratio used was 1:8:40. The sample was mildly agitated for 1 minute and 50 s and was then rinsed in DI water for 3 minutes and blown dry with N_2. The measured etch rate was ~1.6

μm/min. The second stage was performed immediately after the first, apart from the trial investigations, whereby the samples were examined with Alpha-step in order to check the quality and depth of each stage. The ratio for the more aggressive, secondary etch was 8:1:1 for 10s during which, the sample was vigorously agitated. The etch rate for the 8:1:1 ratio etch was 1.00 μm/min. The wafers were then rinsed with DI water for 3 min before being blown dry with N_2. In all the experiments including the initial trials, the etch depth varied between 1.4 μm and 1.6 μm especially when the etching was performed on different days. In addition, because of the aggressive nature of the second etch, the odd fractions of a second are really important. Figure 3.4 shows an example of a badly etched and probably contaminated sample. The sidewalls are extremely rough and the surface of the samples is covered with impurities. Figure 3.5 shows an SEM image of an 8 μm stripe using the two-stage phosphoric etch used for growth.

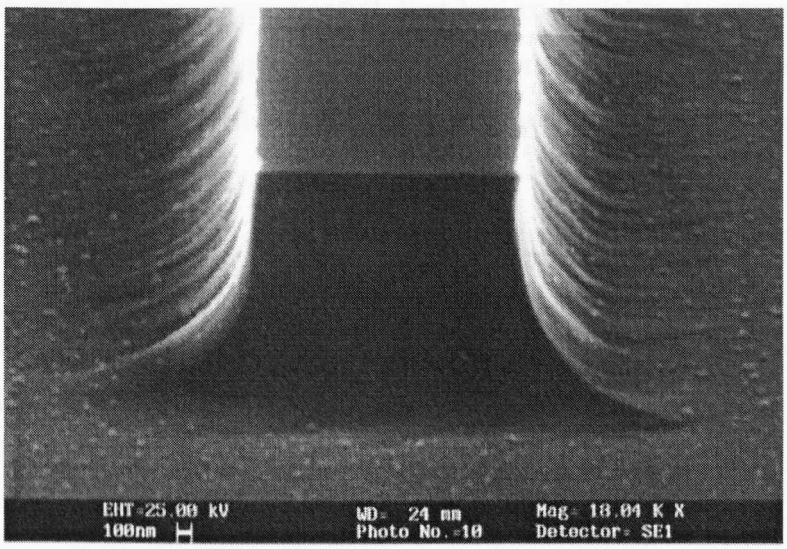


Figure 3.4: A 5 μm stripe etched along the <001> direction using H_3PO_4 : H_2O_2 : H_2O (1:8:40).

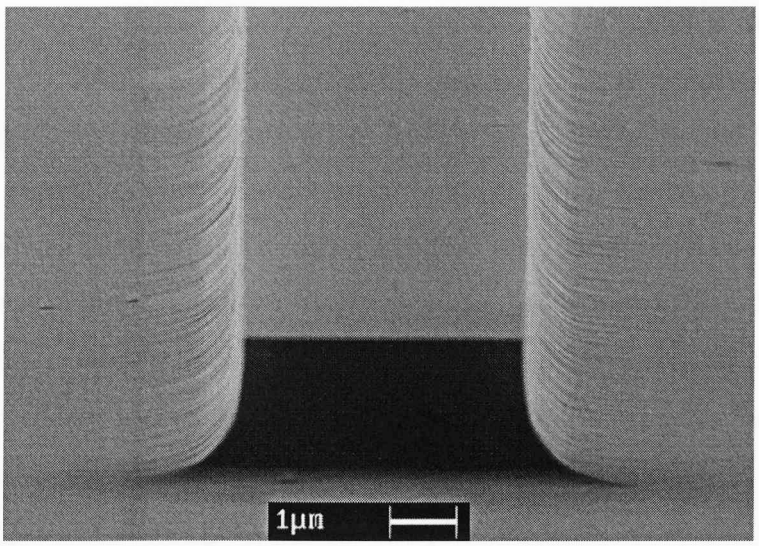


Figure 3.5: An 8 µm stripe etched along the <001> direction using the two stage phosphoric etch $H_3PO_4 : H_2O_2 : H_2O$ (1:8:40/8:1:1)

The clean room environment conditions were kept as constant as possible but small fluctuations in both room and solvent temperatures could not be avoided, causing etch rate discrepancies. Special care had to be taken to ensure the good condition of the solvents and equipment used. In order to minimise discrepancies, the etching was mainly carried out on a number of wafers on the same day.

Nevertheless, for the samples used, great care was taken to achieve as contamination free a surface as possible and produce well defined sidewalls for these investigations. As mentioned above, after the solvent cleaning the etched wafers were O_2 plasma ashed, outgassed and AH cleaned. All the samples provided a good quality (2×4) RHEED reconstruction prior to growth.

3.4. Sample Preparation.

The ridge structures were grown by MBE on patterned GaAs(001) semi-insulating substrates in a VG V80H growth chamber, which also contained an additional chamber for AH cleaning the samples prior to growth.

After O_2 ashing the wafers were generally In-bonded onto a Mo platen and are introduced into the chamber *via* the *fast entry load lock*. The ones that are not going to be used remain in the clean room for later use. The wafer for growth was transferred *via* the trolley-pulley system to the AH chamber where it was carefully

outgassed to 400°C. Subsequently, the sample was AH cleaned at 400°C for 30 min. When the substrate has significantly cooled, it was transferred into the deposition (growth) chamber were it was further outgassed to around 620°C in the presence of arsenic to ensure the complete removal of the native oxide. The mass spectrometer was used to follow this procedure and monitor all the compounds liberated. Finally, the temperature was lowered to that required for growth and the (2×4) RHEED pattern was checked before growth. In the cases of the InAs dot samples, the surface reconstruction was checked also directly after the end of the growth to verify the presence of chevrons, which appear when there is a facetted 3D surface present. Post growth, the samples were removed from the MBE chamber and taken to the SEM and AFM microscopes for analysis.

CHAPTER 4:

Effect of Mesa Width on Ga Adatom Diffusion Processes.

4.1. Introduction.

The epitaxial growth of III-V semiconductor structures on patterned substrates has demonstrated significant potential for the fabrication of new device structures with novel properties [38,119,120]. For example, it has recently been shown that high quality arrays of pyramidal micro-structures can be grown by MBE on square mesas patterned onto GaAs(001) substrates [47]. Structures with {110} pyramid facets were formed, with optical micro-reflection and micro-transmission imaging measurements indicating reflectivities greater than 80 % [50]. It was shown that this type of structure could be used as the top mirror in a novel, micron-scale vertical microcavity device optical work [50]. More recent studies on pre-patterned stripes indicate that this method also shows promise for producing waveguide structures [121]. Fabrication of these types of structure requires a high degree of control over the growth process in order to precisely define the final pyramidal shape and morphology of the final structure.

Growth on patterned substrates is highly complex since new facets evolve during deposition. The diffusion and incorporation processes on these planes will determine both the morphology and shape, as well as the structural quality of the films. Several methods have been employed to investigate the growth mechanisms on patterned GaAs substrates, the most powerful being *in-situ* μ-RHEED, which has been used to provide a direct measure of the Ga adatom diffusion rates during growth [27,33]. Ga diffusion lengths for the low index planes were then derived from these measurements using simple diffusion theory [14,27,33]. The μ-RHEED studies also demonstrated that the Ga adatom migration length and direction are affected by the local V/III ratio or specific As species used during growth [15] [11]. However, these measurements do not provide a complete model for the growth of different facets. Indeed, as is known from the measurements of diffusion lengths on

low index planes, the values obtained can vary significantly, due to variations in growth the conditions [24,122-124]. The results do point to trends and as such prove useful for understanding the growth processes during thin film deposition.

A few groups have used theoretical treatments to obtain the general evolution of the growth ridge structures [125-127]. However, the detailed structure, and the subtle effects of the changing growing parameters with the subsequent interplay of the growing facets, have not been modelled. As a consequence, relatively little is known about how the interplay between evolving facets influence the shape and morphology of the final structure.

A limited amount of experimental work has been carried out in order to address the growth mode evolution on patterned substrates. Williams *et al.* examined the deposition of GaAs on GaAs (001) patterned substrates [48]. The features were wet chemically etched along the <100> directions and consisted of mesa stripes with a sidewall angle of ~90°, in different widths. Different GaAs quantities were deposited under a variety of growth conditions. They discovered that the deposited GaAs forms new {110} facets because Ga diffuses upwards form the {110} facets to the top (001) plane, and the edge position is less energetically favoured. Moreover, once these facets were formed, they became essentially "non-growth" planes. Williams *et al.* also observed a build up of material at the top edges of the (001) plane on both sides of the mesa stripe. This effect was defined as the "Swimming Pool Effect" (SPE). The smaller mesa stripes (5 μm etched mesa) were found to be closed off after the deposition of 1.00 μm of GaAs.

4.2. Experimental Details.

The GaAs(001) substrates were patterned using standard photolithography and wet chemical etching methods; an etch consisting of H_3PO_4:H_2O_2:H_2O in the ratio 1:1:10 was used. This produced mesa stripes widths of 5-15 μm, aligned along <100> and the orthogonal <100> and <010> directions, with sidewalls intersecting the (001) surface at approximately 73°.

After patterning and prior to growth, the substrates were oxygen plasma ashed and transferred immediately to the load lock. They were subsequently moved

to the preparation chamber for outgassing at 400°C and were then cleaned at the same temperature for 30 min at 6×10^{-5} mbar under atomic hydrogen flux. This procedure removed any remaining photoresist and resulted in exceptionally clean substrate surfaces prior to growth, without the prerequisite of thermal substrate cleaning. The patterned substrates were then briefly annealed in the growth chamber at 610°C, under an As_4 flux, to remove any residual native oxides. The surface reconstruction was continuously monitored by RHEED and the substrate temperature measured using an IR-Ircon pyrometer to an accuracy of ±3°C. The As_4 supply was kept constant at a 300 mil valve position. Once a sharp (2×4) RHEED pattern was obtained, the substrate temperature was reduced to 570°C and a GaAs layers of 0.25 and 1.50 μm thickness were deposited at 0.25 μm/h. The incidence flux was approximately 25° to the surface normal from the group III and group V sources. The structures were examined post-growth *ex-situ* by SEM (LEO 440 Stereoscan) and AFM (Digital Instruments 3100 IIIa) using high aspect ratio probes (Nanosensors).

4.3. Growth on the 5 μm Mesas.

Patterning of the GaAs (001) substrates produced mesa structures 100 μm long and 1.3 μm high, as shown by the SEM image in figure 4.1(a). AFM measurements of the as-etched mesa showed that the sidewall angle was approximately 73° with a tailing off at the bottom of the mesa. The 5 μm wide mask feature was reduced in width after etching to ~ 2.7 μm and the 15 μm to ~12.7 μm, due to undercutting. Throughout this chapter, the features will be referred to as their pre-etch size *i.e.* 5 μm and 15 μm wide. The SEM image in figure 4.1(b) shows the ridge structure after deposition of 0.25 μm GaAs. The mesa stripe transforms to a ridge structure consisting of essentially three primary facets. These are shown schematically in figure 1(b) and are labelled top, middle and bottom.

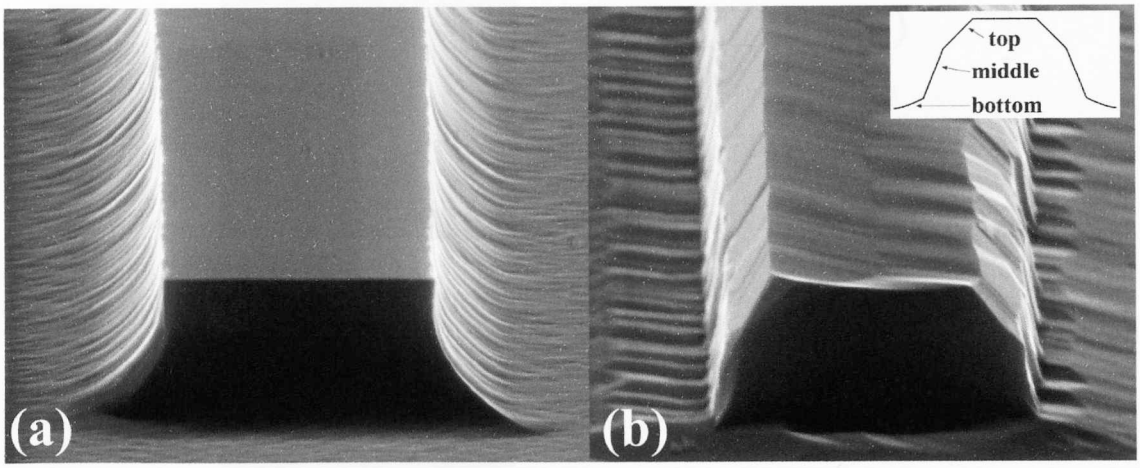


Figure 4.1: (a) SEM image of a 5 μm etched GaAs stripe, (b) SEM image of a 5 μm stripe after the deposition of 0.25 μm GaAs at 570°C, (insert) Schematic showing the different facets formed after GaAs growth.

It can be seen from figure 4.1(b) that there is a build up of material at the edges of the ridges. The effect seen is the bowl-like appearance at the top of the mesa stripes *i.e.* the SPE. It is caused by the relatively short Ga adatom diffusion length on the (001) plane for the growth conditions used, which limits the diffusion of Ga adatoms across the top surface, leading to a build up of material at the edges. The SPE decreases (or increases) according to the growth conditions used. For example, the SPE becomes more significant with increasing V/III ratio (decreasing Ga flux) and/or with decreasing temperature [47].

In figure 4.1(b) the top facet is close to 45° and is consistent with the formation of a {110} facet. This facet is formed for all deposition conditions studied and was not present in the original "as etched" mesa. Additional support for this assignment is provided by the appearance on the facet of micron-sized, triangular-like islands. These type of features are often observed during the homoepitaxial growth of GaAs on planar GaAs(110) substrates, as discussed in Chapter 1.1 [14,15].

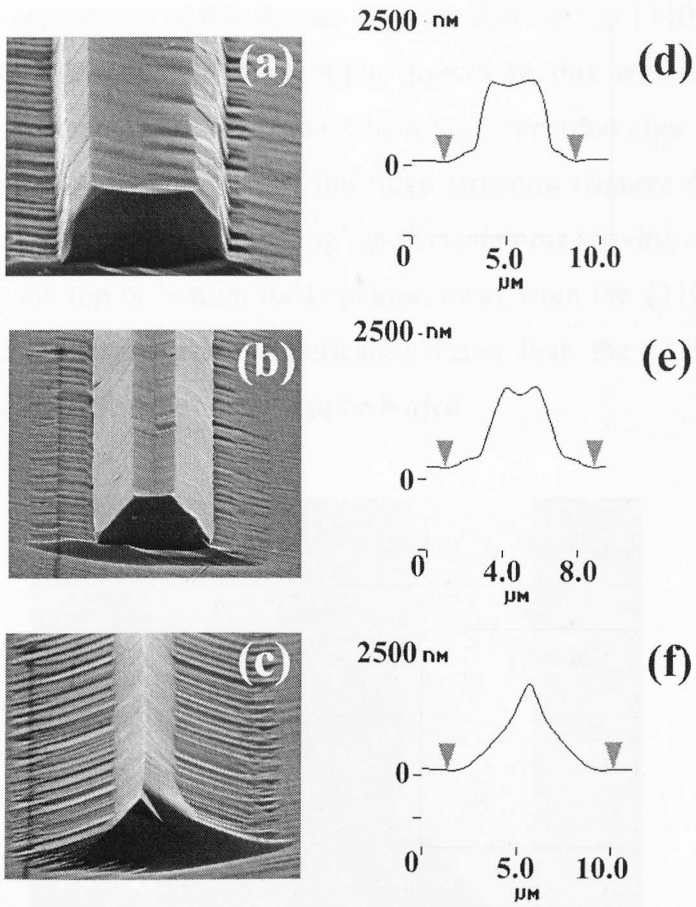


Figure 4.2: SEM images of a 5 μm stripe after depositing: (a) 0.25 μm, (b) 0.5 μm and (c) 1.50 μm of GaAs at 570°C. AFM height cross-sections of the 5 μm stripe after the deposition of (d) 0.25 μm, (e) 0.5 μm, and (f) 1.50 μm of GaAs.

The subsequent interplay of the primary facets highlighted in figure 4.1 was followed as a function of GaAs deposition quantity. Representative SEM images (a-c) and AFM height cross-sections (d-f) are shown in figure 4.2. There is a clear change from figures 4.2 (a, d) (0.25 μm GaAs) to figures 4.2 (b, e) (0.50 μm GaAs). The {110} top facet lengthens considerably and the concomitant increase in the bottom facet length leads to almost complete overgrowth of the middle facet. The classic dip shape at the top of the structure due to Ga diffusion off the {110} facets to the top surface can also be seen in figures 4.2(b, e) [47,48]. The overlapping of the diffusion profiles from both sides of the ridge structure demonstrates that Ga adatoms can diffuse from one side to the other of the mesa. The SEM image in figure 4.2(b) also shows the appearance of a trench between the middle and bottom facet. This is shown more clearly (and highlighted by the arrows) in the image shown in figure 4.3, also recorded after 0.5 μm GaAs

deposition. The appearance of this feature suggests that the top {110} facet acts as a shadow to the incident flux, prohibiting growth in this region. This trench disappears upon further GaAs deposition. The images recorded after the deposition of 1.5 μm GaAs show completion of the ridge structure (figures 4.2(c, f)). The {110} facets are essentially 'non-growing' and Ga adatoms arriving on these facets diffuse to either the top or bottom (001) planes, away from the {110} facets. The bottom facet subsequently grows significantly faster than the {110} facets and consequently the ridge structure begins to be buried.

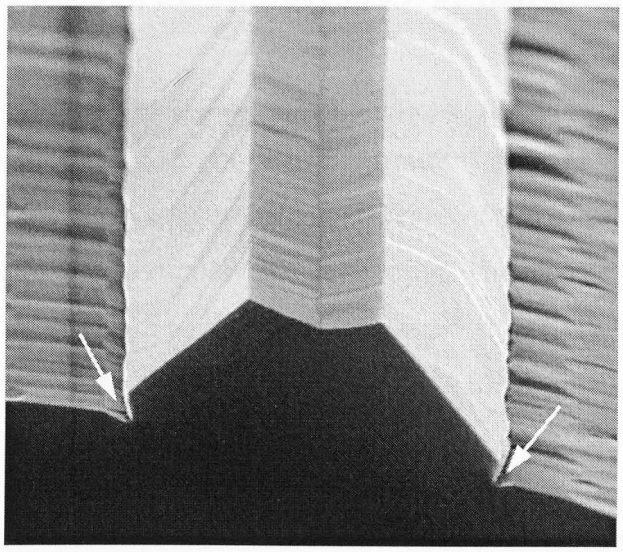


Figure 4.3: SEM image of a cleaved 5 μm stripe after deposition of 0.50 μmGaAs at 570°C.

4.4. Growth on the 15 μm Mesas.

To investigate the effect of increased mesa width on the Ga adatom diffusion kinetics, 15 μm mesa stripes were also examined as a function of GaAs deposition. The 15 μm stripes after the etching process led to mesas of approximately 15 μm width and 1.3 μm height. However, for convenience purposes, they will be referred to as 15 μm wide mesas. Figure 4.4 shows a typical SEM image after the deposition of 0.25 μm GaAs at 570°C. The growth conditions were identical to those used in 4.3 since all stripes were on the same wafer.

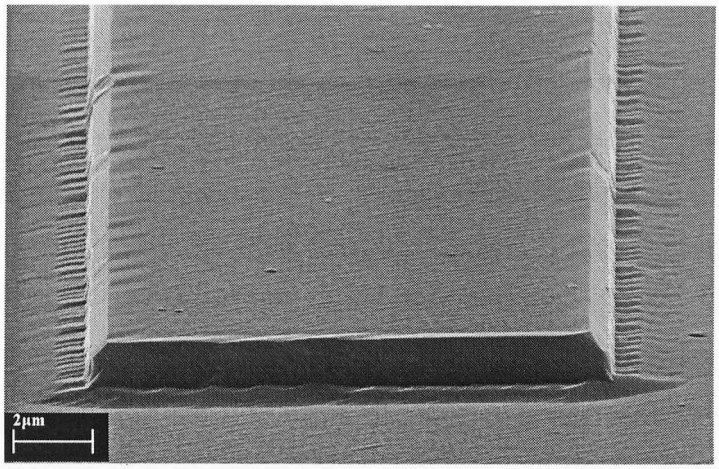


Figure 4.4. SEM image of a 15 μm stripe after 0.25 μm GaAs deposition at 570°C.

The ridge structure formed again consists of three primary facets as previously observed for the 5 μm stripes (figure 4.1). The top facet angle is measured to be 43.5°, again suggesting the presence of {110} facets; the triangular islands formed on the facets support this suggestion. The middle facet has an angle of 67°, which is less than the 73° angle measured directly after etching. Upon further growth the facets progressively changed. SEM images recorded as a function of GaAs deposition are shown in figure 4.5.

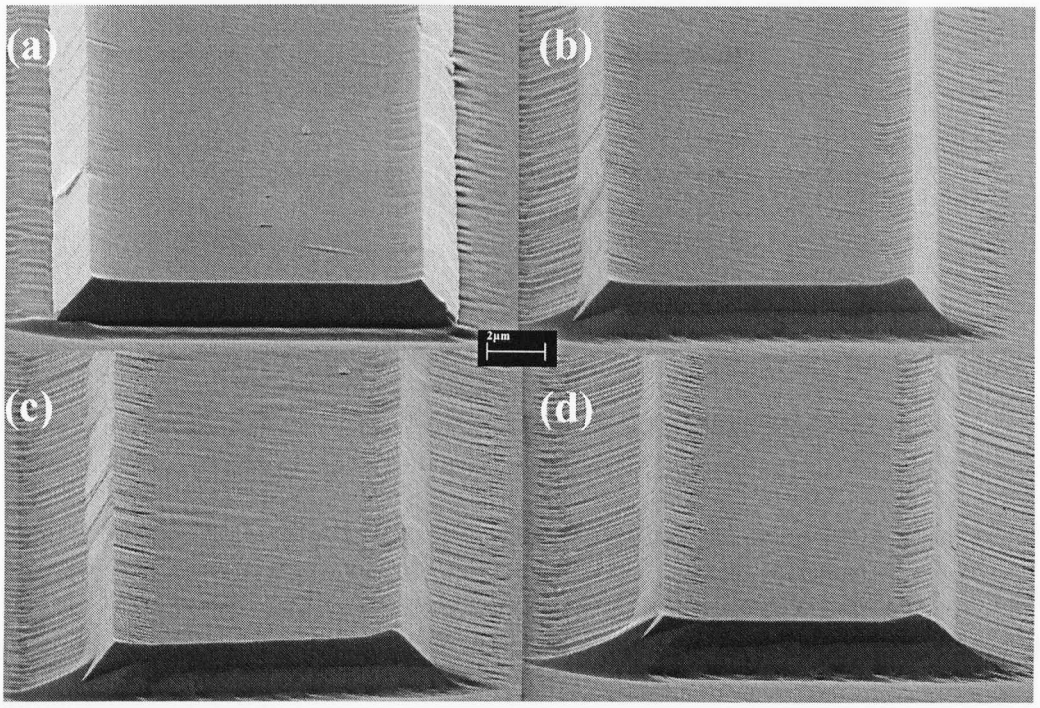


Figure 4.5. SEM images of a 15 μm stripe after the deposition of (a) 0.5 μm, (b) 0.75 μm, (c)1.00 μm and (d) 1.50 μm of GaAs at 570°C using a Ga flux of 0.25 μm/h.

As previously seen with the 5 μm stripe, the length of the top facet increases noticeably after the deposition of 0.5 μm GaAs (figure 4.5(a)). In addition, the bottom facet becomes the primary growing facet after the deposition of 0.75 μm (figures 4.5(b,c)), until the last deposition investigated whereby the middle facet stripe is completely overgrown (figure 4.5(d)). However, the deposition of 1.50 μm of GaAs does not close off the 15 μm stripe (figure 4.5(d)). This is an expected result since theoretically this mesa size should only be closed off after a deposition of 3.17 μm of GaAs, assuming all the Ga adatoms diffuse to the top (001) plane. The cross-sectional area of the ridge can be related to the GaAs deposited using a simplified model: $w=4\times d$, were w is the etched width of the mesa and d is the deposition quantity.

Figure 4.6 shows an SEM image of a cleaved 15 μm stripe after the deposition of 0.50 μm of GaAs.

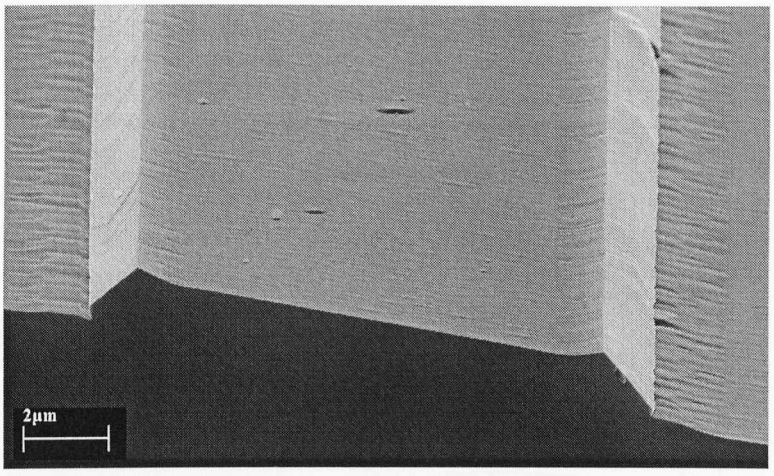


Figure 4.6. SEM image of a cleaved 15 μm stripe after 050 μm deposition of GaAs at 570°C.

The trench seen in figure 4.3 for the smaller stripe is once more clearly present, forming between the middle and the bottom facets. The trench again disappears upon further deposition. The SPE is also a strong characteristic of the morphology evolution.

4.5. Measurements of Facet Angle and Length.

More quantitative measurements of the evolving morphology for the 5 μm stripes are shown in figure. 4.7, which shows plots of both the facet angle (a) and facet length (b) as a function of GaAs deposition quantity. The data was obtained from contact mode AFM measurements of the ridge structures. Both sides of each ridge and the ridges in the two orthogonal directions exhibited the same behaviour; consequently the data obtained for each ridge structure and the two directions have been averaged together.

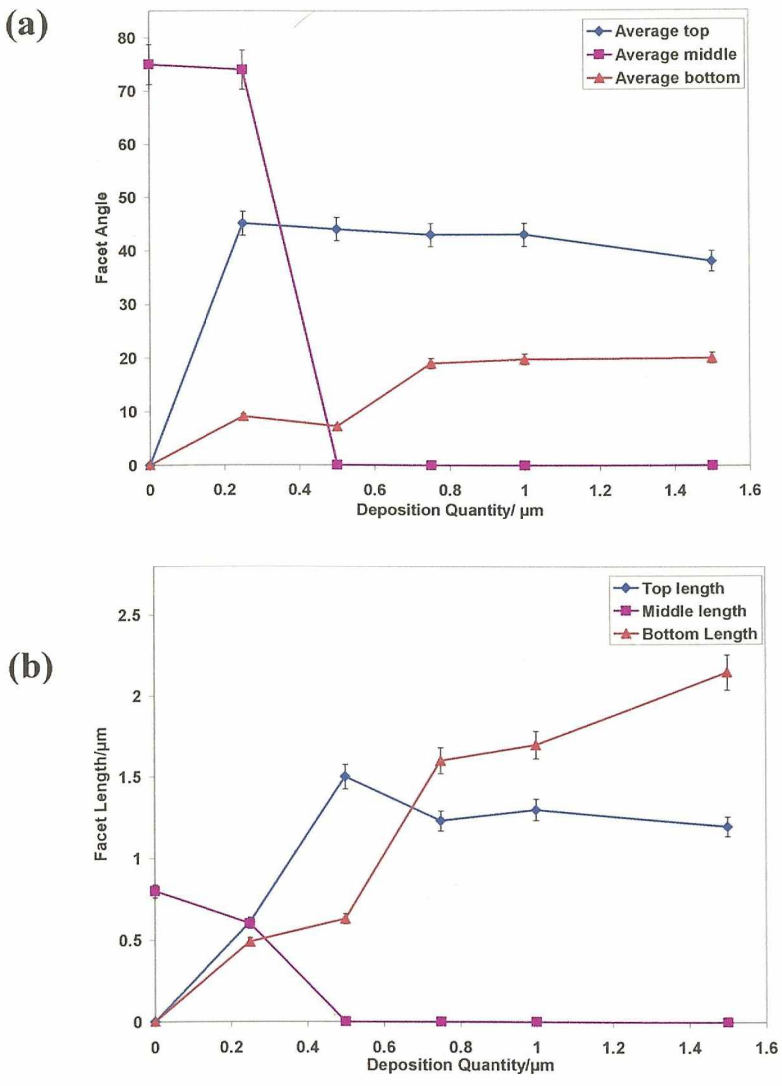


Figure 4.7. Plot of (a) facet angle and (b) facet length as a function of GaAs deposition quantity. The data was obtained from AFM measurements taken from growth on the 5 μm stripes. The facets are divided into: ♦ top; ■ middle; and ▲ bottom.

Figure 4.7 shows that the average angle of the middle facet begins to fall as the deposition quantity increases to ~ 0.5 μm. The initial length of the middle facet (~ 0.7 μm) is shorter than would be expected for a mesa 1.3 μm high, due to the presence of a curved section at the base of the mesa (fig. 1a), which appears to act as a seed for the growth of the bottom facet seen in the SEM and AFM images. Simultaneously, the bottom facet angle increases and reaches a constant value of approximately 20° after ~ 1 μm deposition, suggesting formation of a {310} facet. The length of this bottom facet increases continuously with deposition quantity up to a maximum value of ~ 2.1 μm. This behavior is in marked contrast to that of the top facet where the angle after 0.50 μm deposition is close to 40°. This angle is less than expected for a {110} facet, which is probably a consequence of the micron-sized islands formed on the facet (figure 4.2(a)). Figure 4.7(b) shows that the sidewall angle for the top facet after 1.00 μm GaAs deposition remains essentially stable. However, since the bottom facet takes over after the 0.75 μm deposition, and starts to move upwards, a decrease in the length of the top facet should be expected.

Similar plots are shown in figure 4.8 (a) and (b) for growth on the 15 μm mesas. In this case, the middle facet has a length of 0.80 μm, similar to that measured on the 5 μm wide stripes. This tailing off acts as a seed for the development of the {310}-bottom facets. The middle facet decreases in angle but its length also decreases and after 0.50 μm GaAs deposition, it is consumed by the top {110} facet whose length increases considerably up to 0.50 μm deposition. After this point, the dominant facets appear to be the bottom, which increases dramatically in length and in angle. Figure 4.8 (a) and (b) shows that after the deposition of 0.75 μm of material the angle reaches a value of 20° and the length increases from 0.60 μm to 1.60 μm. this behaviour is quite different for the top facet which reduces slightly in angle and length followed by a larger increase after 1.50 μm deposition. Interestingly, the length of the top facet at this stage of growth, is considerably less than that observed for the 5 μm stripes, which could be attributed to the fact that the larger width mesas have not closed off. An interesting point is also that the top facet length does not increase with further deposition since the bottom facet becomes the dominant one after 0.75 μm deposition which

suggests that the stripes would most probably be completely buried before having the chance to close off.

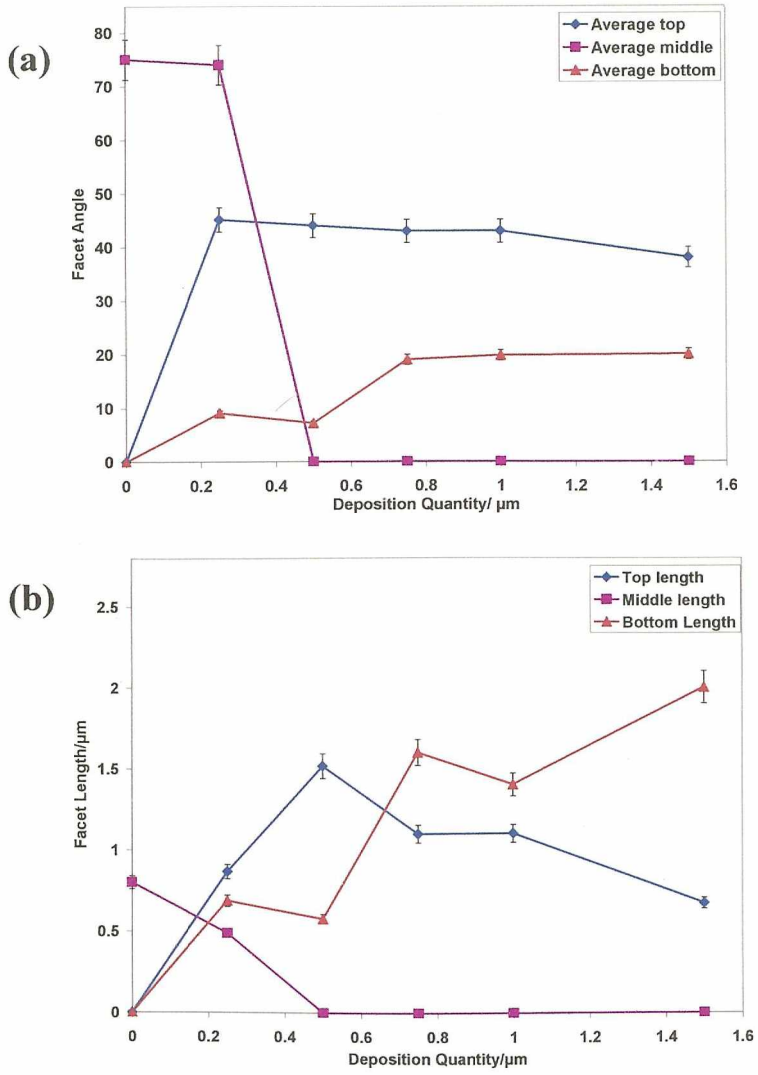


Figure 4.8. Plot of (a) facet angle and (b) facet length as a function of GaAs deposition quantity. The data were obtained from AFM measurements taken from growth on the 15 µm stripes. The facets are divided into: ◆ top; ■ middle; and ▲ bottom.

The implication that some Ga adatoms diffuse from the {110} top facets to the middle facets and cause the top facets to extend and include the middle ones, is also evident for the 15 µm stripes, since the formation of a trench between the middle and the bottom facet occurs after the 0.50 µm deposition (figure 4.6). This suggests that growth near the mesa base is inhibited at this stage of growth, due to the presence of the top {110} facets, which shadow the incident As flux and hence reduce the material accessing this area of the ridge structures.

4.5.1. Summary.

The above information, can be summarised as follows:

- Initial growth is dominated by the growth of this new {110} facet.
- The SPE affect is apparent on the edge of the (001) mesa top.
- A bottom {310} facet starts to slowly develop and to dominate in the later stages of growth.
- A trench is formed between the top and bottom facets, which limits the mesa overgrowth while present.

4.6. Discussion.

This investigation proved extremely important for understanding the kinetics of Ga adatom diffusion processes on GaAs. After the deposition of 0.25 μm of GaAs, three primary facets are always present for all mesa sizes studied. The top has an angle of 45° and is identified as an {110} facet, the middle facets which are the facets obtained after etching and has an angle of 75° and the bottom facets with an angle of 9°. In this discussion we focus on: i) the SPE effect and how it intervenes with the formation of the {110} facet ii) how formation of the {110} facet, iii) the formation of the trench and how it affects subsequent growth; and iv) the domination of the bottom facet after ~0.75 μm deposition. Also, a comparison with previous work carried out on patterned substrates with 90°sidewalls is also presented.

4.6.1. Swimming Pool Effect (SPE).

Figures 4.2 (a) and (b) highlight the clear build up of material on the top (001) surface of the ridges, near the mesa edges. This effect is commonly referred to as the swimming pool effect (SPE) and has been seen in other investigations of

GaAs growth on patterned substrates [47,48]. The magnitude of the SPE is strongly dependent on the growth conditions and the effect increases with increasing V/III ratio and decreasing temperature. For at these conditions the Ga migration length on the (001) plane is reduced and Ga adatoms are forced to incorporate more rapidly after migrating off the {110} facets. Figure 4.9 shows a schematic diagram of the adatom migration process at the top of the mesa. Ga diffuses off the {110} facet to the top (001) plane, but because of the relatively short diffusion length on that surface, it incorporates close to the edges on both sides of the stripe. This produces the small bowl-like shape at the top edges of the stripes. It should be noted that some of the Ga adatoms can also diffuse downwards to the bottom facet.

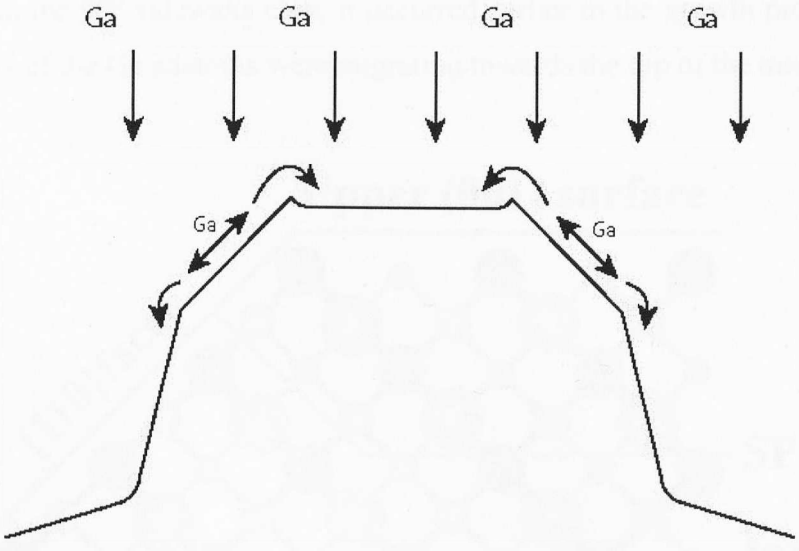


Figure 4.9. Schematic diagram of Ga adatom diffusion on the {110} facets during the early stages of growth.

4.6.2. Formation of the {110} Facet.

The {110} facets form in order to keep the surface in a state of minimum energy during growth. Sangster *et al.* suggested that in order to keep the surface energy at a minimum, the number of dangling bonds should not increase [128]. If one atom were added at one of the two outer lattice positions on the top edge of the stripe, the number of dangling bonds would increase by one since the available dangling bonds for incorporation at the edge is only one. Therefore, the deposited Ga adatoms would have to move one lattice position inwards towards the centre of

the ridge structure compared to the previous layer as demonstrated in figure 4.10, thus leading to the formation of the {110} facet.

The {110} facets require a stable growth regime to develop and lengthen. Therefore it is assumed that stable facet growth only occurs within a specific range of impinging V/III ratios. If the local V/III ratio decreases during growth, the facet becomes unstable and in order to maintain an acceptable growth environment, the facet has to reduce its angular inclination to allow for more of the incoming flux to be directed to it, improving the *local* growth conditions. This new facet is closer to the (001) plane and it receives a greater direct As flux. This may be the reason for the formation of a 21° facet after the deposition of 1.50 μm of material for the 15 μm stripes. A similar effect has been reported for mesas with 90° sidewalls. However, in the 90° sidewalls case, it occurred earlier in the growth process since the majority of the Ga adatoms were migrating towards the top of the mesa.

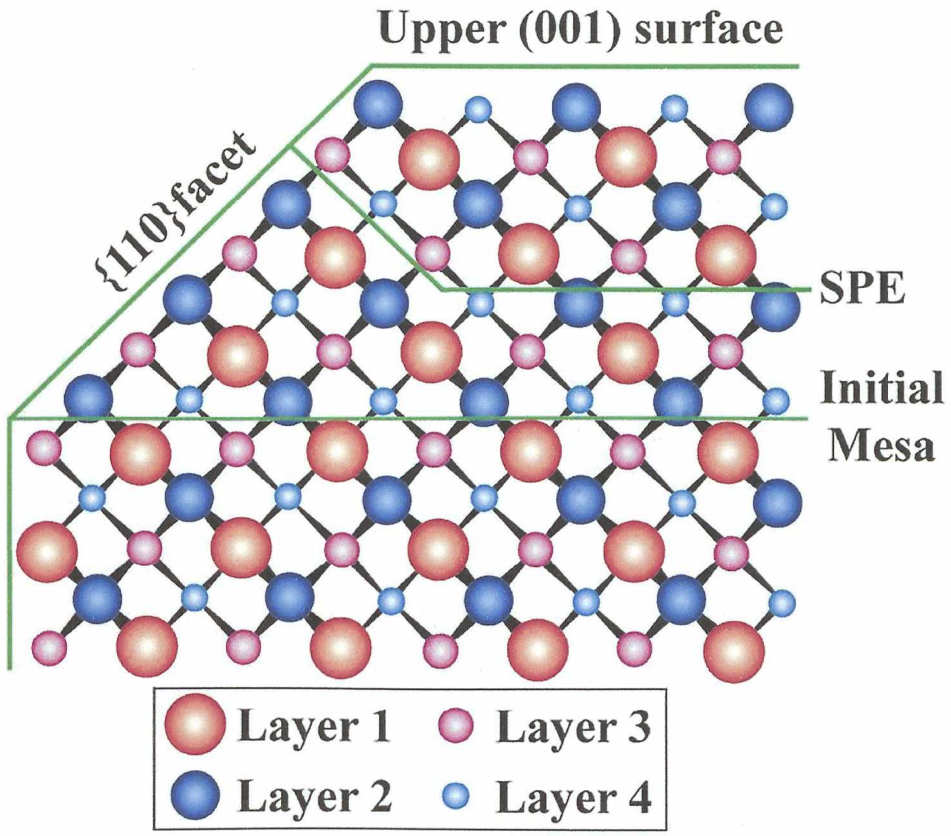


Figure 4.10. Schematic 3D representation of the GaAs lattice representing the top left edge of a stripe after the deposition of three layers of GaAs. The size of atoms decreases with their relative position of the viewer. The red coloured atoms represent Ga and the blue As. [48].

The SEM images in figures 4.2 and 4.5, show that the top {110} facet has some roughening of the surface morphology in the form of triangular "micro-steps" which are present in all growths and for all samples. The triangular shapes are always aligned in specific directions either towards or away from the {n11} type directions and are similar to those reported during the homoepitaxial growth of GaAs on planar GaAs (110) substrates [14,15]. These triangular shapes are specific to As_4 growth as opposed to As_2 and are present at high substrate temperatures and/or low V/III ratio (Chapter 1.3). These triangular "micro-steps" are aligned in both the LHS and RHS of the stripes. However, the degree of roughness, caused be these triangular micro steps, differs with the specific growth conditions used and the GaAs deposition quantity. This is apparent in figures 2(a-c) for the 5 μm stripes and figures 5 (a-d) for the 15 μm stripes, where the roughness can be seen to reduce with increasing GaAs deposition.

The Ga diffusion length on the (110) plane is known to be significantly larger than on the (001) surface [33,129] and Ga adatoms can move freely along the surface before migrating towards the (001) surface and incorporation. When the {110} facet becomes longer, the probability of the landing Ga adatoms leaving the {110} facet becomes smaller and they are subsequently more likely to be incorporated in the facet making it smoother especially when high V/III ratios and low growth temperatures are used [14,15]. These results are consistent with previous studies on the growth of GaAs on substrates with vertically etched sidewalls by Williams *et al.* [48]. Once the {110} facet is formed, there is little evidence to suggest further growth since the local As concentration on the facet is low. This was seen previously in the investigation of AlAs/GaAs heteroepitaxial growth on GaAs(001) patterned substrates [130]. For the GaAs growth, the {110} facets upon formation had very little further growth on them compared with the AlAs growth whereby the {110} facets, once formed, were seen to grow outwards with additional deposition. The most As rich planes are the upper and the lower (001) because of the low inclination angle with the incident As flux. The {110} facets, being at an angle, have less of the incident As flux landing on them. In addition, the lower As_4 incorporation coefficient on the {110} makes them less susceptible to further growth. Moreover, the Ga adatom diffusion length on the {110} facets is considerably longer than for the (001) planes which gives rise to the preferential migration of Ga adatoms to either the top (001) plane or the bottom

facet. However, it has been observed that in lower temperatures where the As concentration is increased and the Ga diffusion length is smaller, growth does occur.

4.6.3. Formation of the Trench and How it Affects Growth for the {110} Facets.

As seen in figures 4.3 and 4.6, a trench appears after the deposition of 0.50 μm GaAs. The changing angle of the middle facet indicates that facets with angles between ~ 73° and 45° are not stable for these growth conditions, and that the middle facet appears to favour the {110} surface. This suggests that kinetics play a crucial role in determining which facets are formed since from pure thermodynamic considerations it is well know that {111} surfaces are the most energetically stable [131]. It can also be seen that the top facet does not increase in length, as might be expected if the majority of the Ga adatoms were diffusing to the top surface.

There are two possible scenarios for the growth dynamics involved in the formation of the {110} facet. The first suggests that it is formed through outward rotation of the middle facet, which would involve the diffusion of Ga adatoms to the bottom of the middle facet, gradually reducing the angle to 45°. A second possibility is that Ga adatoms diffuse from the top to the middle therefore extending the {110} face to include the middle facet. The SEM image in figure 4.3 shows that after deposition of 0.50 μm GaAs, a trench appears running along the stripes between the middle and the bottom facets. This suggests that the top facet has acted as a shadow to the incoming flux and inhibits growth at this point. The middle facet therefore grows as an extension of the top {110} facets. Figure 4.11 shows a schematic representation of the Ga adatom diffusion processes after 0.25 μm deposition of GaAs. The majority of Ga seems to diffuse from the top {110} facet downwards and consumes the 73° facet. Some migrates towards the (001) top plane and incorporates there, and a minority is incorporated at the {110} facet. However, the encircled area shown in figure 4.11 is As deficient because the top {110} facet shadows the incident As source flux at that point. As a consequence, some Ga adatoms cannot incorporate and they migrate to the bottom facet,

resulting in the formation of the trench. Due to the presence of this trench, Ga cannot easily diffuse to the bottom of the 45°facet. It is assumed that the growth on the sidewalls follows the second suggestion, whereby Ga from the {110} facet diffuses downwards and eventually is incorporated, extending the lower edge of the {110} facet. As the deposition quantity increases, the growing {110} facet becomes a greater secondary source of Ga adatoms and, due to the long diffusion length of the Ga adatoms of the {110} planes, a large proportion of them migrate and become incorporated on the top (001) surface. Consequently, after 1.00 μm of material is deposited, the stripes are closed off.

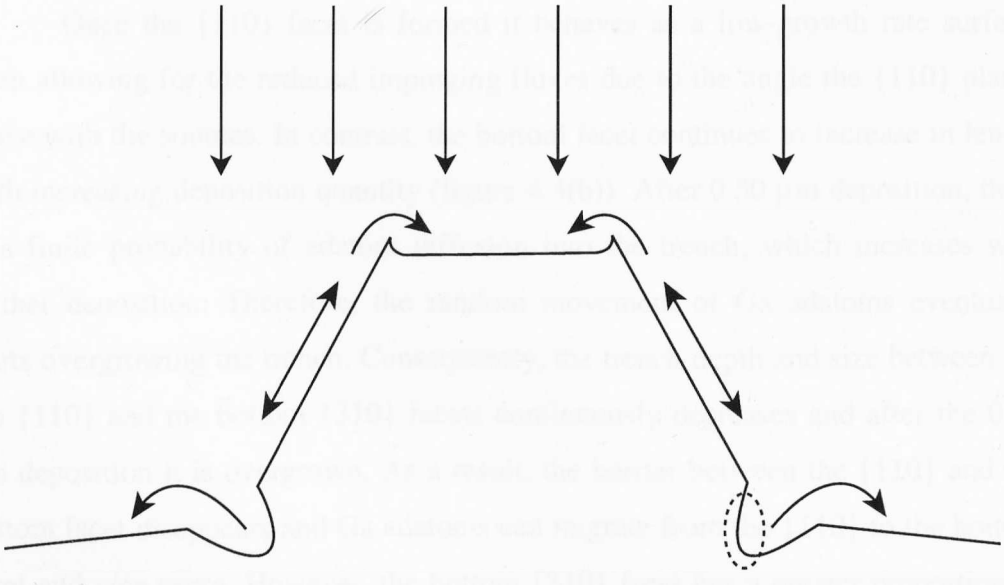


Figure 4.11. Schematic showing the assumed flow directions of the surface Ga species after the deposition of 0.50 μm of GaAs.

For the smaller width stripes, a small decrease in length is observed for the {110} facets once the stripe is closed off, since the bottom facet starts moving upwards burying the structure. Also, for the 15 μm stripes that are far from closed off, the length of the {110} facet, that is expected to increase, remains constant mainly due to competition between the {110} and the bottom facet.

4.6.4. Bottom Facet Domination.

The SEM and AFM images show that the ridges are closed-off after deposition of between 0.75 μm and 1.00 μm of material for a 5 μm stripe.

However, complete closure should in principle occur after ~ 0.68 μm deposition, provided all the Ga adatoms diffuse from the {110} to the top facet. The implication is that a significant proportion of the Ga adatoms also diffuse to the bottom facet, therefore more GaAs is required for completion of the ridge structure. This is evident in the images since the bottom facet increases in length dramatically after the deposition of 0.75 μm. It should be noted, that this is not observed for the ridge structures with vertical sidewalls [47], the difference in growth behaviour is due to the As population available for incorporation. It appears therefore, that the inclination of the sidewalls away from the vertical reduces the energy barrier to diffusion of Ga adatoms down the ridge structure to the base areas.

Once the {110} facet is formed it behaves as a low-growth rate surface, even allowing for the reduced impinging fluxes due to the angle the {110} planes make with the sources. In contrast, the bottom facet continues to increase in length with increasing deposition quantity (figure 4.4(b)). After 0.50 μm deposition, there is a finite probability of adatom diffusion into the trench, which increases with further deposition. Therefore, the random movement of Ga adatoms eventually starts overgrowing the trench. Consequently, the trench depth and size between the top {110} and the bottom {310} facets continuously decreases and after the 0.75 μm deposition it is overgrown. As a result, the barrier between the {110} and the bottom facet disappears and Ga adatoms can migrate from the {110} to the bottom facet and *vice versa*. However, the bottom {310} facet has a greater proportion of (001) planes and a higher local As flux, therefore a higher As incorporation coefficient. Since this area has a higher As concentration than the {110} facet, a considerable amount of Ga migrating to the {310} will incorporate. It would appear therefore, that the lower {310} facet grows faster than the {110} surfaces and thus consuming the {110} surface earlier. After the completion of the stripes, since there is no top (001) plane, the dominant facet *i.e.* the fastest growing crystal surface, becomes the bottom {310}, which starts burying the structure. At approximately 0.90 μm GaAs deposition the edge of the lower facet reaches the etched mesa depth and leads to overgrowth of the {110} facet.

To summarise, the schematic in figure 4.12 demonstrates a possible scenario of the growth sequence for the 5 μm stripes. There are three main stages for the overgrowth on the stripes. In the first stage (figure 4.12(b)), the {110} facets have formed, most probably in order to reduce the surface energy. In the second

stage, a trench appears between the bottom facet and the {110} planes, and the 75° facets disappears as a consequence of Ga adatoms migrating from top part of the {110} facets downwards, consuming the middle facet. In the last stage, the 5 μm stripes are closed off and the bottom {310}-type facets become the dominant ones since they are the most As rich surfaces, leading to the overgrowth of the ridge.

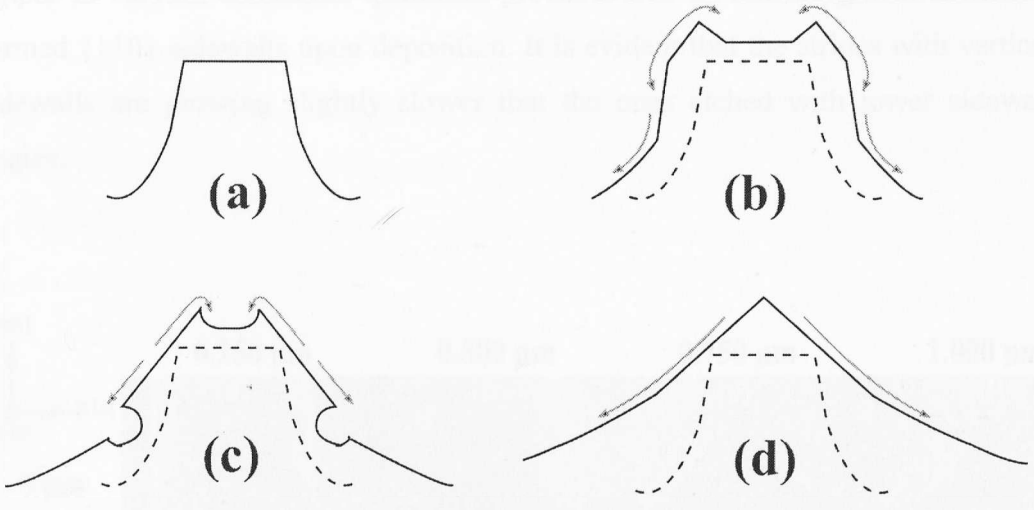


Figure 4.12. Schematic model of Ga diffusion during deposition. (a) Etched stripe, (b) 0.25 μm, (c) 0.50 μm and (d) 1.00 μm GaAs.

4.6.5. Changes for the 15 μm Stripes.

For the 15 μm stripes the same trend was observed until the deposition of 1.00 μm of material. However, upon further deposition, the {110} facets were reduced in angle to ~35° and another facet appeared at the cusp of the two edges of the ridge with an angle of 21°. These new facets were possibly formed in order to reduce the total surface energy. Upon further deposition, the local V/III ratio decreased and growth on the {110} plane became unstable. In order to maintain an acceptable growth environment, the facet had to reduce its angular inclination to improve the As population.

4.6.6. Comparison With Work Done on 90° Sidewalls.

Similar work has been performed on GaAs patterned substrates with stripes having an angle ~90° [132]. The stripes were also oriented in the <100> directions and were similar in size. Figure 4.13 shows SEM image of the 5 μm and 15 μm stripes in varying deposition quantities grown at 570°C. All the grown structures formed {110} sidewalls upon deposition. It is evident that the stripes with vertical sidewalls are growing slightly slower that the ones etched with lower sidewall angles.

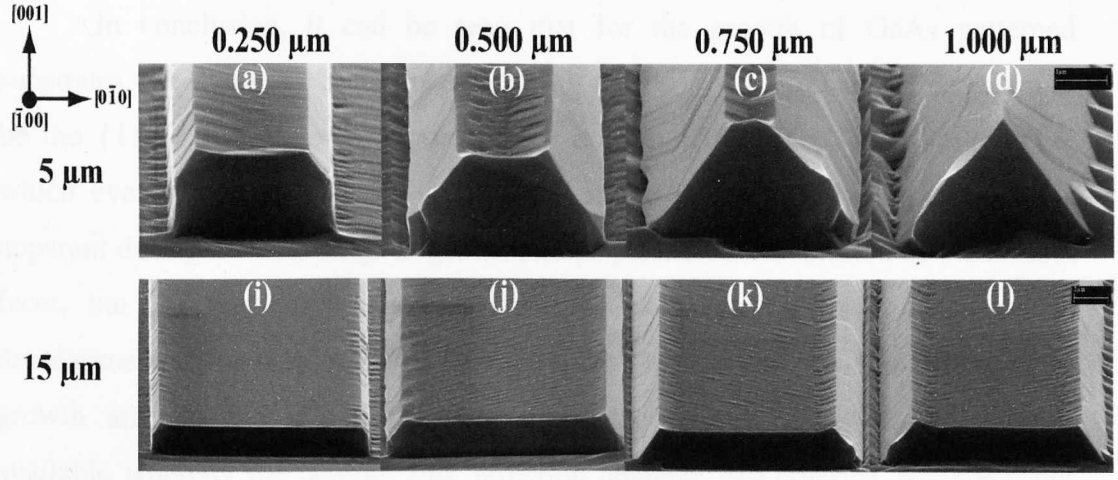


Figure 4.13. SEM images of 5 μm and 15 μm stripes after 0.25 μm, 0.50 μm, 0.75 μm and 1.0 μm GaAs deposition at 570°C using a 0.25 μm/h Ga flux. [132]

It can be seen from figure 4.2(b) that the (001) top surface is shorter in length than the image in figure 4.13 (b). This can be attributed to the fact that the As pressure for the vertical sidewall experiments was higher than for the ones with lower angle. This reduces the Ga migration length and as a consequence, a smaller amount of Ga escapes the {110} facets and is available for incorporation on the top (001) plane. Moreover, the trench that is apparent after 0.50 μm deposition on the lower angle stripes on the 73° ridges is also present on the vertical sidewall mesas, but does not disappear upon further deposition. In fact it remains present even after the completion of the stripes at 1.00 μm deposition. A possible reason for this behaviour could be the higher As pressure during growth which shortens the Ga

diffusion length and lowers the probability of Ga migration into the trench and incorporation there. This inhibits the overgrowth of the {110} facets and the length of the {110} facets was generally longer for the vertical sidewall experiments. For the 15 μm stripes the behaviour is similar and for that reason, there is a greater probability for the ridges to close off upon further deposition, without reducing the angle of the top {110} facet as seen for the lower sidewall angle ridges. However, this is speculation since the experiments stopped after the deposition of 1.00 μm of GaAs and in the case of the 73° angle, the appearance of the top 21° angle was observed after 1.50 μm deposition. Interestingly, it was observed, that the Ga adatoms tended to migrate in greater proportion upwards to the top (001) whereas in the lower sidewall angle case, a lot of the migrating Ga atoms are incorporated on the bottom facet.

In conclusion, it can be seen that for the growth of GaAs patterned substrates, the dominant facet present during the early stages of growth appears to be the {110}, and as growth proceeds, a bottom {310} facet starts developing which eventually leads to the overgrowth of the ridge structure. A trench was apparent during the first stage of growth, helps prohibit the evolution of the bottom facet, but for the later stages, it becomes overgrown allowing the upward development of the bottom facet. Therefore, the Ga adatoms at the initial stages of growth are directed mostly upwards, until the bottom {310} facet becomes available whereby the adatom flux direction changes. By contrast, growth using ~90° sidewalls, because of the extended presence of the trench blocking any adatom migration from the base areas surrounding the ridges, limited the {110} facet overgrowth and produces longer facets.

CHAPTER 5

Influence of the Growth Conditions on GaAs Deposition on Mesa Stripes.

5.1. Introduction.

Substantial work has been focused on achieving high quality growth on patterned substrates, but few studies have investigated the detailed surface morphology for a wide range of growth conditions as a function of the quantity of the material deposited. This provides the basis for obtaining a better understanding of the growth kinetics and the effect of the deposition conditions on the Ga adatom diffusion behaviour. In this work, the emphasis is on GaAs growth on mesa structures with ~73° sidewalls using different substrate temperatures, Ga fluxes and As species. The use of a higher Ga flux (0.5 μm/h)/(lower V/III ratio) and a lower substrate temperature (480°C), compared to 0.25 μm/h flux and 570°C used previously, provides an effectively lower and higher V/III ratio respectively, and revealed some interesting changes in the evolving morphology of the ridge stripes. In addition, the change from As_4 to As_2 species provided useful information on the Ga adatom diffusion on the mesa ridges. The initial part of this chapter deals with the effects of increasing the incident Ga flux on the 5 μm and 15 μm stripes with increasing deposition quantity. The second section concentrates on the effect of decreasing the growth temperature for the same quantity of deposited material. The third part focuses on the change of incident As species from As_4 to As_2, for low Ga flux rate and the final segment investigates the growth using an As_2 flux at a higher Ga flux rate.

5.2. Experimental Details.

The experimental conditions were similar to the ones used in chapter 4. Three separate sets of samples were grown. The first set was grown under a higher (than chapter 4) Ga flux (0.5 μm/h) with different deposition quantities (0.25 μm-1.5 μm) and a substrate temperature of 570°C. The second set of samples was

grown using a lower Ga flux of 0.25 μm/h for the same deposition quantities and a lower growth temperature of 480°C. The third set of samples was grown using an As_2 flux whilst keeping the other growth parameters the same. The samples were analysed with SEM and AFM, *ex-situ,* after growth.

5.3. Growth Using a 0.5 μm/h Ga Flux at 570°C.

The patterned mesas had an average height of 1.30 μm and were 100 μm long, as in the previous chapter. The width of the 5.00 μm stripe was reduced after etching to ~2.70 μm as measured by AFM. Figure 5.1 shows the morphology of a 5 μm mesa after the deposition of 0.25 μm of GaAs at 0.50 μm/h Ga flux.

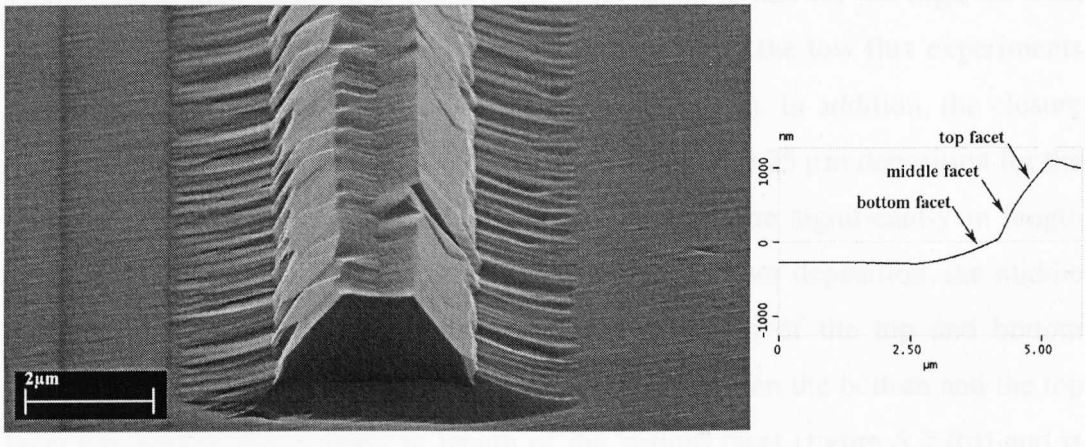


Figure 5.1. SEM image of a 5 μm ridge after 0.25 μm GaAs deposition at 0.50 μm/h Ga flux, 570°C. On the right hand side an AFM cross-section of the ridge.

There are three facets present; the top facet had an angle of 43°, the middle facet an angle of 56° and a bottom 14° facet. The {110} top facet appears to be rougher than the lower Ga flux experiments. The SPE at the top edges of the ridge is clearly visible. Interestingly the middle facet has reduced quite significantly in length when compared with the lower Ga flux experiments.

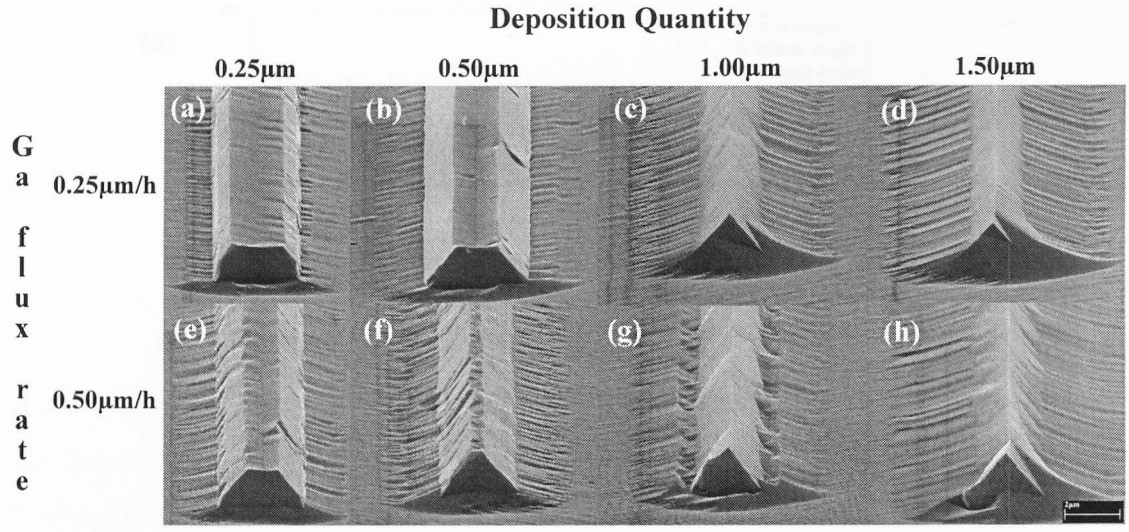


Figure 5.2: SEM images for the (a-d) low Ga flux and, (e-h) high Ga flux at for different GaAs deposition quantities.

Figure 5.2 shows SEM images of the 5 μm ridges taken at both fluxes and various deposition quantities. The overall observation is that for the high Ga flux, the {110} top facet appears to be rougher compared with the low flux experiments – especially for the first two depositions (figure 5.2(e, f)). In addition, the closure of the ridges occurs faster as expected. In more detail, at 0.25 μm deposition for the high flux experiments the middle facet has reduced quite significantly in length compared with the low flux (figure 5.2(a, e)). Upon further deposition, the middle facet disappears with the subsequent increase in length of the top and bottom facets. However, the trench that frequently appears between the bottom and the top facet has limited the increase in length of the bottom facet (figure 5.2 (b)) and is still present after 1.00 μm deposition for the 0.50 μm/h Ga flux. The ridge was completed after the 0.75 μm depositions i.e. earlier than for the lower flux and the overgrowth of the ridge is more prominent. The middle facet disappears after the deposition of 0.25 μm for both fluxes.

Quantitative results of the evolution of the morphology for the higher flux experiments are shown in figure 5.3 which presents plots of the facet angle (a) and facet length (b) versus the deposition quantity for the 5 μm ridge.

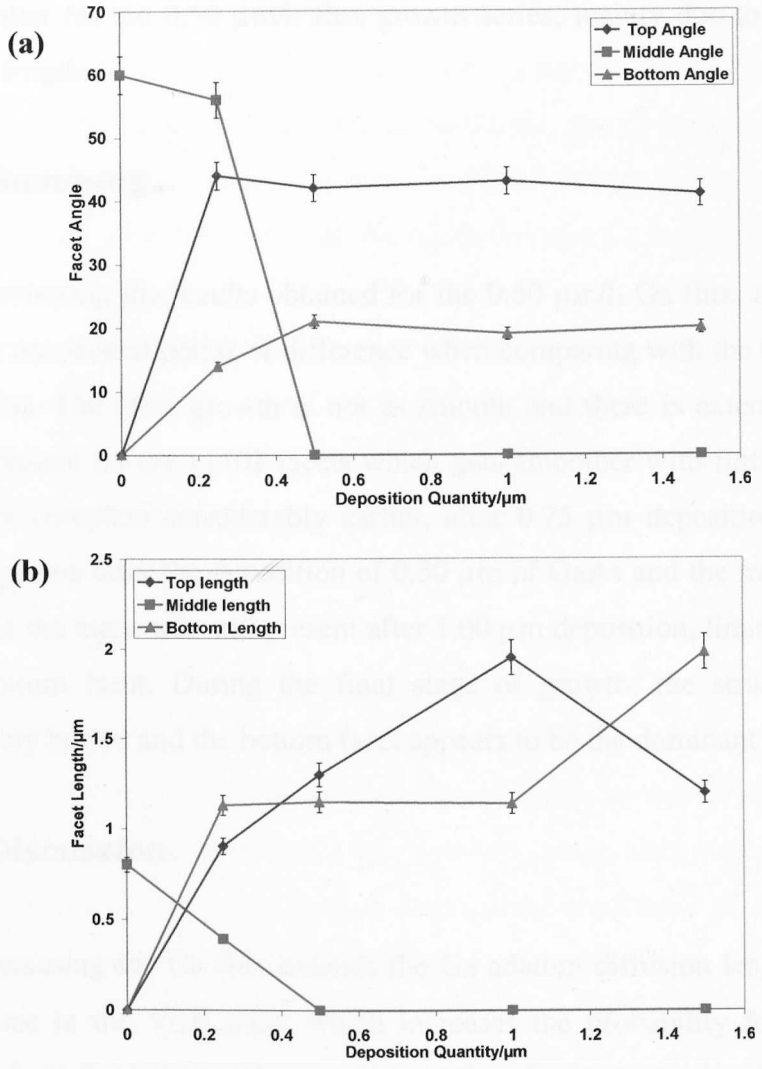


Figure 5.3. Plot of (a) facet angle and (b) facet length as a function of GaAs deposition quantity. The data were obtained from AFM measurements taken from growth on the 5 μm ridges. The facets are divided into: ◆ top; ■ middle; and ▲ bottom.

The top facet for the 5 μm wide ridges remains stable throughout the growth at approximately 43°. The bottom facet appears to have a constant angle of 19° and the middle facet having initially a lower angle due to etching differences, disappears after the deposition of 0.25–0.50 μm GaAs. The top facet length increases throughout the growth series until reaching a maximum after 1.00 μm deposition (figure 5.3 (b)). After the deposition of 1.00 μm GaAs, it reaches its longest value suggesting that most of the Ga adatoms migrate towards the top (001) plane and that there is a reduction in the bottom facet length because of the presence of the trench. Upon further deposition, the top facet decreases, the trench disappears and the bottom facet dominates this stage of growth. The SPE appears

to be smaller for the 0.50 μm/h flux growth series, mainly due to the higher Ga diffusion length.

5.3.1. Summary.

Reviewing the results obtained for the 0.50 μm/h Ga flux, at 570°C under As_4, there are several points of difference when comparing with the 0.25 μm/h flux experiments. The facet growth is not as smooth and there is extensive triangular faceting present on the {110} facets which gets smoother with further deposition. The ridges complete considerably earlier, after 0.75 μm deposition. The middle facet disappears after the deposition of 0.50 μm of GaAs and the trench formed at the base of the mesa was still present after 1.00 μm deposition, limiting the growth of the bottom facet. During the final stage of growth, the structure becomes considerably buried and the bottom facet appears to be the dominant one.

5.3.2. Discussion.

Increasing the Ga flux extends the Ga adatom diffusion length because of the decrease in the V/III ratio, which increases the probability for Ga adatoms migrating from the {110} to the top (001) surface for incorporation. In principle, as already mentioned in Chapter 4, the 5 μm stripes should complete after the deposition of ~0.68 μm of GaAs, provided that all Ga diffuses to the top (001) plane. This is very close to the point that ridge completion occurs in this series of samples i.e. ≤0.75 μm, suggesting that most of the Ga migrates towards the ridge top at least until 0.75 μm of GaAs was deposited. As a consequence, this also limits growth on the {110} facets, which explains the roughness observed throughout this growth series. This roughness is seen in the form of triangular faceting, which was previously observed by Holmes *et al.* [14] and Tok and co-workers [15], who have investigated GaAs growth on planar (110) surfaces– also discussed in section 1.4. It was found that for low V/III flux ratios, the triangular faceting was more prominent and the triangular features were oriented along the <112> and <110> step directions.

The bottom facet evolution seems to be suppressed for the 0.50 μm/h Ga flux experiments, until the 1.00 μm deposition. A possible reason for this

behaviour could be the large Ga adatom diffusion length, which sustains the trench until the last stages of growth and therefore prohibits the development of the bottom facet. The sufficiently low As concentration, due to the low V/III flux ratio provides greater freedom for Ga adatoms to diffuse further across the mesas to the most favourable sites. This leads to the much reduced Ga incorporation at the As depleted area between the top and the bottom facet sustaining the trench until later stages of growth compared with the low Ga flux experiments. The appearance of this trench prohibits the bottom facet growth sufficiently and therefore limits the overgrowth of the stripe by the {310} bottom facets. Similar results were observed for the growth on 90° sidewalls, where the trench was present throughout the growth hence the overgrowth of the stripe was limited [48].

There was, however, a small irregularity in the results of this investigation, the reason is that two different *as-etched* wafers were used to carry out the sample growth for the series. The first was used for the 0.25 μm, 0.50 μm and 0.75 μm depositions and this initial wafer had sidewalls which measured an angle of 60°, rather than 73° that was used in all other growth series. This was unexpected and was most probably due to changes in the ambient conditions of the clean room facility used to carry out the wet chemical etching procedure. Nonetheless, this unfortunate change to the original sidewall angle has proved to be a useful aid to our understanding of the effect of the initial sidewall angle on the growth kinetics.

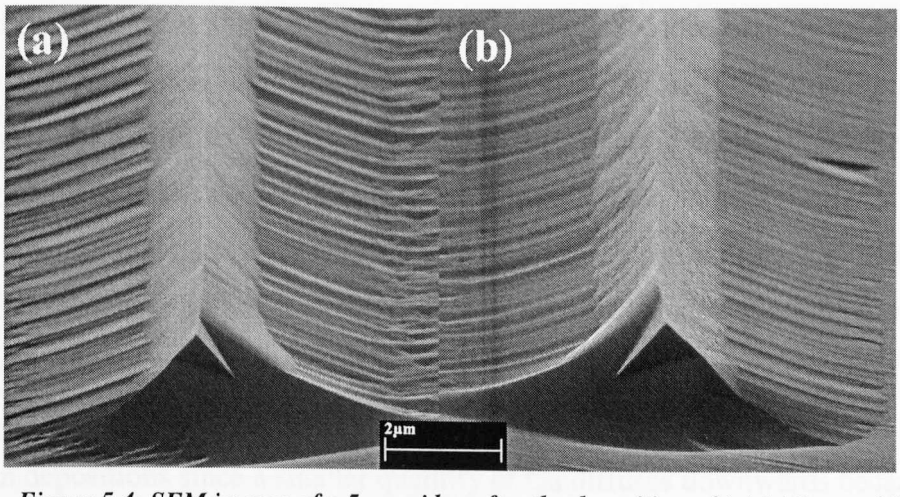


Figure 5.4: SEM images of a 5 μm ridge after the deposition of (a) 1.50 μm of GaAs at 0.25 μm/h Ga flux and (b) 0.75 μm at 0.50 μm/h Ga flux.

After the deposition of 0.75 μm of GaAs for 0.50 μm/h Ga flux at a substrate temperature of 570°C, there was a considerable decrease in the facet angle and length which was comparable to 1.50 μm of deposition quantity for the 0.25 μm/h Ga flux experiments (figure 5.4).

Growth under the higher Ga flux reduces the V/III ratio, increasing the Ga diffusion length, and consequently Ga adatoms can travel greater distances and incorporate at more favourable lattice sites. In this case, the most energetically favoured planes for incorporation are the (001) and the {310} [35,44]. This leads to a faster ridge completion and the overgrowth of the base of the {110} facets. However, this may not be the only reason to explain such rapid completion and overgrowth. The initial sidewall angle of 60° is a less favourable facet than the (001)/{310} surfaces but more kinetically favoured than the {110} facets. For that reason, the angle reduces during growth in order to increase the (001) nature of the growing surface. Increasing the As quantity reaching the surface makes it more favourable for GaAs formation. Finally, this facet is consumed by the {310} facet. Since the initial angle of 60° is less steep, the trench that normally forms because of shadowing from the top {110} facets extending outwards, is not present and consequently there is a greater chance of the bottom facet starting to dominate the ridge growth, leading to the burial of the stripe at this early stage (0.75 μm deposition). Conversely, for the 1.00 μm deposition growth in the series, the sidewall angle had the "normal" *as etched* value of 70°. SEM and AFM images showed an increase in the {110} facet angle and length, a decrease in the length of the {310} bottom facet and the trench re-appearing. This suggests that the normal facet evolution would follow this trend rather than the one observed for the first 3 depositions, due to the shallower than usual sidewall angle.

The same general observations apply for the 15 μm stripes. The difference being that the ridges do not close off, which is expected since the material required for completion is greater than 1.50 μm of GaAs, as explained in Chapter 4. In addition, the bottom facet length is shorter that its smaller ridge equivalent for the 1.50 μm depositions since a smaller quantity of Ga diffuses downwards because the top (100) plane is still available for growth.

5.4. Growth using a 0.25 μm/h Ga Flux at 480°.

In a further set of experiments, the effects of substrate temperature on 73° sidewall mesa stripes was investigated. The samples were grown in an identical way to those described in Chapter 4, except that the substrate temperature used was reduced to 480°C. The decrease in temperature significantly reduces the Ga adatom diffusion length, leading to changes in the facet evolution.

Figure 5.5 shows a SEM image of a 5 μm ridge after the deposition of 0.25 μm GaAs. Two primary facets are present the upper {110}, and the middle with an angle of 69°. There is also a very small bottom facet, measured to have an angle of 13°. The top facet being is short relative to the higher temperature growth and the middle facet well defined. The {110} facet is smoother than it's higher temperature equivalent. Moreover, the {110} facet appears to be growing slightly outwards.

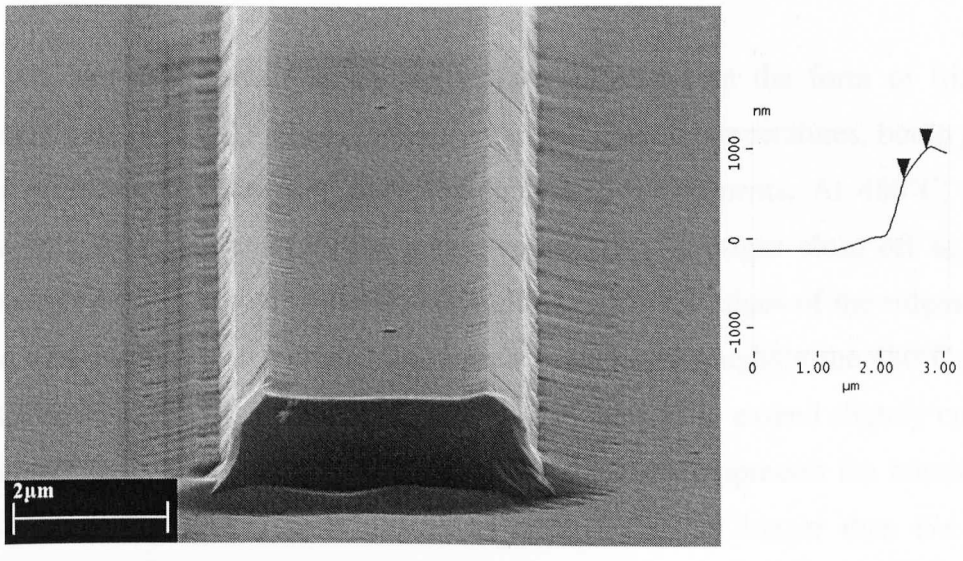


Figure 5.5. SEM image of a 5 μm ridge after the deposition of 0.25 μm of GaAs at 480°C. The Ga flux is 0.25 μm/h. On the right hand size is an AFM cross-section of the ridge.

Figure 5.6 shows SEM images of the resulting 5 μm ridges after the deposition of 0.25–1.50 μm GaAs, at a substrate temperature of 480°C (a –d) and 570°C (e– h).

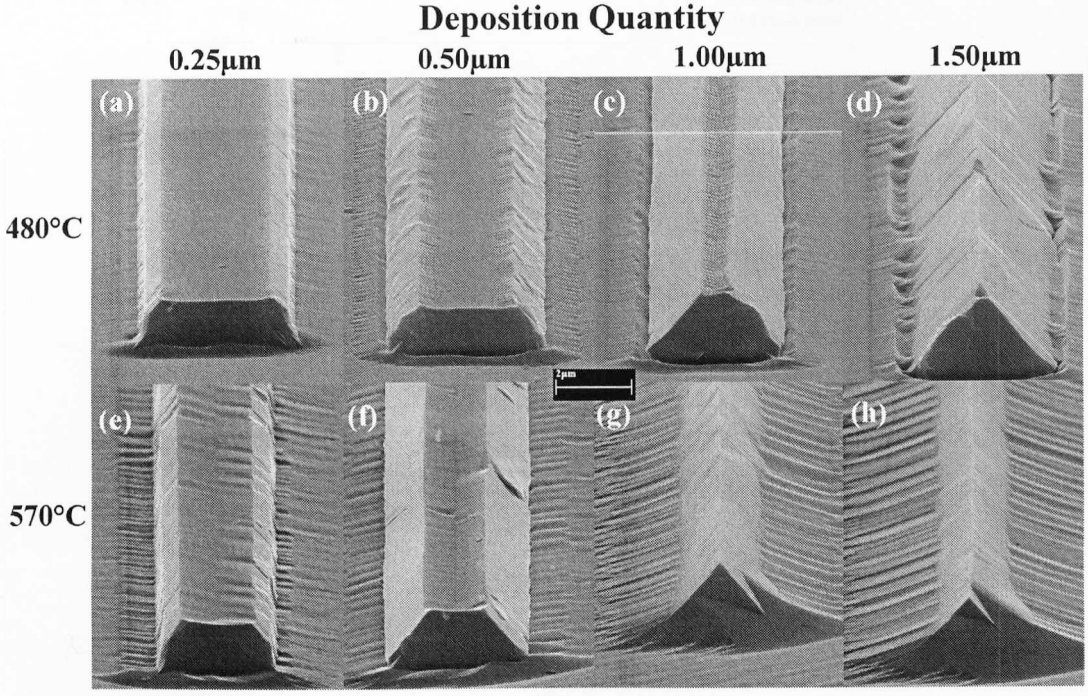


Figure 5.6: SEM images for (a-d) low temperature growth (480°C) and, (e-h) 570°C growth at various GaAs deposition quantities.

For this growth series, the surface roughness in the form of triangular faceting on the {110} planes is similar for both growth temperatures, but in general the surface roughness is greater for the 570°C experiments. At 480°C, growth exhibits slower facet evolution and consequently the ridges close off at a later stage. In addition more material accumulates at the top edges of the ridges due to the SPE (figure5.6 (b)) effect. The trench is present throughout the 480°C growth experiments. In greater detail, the {110} facet appears to extend slightly outwards (figures (a, b, c)) forming a large trench which then suppresses the bottom facet evolution. The {110} facet appear to be considerably longer than it's higher temperature equivalent (figures 5.6 (d, h)).

AFM measurements for this growth series provided quantitative results of the evolving ridge morphology for 480°C growth series. Figure 5.7 demonstrates this variation with plots of both facet angle (a), and facet length (b), for the 5 μm ridges.

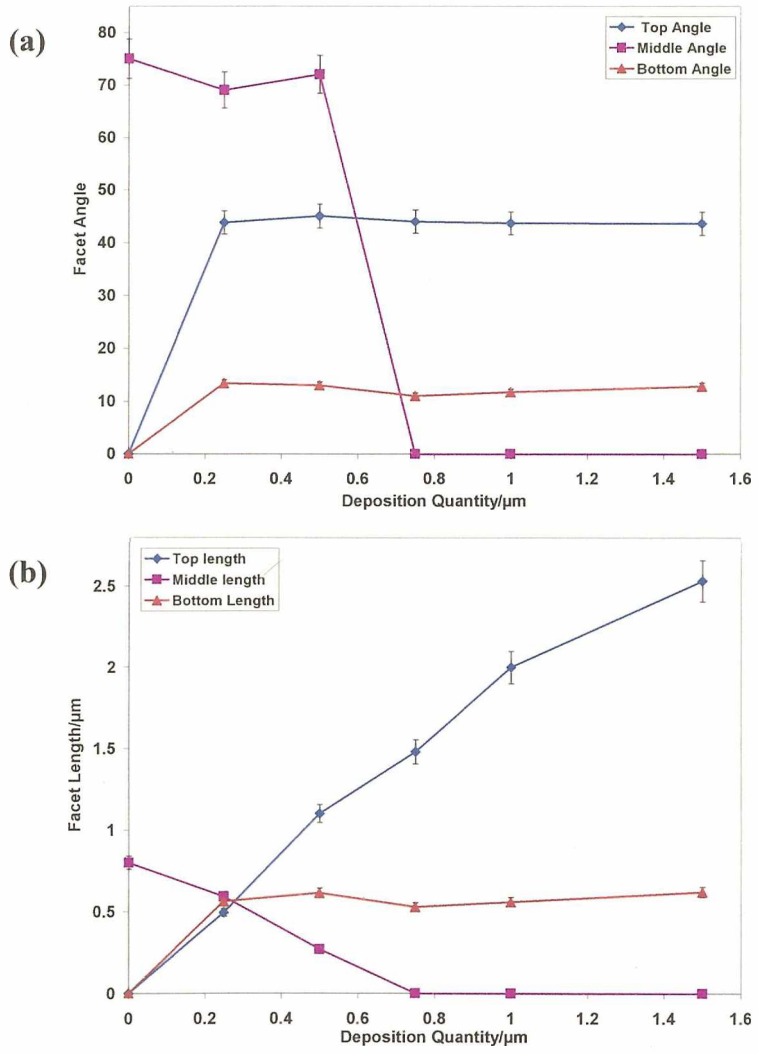


Figure 5.7. Plot of (a) facet angle and (b) facet length as a function of GaAs deposition quantity. The data were obtained from AFM measurements taken from growth on the 5 μm ridges for the 480°C growth temperature. The facets are divided into: ◆ top; ■ middle; and ▲ bottom.

It can be seen that the facet angle remains stable at around 45° throughout the growth series, which is due to the fact that the ridges only close off between the 1.00–1.50 μm deposition. Thus the (001) top plane was always available, and the length of the {110} facets increased continually, until it reached the longest value observed during these investigations: 2.5 μm. The ridge structure was therefore not buried, nor did the {110} facets overgrow from the bottom facet. The bottom facet did not increase in angle, or length, but remained at 13° and 0.60 μm respectively. Indicating that at 480°C, the Ga was trapped on the {110} planes and could not reach part of the lower edge to form a bottom facet, aided by the {110} overhang making a big trench. The middle facet decreases slightly in angle and length after

0.25 μm deposition. However, after deposition of 0.75 μm of GaAs, the facet angle increases. This is additional evidence along with the SEM observations that the {110} facet grows outwards. With continued deposition, the middle facet remained present, but became steeper after each deposition, until 1.00 μm has been deposited. Unfortunately, the AFM cannot follow this facet evolution accurately due to tip limitations caused by the {110} overhang, which was discussed in section 2.5.2.

The 15 μm ridges also demonstrated similar trends and a maximum measured {110} facet length.

5.4.1. Summary.

The following trends were observed for the growth experiments at a substrate temperature of 480°C. The facet evolution was slower than for the 570°C series, and the ridge completion occurred at 1.00 μm deposition. The surface smoothness was better than the 570°C temperature results, and the SPE more prominent. A trench between the top and middle facet was present throughout the growth series and the top {110} facet was observed to expand outwards, resulting in a more steeply angled middle facet. The bottom facet has been efficiently suppressed by the trench and does not facilitate overgrowth.

5.4.2. Discussion.

When the growth temperature was decreased to 480°C, at a Ga flux of 0.25 μm/h, under an As_4 flux, the Ga adatom migration length decreased considerably. This provides more information on the facet evolution. Since the Ga adatoms landing on the {110} facets have a lower escape probability, due to their smaller diffusion lengths, the {110} planes grow more effectively. Ridge completion is therefore slower than for other experiments, because a larger proportion of the arriving Ga adatoms incorporate into the {110} facets, rather than migrating off them, upwards to the (001) plane. This reduced Ga mobility causes the relatively large SPE observed at the top edges of the ridge, observed in the SEM and AFM investigations, since the lower Ga diffusion length prevents Ga adatoms migrating

large distances, away from the ends of the {110} facets. This forces a build up of material near the edge of the ridge top.

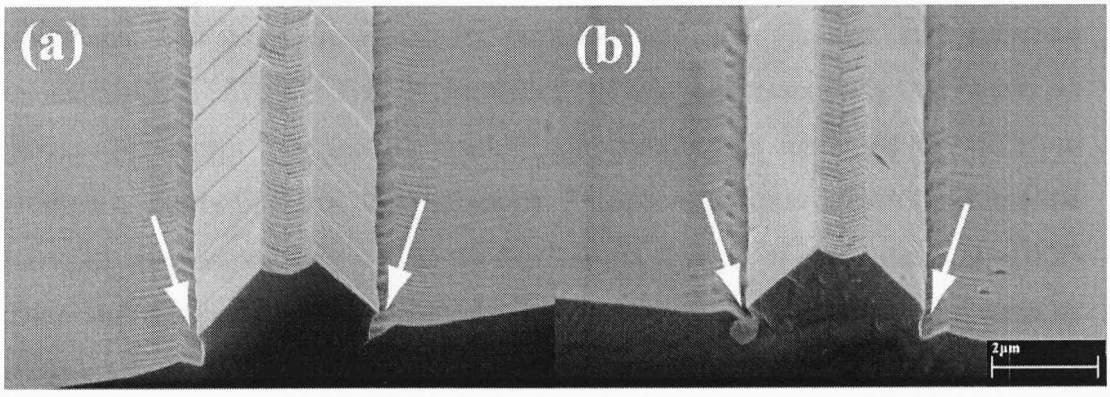


Figure 5.8. SEM images of a cleaved 5 μm ridge after the deposition of (a) 0.75 μm and (b) 1.00 μm of GaAs at 480°C.

Cleaved SEM images of a 5 μm ridge after the deposition of (a) 0.75 μm and (b) 1.00 μm at 480°C substrate temperature are shown in figure 5.8. It can be seen that the middle facet is steeper than the initial sidewall. This is most likely to be caused by Ga adatoms incorporating into the {110} facets causing them to extend in a parallel direction for the reasons explain above. However, the AFM cannot follow this observation since the facet is actually inclining inward and the tip cannot access this area of the structures. Development of large {110} facets causes additional shadowing of the source As flux (discussed in section 4.5.3) to base areas of ridges, forming a deeper trench. This inhibits the expansion of the bottom facet and hence limits the onset of the overgrowth of the base of the ridge. As a consequence, the {110} facets during the 480°C growth series, are the longest observed for all experiments undertaken, after the 1.5 μm deposition. This observation is in agreement with the work done by Tok *et al.* in which low temperature and high V/III ratios are the best conditions for (110) planar growth [7,15].

5.5. *Effect of As_4 and As_2.*

Both As_2 and As_4 species were used as incident fluxes for growth at 0.25 μm/h and 0.50 μm/h Ga fluxes for both low and high Ga flux at a substrate temperature of 570°C. The experimental details are essentially the same as previously, except that the As cracker temperature was increased to 965°C to produce a steady beam of As_2 molecules. The valve position was 300mil and the substrate temperature 570°C. The Ga flux for the first set of experiments was 0.25 μm/h and 0.50 μm/h for the second. The deposition quantities were the same as those used previously.

5.5.1. *Growth Using 0.25 μm/h Ga Flux at 570°C, Under As_2.*

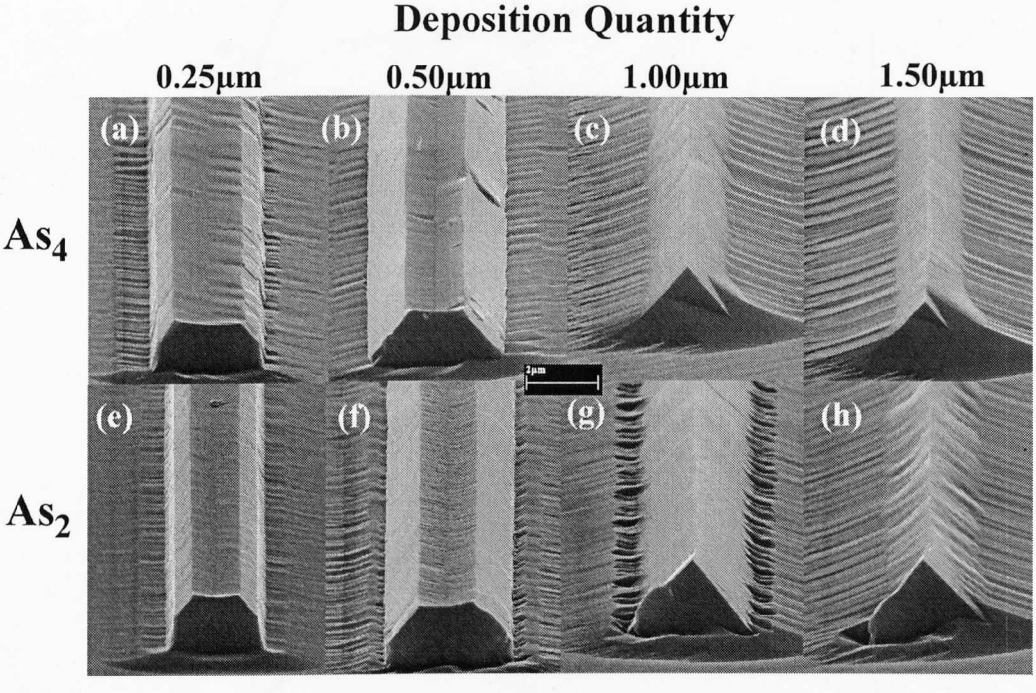


Figure 5.9: SEM images of a 5 μm ridges under As_4 (a, d) and As_2 (e, f) at different deposition quantities.

As seen in figure 5.9, growth under As_2 (e- f) produced smoother ridges with less triangular faceting on the {110} facets. The {110} facet evolution appears to be somewhat slower when compared with the As_4 series figures 5.8 (b, c) as the middle facet for the As_2 series is still present. The SPE affect appears to be slightly less prominent for the As_2 series. The trench is still noticeable until the 1.00 μm

deposition resulting in the suppressed bottom facet development. The {110} facets are longer for the As_2 growth series for the equivalent deposition quantity (figure 5.9 (g, h)).

For the quantitative information on the 5 μm stripes, figure 5.10 shows the evolution of the facet angle (a) and facet length (b) with increasing deposition quantity as measured by AFM.

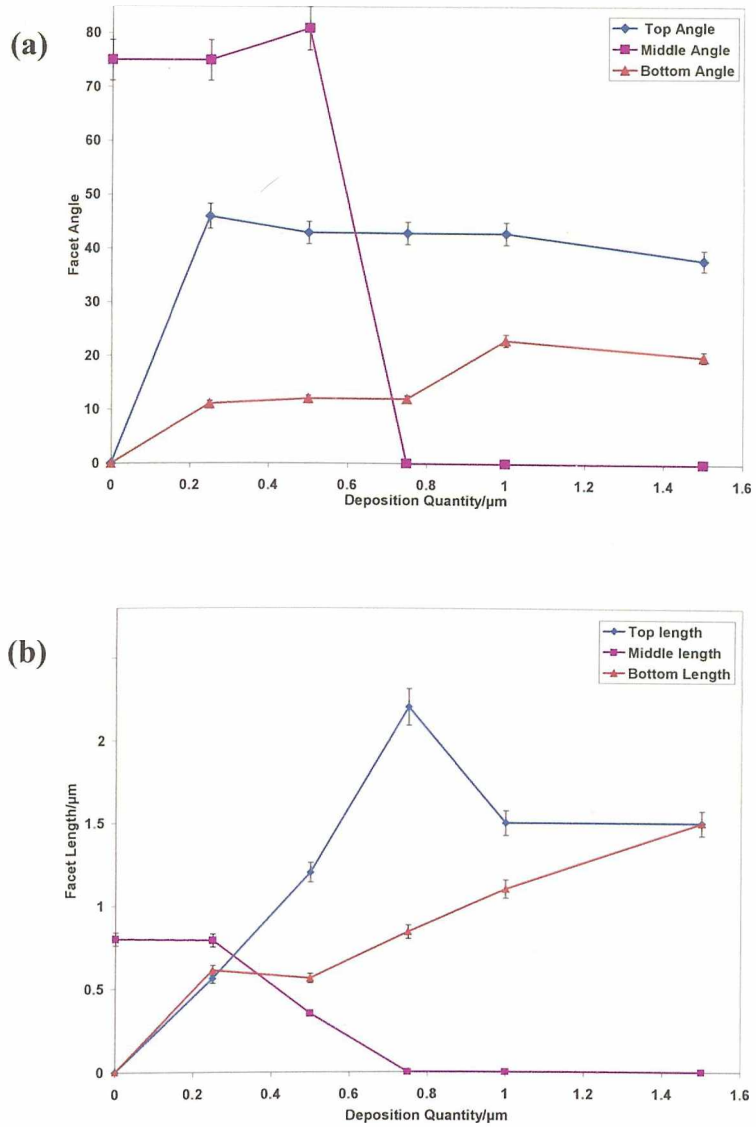


Figure 5.10. Plot of (a) facet angle and (b) facet length as a function of GaAs deposition quantity. The data were obtained from AFM measurements taken from growth on the 5 μm ridges for the 570° growth temperature under As_2. The facets are divided into: ◆ top; ■ middle; and ▲ bottom.

For the middle facet, it can be seen that there is a slight increase in the angle after the 0.50 μm deposition, suggesting that there is a possibility the ridge grows

outwards. However, even though the AFM measurement at this point could be misleading due to tip limitations, SEM imaging verified this observation. The {110} facets angle, remains at a constant value up to the 1.50 μm deposition, whereupon it decreases slightly. The {110} facet length reaches a value of ~2.2 μm after 1.00 μm deposition, at which point it decreases. Interestingly, this is the point where the trench that formed early in the growth has started diminishing. The bottom facet length values are generally lower for the As_2 growth series; as an example the value for the bottom facet after the 1.00 μm deposition is 1.10 μm for the As_2 series and 1.70 μm for the As_4 series. This is most probably mainly due to the presence of the trench at this late stage of growth for the As_2 series.

5.5.1.1 Summary.

For the As_2 growth series under 0.25 μm/h Ga flux growth series, the following observations were made:

i) The top facet extended continuously with increasing deposition quantity reaching a maximum value of 2.2 μm after 0.75 μm, whereupon, it deceased significantly. The SPE is visible during all the depositions but less prominent than for the equivalent As_4 series as seen in SEM images.

ii) The middle facet shows a slight increase in angle after the 0.50 μm deposition, suggesting a slight outward extension of the {110} facet.

iii) A trench is present for the first four depositions, which slows the ridge overgrowth.

iv) The bottom facet length gradually increases, followed by a more rapid increase for the last two stages of growth after the trench has disappeared.

v) For the 15 μm ridges, the facet evolution trends are analogous. However, the ridges are not completed, as expected, and after the final deposition quantity the bottom facets are longer than those observed for the 5 μm ridges, suggesting faster overgrowth.

5.5.1.2 Discussion.

Changing the As species has some interesting consequences with regard to the {110} facet evolution. When the As_4 is converted to As_2 by thermal cracking, the maximum As sticking coefficient increases from 0.5 to 1 [9,10]. By keeping the number of As atoms constant, it was found by Ogura [36] that the diffusion length of Ga on the (001) decreases with a higher As_2/As_4 ratio. It was also found that the As_2 molecules are incorporated easier than As_4 in the GaAs epilayer Ogura *et al.* [133]. As already mentioned in 1.4, Holmes *et al.* [13] investigated the differences between As_2 and As_4 using RHEED oscillations on the GaAs (110) and found that RHEED oscillations were obtained over a much wider range of conditions for As_2 and that the use of As_2 produced smoother surfaces.

The reduction of the Ga adatom diffusion length, due to increase of the V/III ratio, has almost the same effect as reducing the substrate temperature. Thus, at a high V/III ratio/low substrate temperature, a larger proportion of the Ga landing on the {110} facets gets incorporated, and the facet grows slightly outwards leading to the shadowing of the middle facet. Figure 5.11(a), which shows a cleaved SEM image of a 5 μm ridge after the 0.50 μm deposition, demonstrates the change to the middle facet, which appears to be steeper than the initial 73° sidewall.

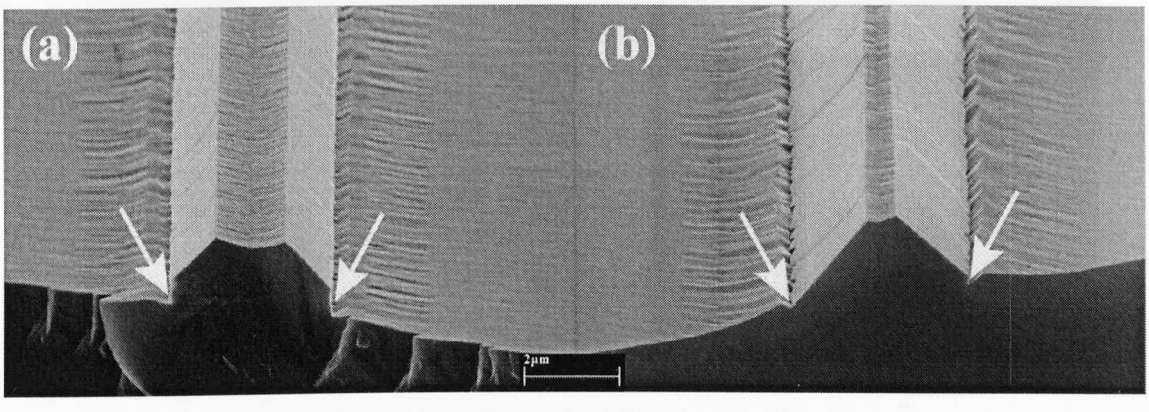


Figure 5.11. SEM images of a cleaved 5 μm ridge after the deposition of (a) 0.50 μm and (b) 0.75 μm of GaAs at 570°C under As_2.

Figure 5.11(b) shows the ridge after 0.75 μm deposition. The trench at the mesa base is large since the outward extension of the {110} facets shadows the

base area of the mesa, from the incoming As flux, so that Ga incorporation in this region is severely limited due to the V/III ratio being too low. The longest {110} facets are observed for the 0.75 μm deposition, even though the ridge is not completed, because with further deposition, the trench slowly fills in allowing Ga to migrate to the bottom facet and begin to overgrow the base of the ridge. This is an interesting point since it would be expected that the longest {110} facets would be the ones where the ridge is competed. This is not the case however, since the trench fills in after the 1.00 μm deposition and the bottom {310} facet has increased significantly and starts overgrowing the lower edge of the top {110} facets.

5.5.2. Growth Using a 0.50 μm/h Ga Flux at 570°C, under As_2.

In another set of experiments, the Ga flux was increased to 0.50 μm/h, keeping all other conditions the same. Increasing the Ga flux reduces the V/III flux ratio, which increases the Ga adatom diffusion length.

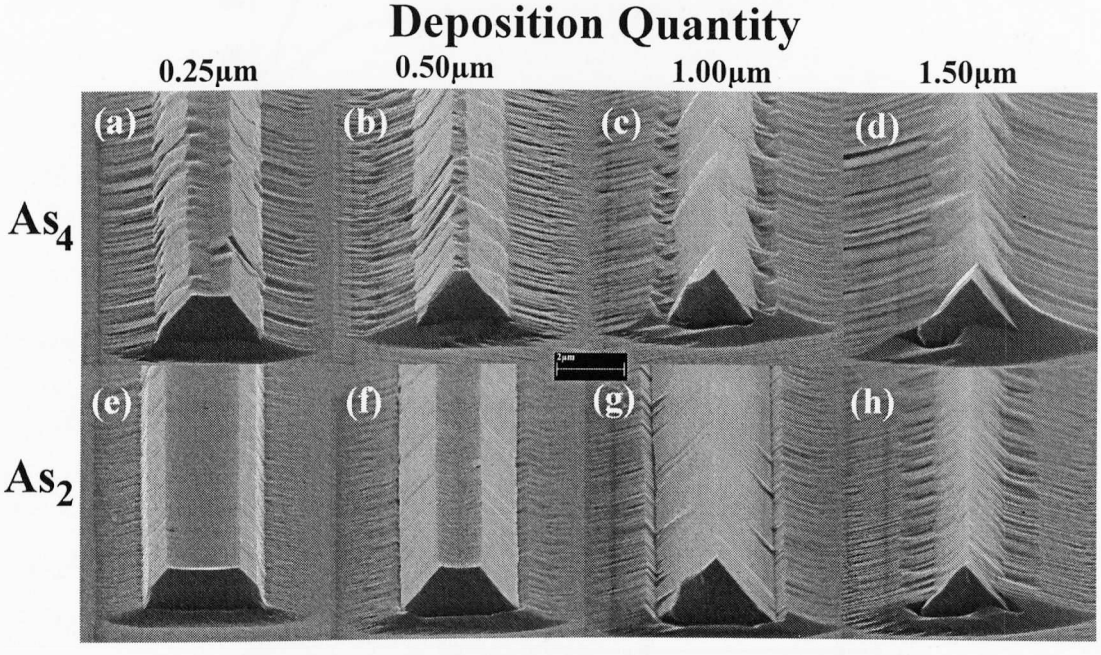


Figure 5.12: SEM images of 5 μm ridges after various depositions under As_4 (a–d) and As_2 (e–f) for 0.50 μm/h Ga flux.

Figure 5.12 shows SEM images comparing the As_4 versus the As_2 growth series for a 0.50 μm/h Ga flux. The As_2 growth appears to be smoother on the

general areas of the wafers, and forms less triangular roughness on the {110} facets. The facet evolution seems to be considerably slower, a good representative image being of the 0.50 μm deposition (figure 5.12 (b, f)). The ridges complete after 1.00 μm deposition, ~0.25 μm later that for the As_4 growth series. The SPE is present in both growth series, but somewhat more noticeable for the As_2 growth. A trench is present in all the depositions and only reducing after the 1.50 μm deposition. The longest and smoothest {110} facets for these two series are observed after the deposition of 1.00 μm for the As_2 series (figure 5.12 (g)).

Figure 5.13 shows facet trend for (a) angle and (b) length with increasing deposition quantity of the 5 μm stripes.

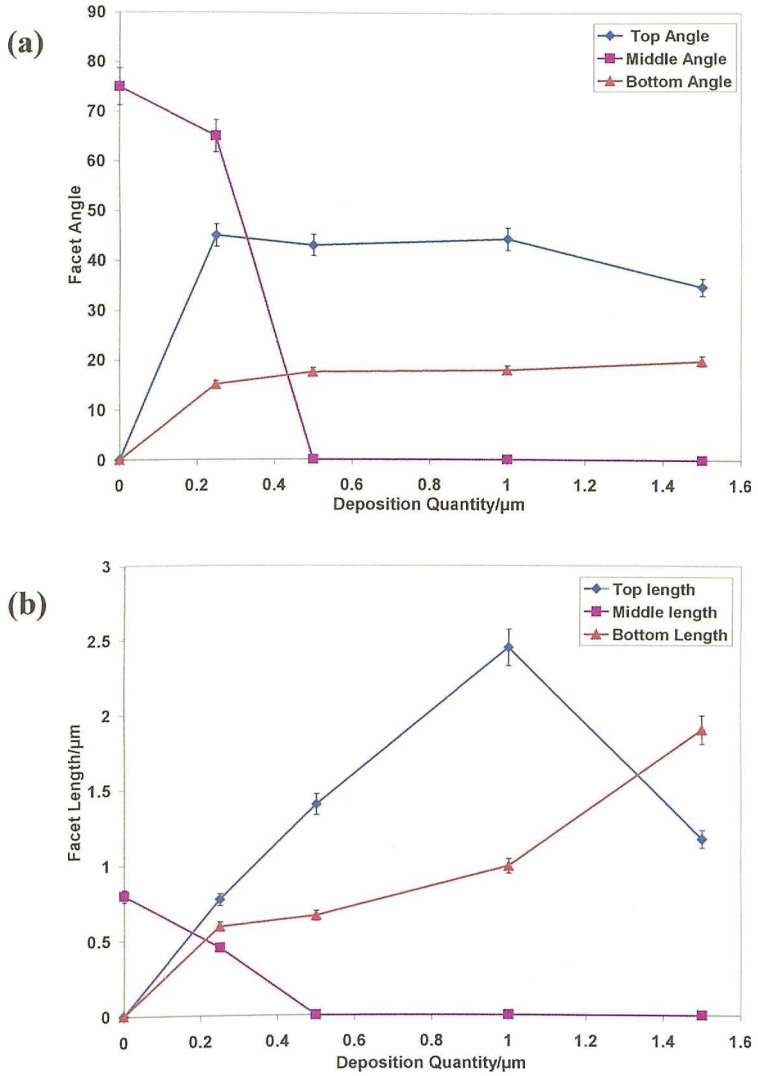


Figure 5.13. Plot of (a) facet angle and (b) facet length as a function of GaAs deposition quantity. The data were obtained for the 5 μm stripes for the 570° growth temperature under high Ga flux, under As_2. The facets are divided into: ♦ top; ■ middle; and ▲ bottom.

The middle facet angle and length decrease after 0.25 μm deposition and the middle facet disappears with further deposition. The top facet has an angle of 44° for the duration of the growth, until the last deposition whereupon it decreases. The facet length increases to reach a maximum value of 2.45 μm, the largest value observed for any series, with a close second that of the 480°C growth series. The bottom facet length increases with further deposition similarly, as it does for the As_4 growth series, which is interesting since after the 1.00 μm deposition for example, the {110} facet is also surprisingly long.

5.5.2.1. Summary.

For the higher Ga flux experiments under As_2, the growth was smoother and the facet evolution slower than for the As_4 series. The top {110} facet length increases with deposition quantity reaching its maximum value after 1.00 μm deposition. The facet evolution was slower than with As_4, giving ridge completion after 1.00 μm deposition. The trench was present throughout the growth finally being buried in after the 1.50 μm deposition. The same trends were observed for the 15 μm ridges, with the only difference being the increased {310} facet lengths after the final deposition, compared with the 5 μm ridges.

5.5.2.2. Discussion.

For the constant Ga flux and the use of a different As species growth series, the Ga adatom diffusion length for the As_2 growth series is smaller compared with the As_4 due to the increase in the effective V/III ratio. Thus the amount of Ga diffusing to the top (001) surface is greatly reduced leading to a slower facet evolution and subsequent ridge completion.

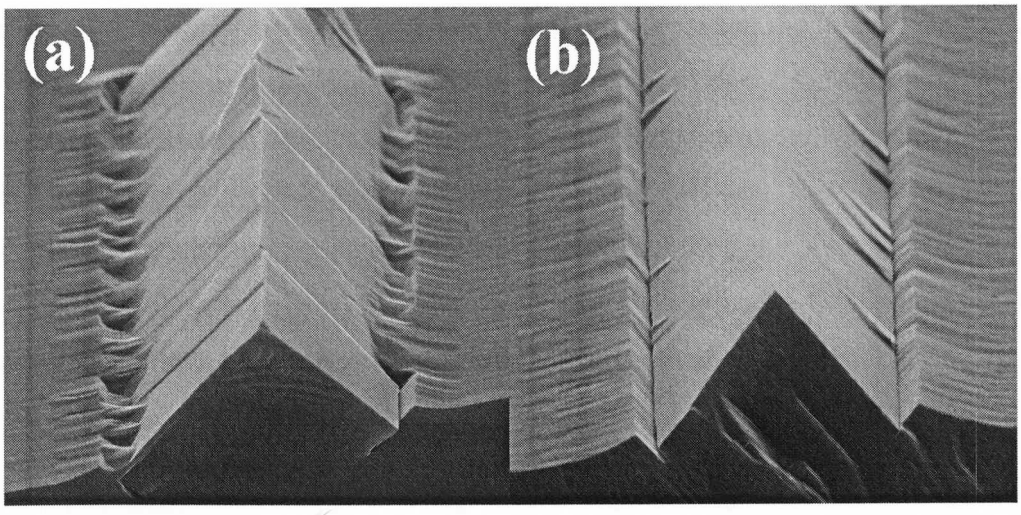


Figure 5.14: SEM images of cleaved 5 μm ridge for (a) the 480°C, As_4, 0.25 μm/h Ga flux, and (b) the 570°C, As_2, 0.50 μm/h Ga flux.

The relatively low Ga adatom migration length also suggests growth on the {110} facets which extend outwards. This is evident from the SEM images and shown in figure 5.14, a SEM image of cleaved samples for (a) the 480°C, As_4, 0.25 μm/h Ga flux and (b) for the 570°C, As_2, 0.50 μm/h Ga flux. These are the two sets of deposition conditions in which the longest {110} facets were formed. It can be seen in figure 5.14 (b), that at the base of the ridge, the {110} facets extend outwards as they did for the lower flux and temperature series where this phenomenon is more prominent (figure 5.14 (a)). In addition, the bottom facets in figure 5.14 (b), appear to be at a higher level than an imaginary extension to the {110} ones. This is the first observation of such a phenomenon and it is possibly due to the trench being extremely large so that is almost completely stopping growth at that point.

Moreover, the lower triangular faceting of the {110} facets is expected, since it has been seen previously that As_2 incorporates more efficiently and produces smoother surfaces.

5.5.2.3. Comparison Between High/Low Ga Flux for As_2 series.

Increasing the Ga flux under As_2, increases the ridge growth rate more than for the lower Ga fluxes, which is expected, as a result of the Ga migration length

increasing, allowing a larger proportion of Ga to migrate from the {110} facets to the top (001) plane. However, there is a competition between the increase in the Ga diffusion length due to the higher flux and the decrease of the Ga diffusion length due to the presence of As_2. Figure 5.15, shows the ridge evolution for the high Ga flux growth series which occurs, faster than for the low flux. However, the difference is not as apparent as that seen when comparing the As_4 growth for the high and low fluxes (figure 5.2). This could be a consequence of the change of As species to As_2 which counteracted the very fast ridge evolution.

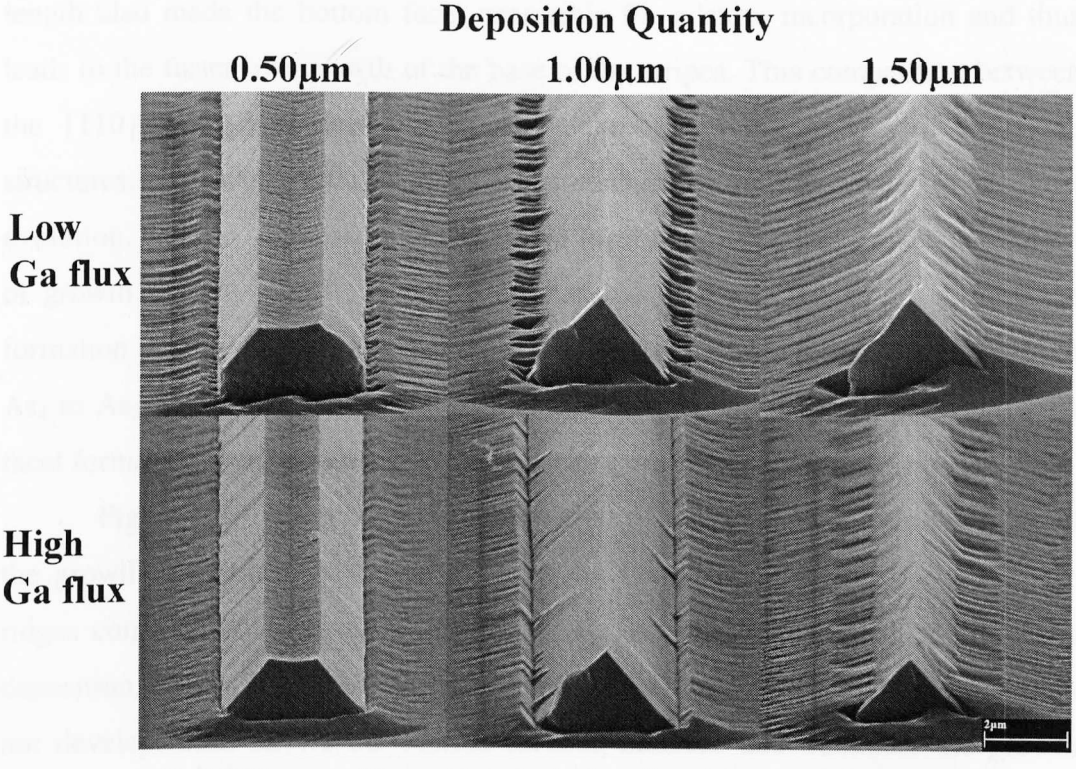


Figure 5.15: SEM images of 5 µm ridges the 0.25 µm/h and 0.50 µm/h Ga fluxes for As_2 experiments at various depositions.

The Ga diffusion length apparently is long enough to allow trench formation and thus suppression of the bottom facet but also short enough to prevent the extra roughness and quicker overgrowth of the ridge.

5.6. Discussion.

Investigating the effects of altering various factors that relate to the ridge growth conditions sheds more light onto the preliminary investigations presented in Chapter 4, for the growth on 75° sidewall patterned substrates. Increasing the Ga flux extends the Ga adatom diffusion length, which provides a higher probability for Ga adatoms to migrate to the top (001) surface for incorporation. This also limits growth on the {110} facets, which explains the roughness observed throughout this growth series. However, the increase of the Ga adatom diffusion length also made the bottom facet accessible for adatom incorporation and thus leads to the faster overgrowth of the base of the stripes. This competition between the {110} and {310} facets is apparent throughout the growth of the ridge structures. Decreasing the substrate temperature leads to much slower {110} facet evolution, and the suppression of the {310} facet domination during the last stages of growth. It also causes the outward extension of the {110} facets making the formation of a trench at the mesa base more likely. Changing the As species from As_4 to As_2 generated a smoother growth with longer {110} facets and less {310} facet formation and base area overgrowth.

Figure 5.23 is schematic representation of the ridge evolution for most of the growth conditions used. For the high Ga flux, 570°C, As_4 experiments, the ridges complete faster than for the other experiments, after only 0.75 μm GaAs deposition. However, due to the high Ga adatom migration length, the trench does not develop. This allows the bottom facet to increase and dominate the growth from an earlier stage, leading to greater overgrowth of the ridge bases. When the temperature and Ga flux rate were reduced, the ridges developed more slowly, due to the reduced Ga migration length, which allows the incorporation of Ga adatoms into the {110} facets causing them to extend outwards. This facilitates a rapid increase in size of the trench, which reduces the overgrowth of the ridge base by the bottom {310} facet. As a result, the {110} facets for these growth series are considerably longer than for the other experiments.

Changing the As species from As_4 to As_2, increases the As incorporation rate, reducing the Ga adatom diffusion length. Similar to the low substrate temperature growths, the increased Ga incorporation rate on the {110} facets leads

to a small outward extension of them. This was observed from the SEM images as the middle facet becomes steeper after 0.5 μm GaAs deposition. This is especially prevalent in the lower Ga flux experiment, since the ridge growth proceeds more slowly and the early stages of deposition have a better chance of being observed. Distinguishing between the low and high Ga flux under As_2, the ridge development is faster for the higher Ga flux experiments, since these have a larger Ga adatom diffusion length.

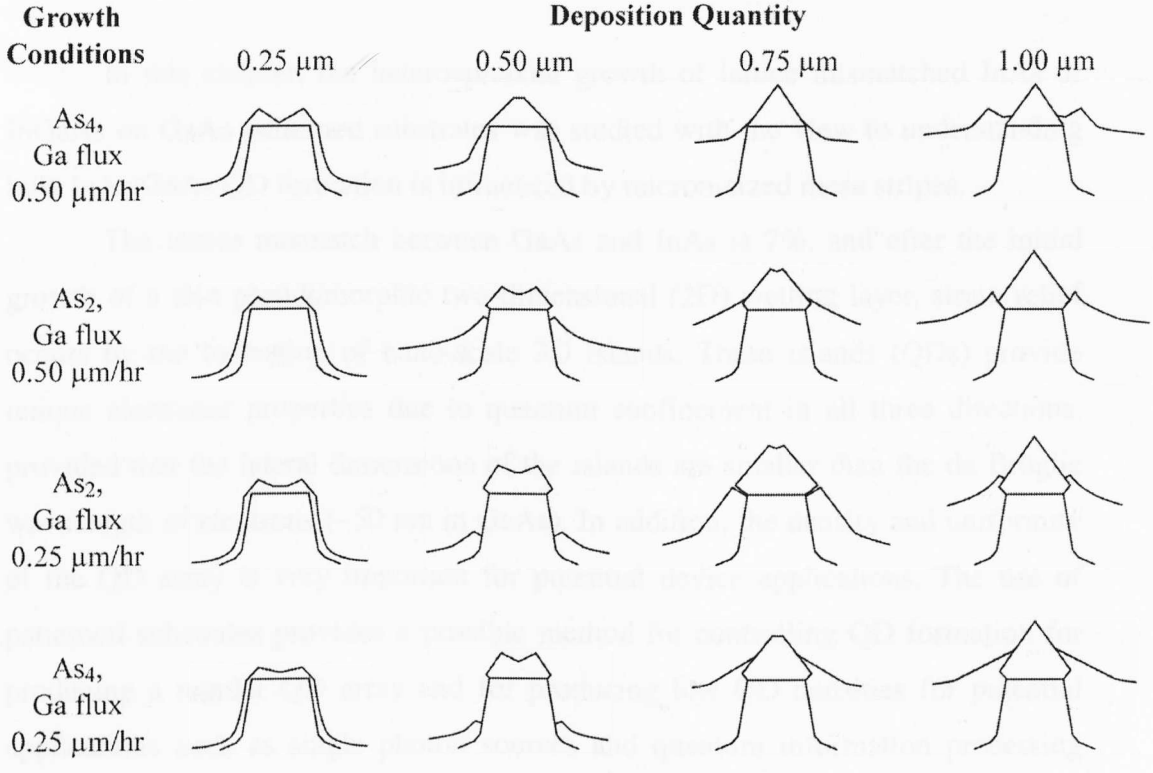


Figure 5.23. Schematic representation of the facet evolution for the different growth conditions investigated.

In conclusion, low substrate temperatures, and high V/III ratios, using an As_2 flux produces the longest {110} facets and the smoothest ridges, with the minimum amount of base overgrowth by the bottom {310} facets.

CHAPTER 6

Effect of Initial Mesa Width on InAs QD Formation.

6.1. Introduction.

In this chapter, the heteroepitaxial growth of lattice mismatched InAs or InGaAs on GaAs patterned substrates was studied with the view to understanding how InAs/GaAs QD formation is influenced by micron-sized mesa stripes.

The lattice mismatch between GaAs and InAs is 7%, and after the initial growth of a thin pseudomorphic two-dimensional (2D) wetting layer, strain relief occurs by the formation of nano-scale 3D islands. These islands (QDs) provide unique electronic properties due to quantum confinement in all three directions, provided that the lateral dimensions of the islands are smaller than the de Broglie wavelength of electrons (~50 nm in GaAs). In addition, the density and uniformity of the QD array is very important for potential device applications. The use of patterned substrates provides a possible method for controlling QD formation for producing a regular QD array and for producing low QD densities for potential applications such as single photon sources and quantum information processing [134-136].

For the initial stages of research though, the growth conditions and their affect on the formation of the QDs need to be addressed.

6.2. Experimental Details.

The structures were grown by solid source MBE on pre-patterned GaAs(001) semi-insulating substrates. The substrates were patterned using standard photolithography and wet chemical etching methods; producing mesa stripes of

widths ~2.7-12.7 μm (post-etch) and height ~ 1.4 μm aligned along the <100> direction, and with the sidewalls intersecting the (001) surface at ~85°. The cleaning procedure was the same as in Chapters 4 and 5. The substrates were subsequently annealed in the growth chamber to 620°C under an As_4 flux to remove any remaining oxide. The surface reconstruction was monitored using RHEED. Once a sharp (2×4) RHEED pattern was observed, a 0.3μm thick GaAs buffer layer was deposited at a Ga flux of 1 μm/h at 620°C, in order to improve the surface morphology and to prevent the undesirable influence of any residual surface oxygen. The buffer layer also provides {110} planes. For this growth series, the substrate temperature was dropped to 480°C. The QDs were formed by deposition of 2-6 ML InAs at 0.20 μm/h. The RHEED pattern was checked after InAs deposition and chevrons were observed for all samples, confirming the 3D growth needed for QD formation. During growth, all the samples were rotated at a speed of 12 rpm. After growth all samples were then removed from the growth chamber and were characterised using AFM and SEM. All AFM images required background subtraction or flattening but the data was otherwise unprocessed.

AFM measurements showed that the sidewalls were slightly rough and with a sidewall angle of ~90° and a tailing off at the bottom of the mesa. The AFM and SEM measurements were taken laterally along the <010> and $<\bar{1}00>$ directions. For each stripe, measurements were taken at three positions the top, middle and bottom laterally along the axis of the stripes. No clear differences were observed between these measurements and all values presented here are an average of these three.

Errors, Uncertainties and Instrument Limitations

The AFM measurements were performed using a contact mode technique and Non-HAR Nanosensors tips for contact mode. Most of the scans were of good quality and non-problematic. During some of the smaller scans sizes (down to 600 nm), despite the fact that all precautions were taken, the tip lost contact with the surface on occasions and jumped. This was due to the limitation of the scan area being similar to the width of the mesa stripe and since the mesas were 1.4 μm high, it sometimes proved very difficult to achieve high quality scans on the smallest mesa sizes. The error in density for the 15 μm stripe is estimated to be around

0.2×10^{10} cm^{-2}; for the 5 μm stripes it is 0.04×10^{10} cm^{-2}, for the 450°C growth and 3ML InAs coverage. However, since the scan size for the 5 μm stripes is considerably smaller, in the experiments where the dot density was low, the probability of no dots being present in some scans is greater. This especially applied to the 0.02 μm/h In flux experiments where all measured dot densities are very low.

6.3. *Effect of Different Mesa Widths on the In Adatom Diffusion.*

6.3.1. *General Observations for the Formation of QDs.*

The first set of experiments was performed in order to investigate InAs/GaAs island formation on different mesa widths under the same growth conditions and to compare it with the island formation on planar areas of the substrates away from the mesas.

Figure 6.1 shows AFM images for the flat region and on the central area of the 15 μm stripes for 2 ML, 4 ML, and 6 ML InAs coverage. It can be seen that the dot density increases with InAs coverage for both the flat region of the wafer and for the 15 μm stripes. No dots are present on the central area of the 15 μm stripe after 2 ML deposition, but they do appear with increasing InAs coverage. It can be seen that the large mesas behave similarly to the planar region for 4 ML and 6 ML coverage with QDs forming with similar size, though with somewhat smaller density. After the deposition of 6 ML of InAs, the dots coalesce for both the flat and the 15 μm stripes. The term *coalescence* here is defined as the merging of two or more 3D islands into the formation of a bigger 3D island. Dot formation can then be considered in stages; at first there is a dramatic increase in the number of 3D islands. In the second stage, these new larger islands start to merge, and a general roughness is apparent, as shown in figure 6.1 for the 6 ML coverage. At this higher coverage point the distinction between any two islands becomes extremely hard.

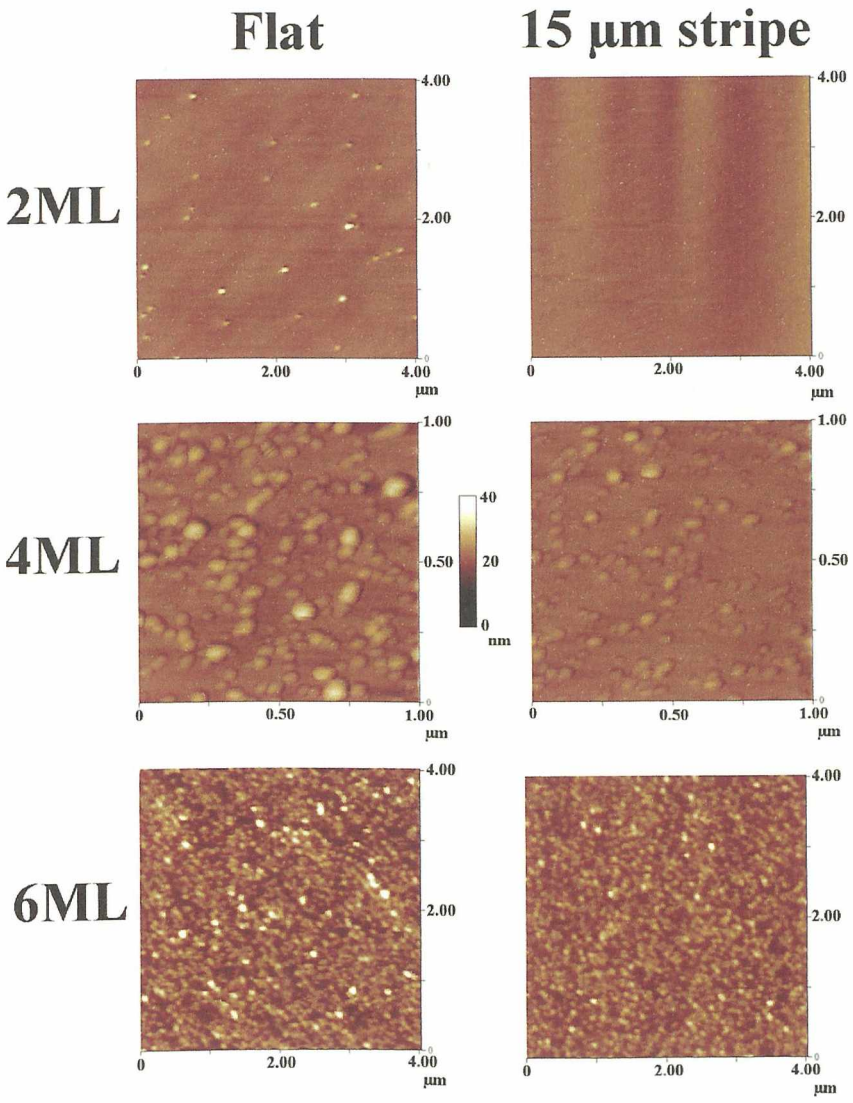


Figure 6.1: AFM images showing the QD formation at various InAs coverages for the planar region and the central area of the 15 μm stripes at 480°C with an In flux of 0.2 μm/h.

Figure 6.2 presents AFM images of QDs forming on the 15 μm and 8 μm stripes for 3 ML and 4 ML InAs coverage. The dot density for the 15 μm stripe appears to be larger than for the 8 μm stripe, whilst for the 5 μm stripes (not shown in figure) dots began to appear after 4 ML deposition. With increasing InAs coverage, the QD density increases for both the 8 and 15 μm stripes with the dots randomly distributed until for the 15 μm mesas stripes the first signs of coalescence appeared.

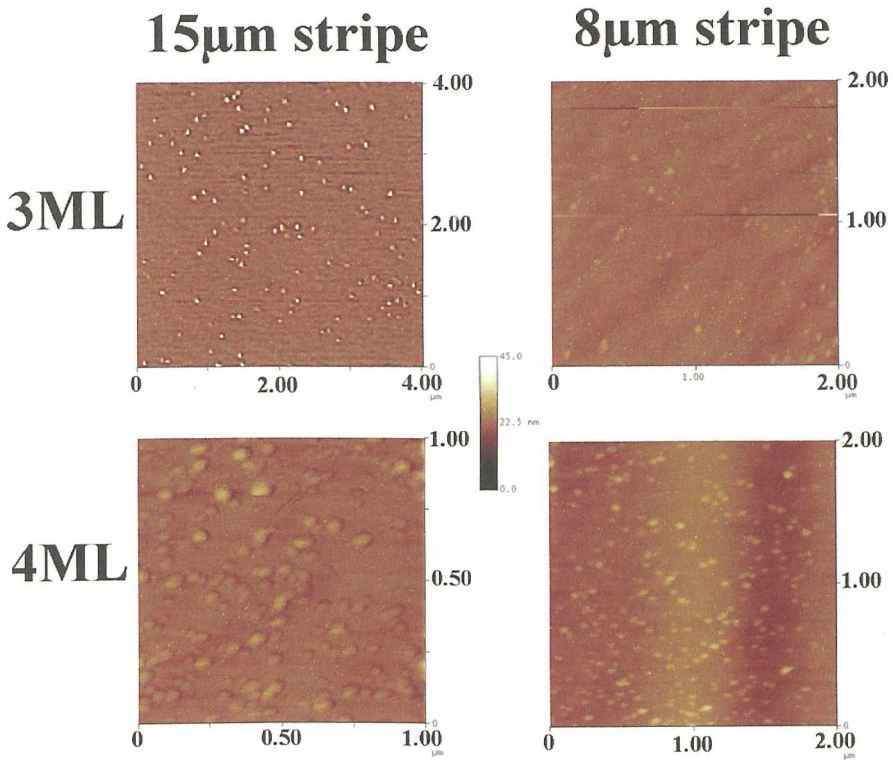


Figure 6.2. AFM images of 3 ML and 4 ML InAs coverage on the 15 μm and 8 μm stripes after deposition at 480°C.

In more detail, figure 6.3 shows AFM images of the central regions of all the stripe widths and the planar region for the 4 ML coverage. It should be noted that the image dimensions for the 5 μm mesa stripe are smaller (0.6 μm^2) than the other three (1 μm^2). The dots appear to decrease in size and density with decreasing stripe width. QDs on the flat region have increased considerably in size and some have already started to coalesce. This however, is only seen for the flat region and to a smaller degree for the QDs on the 15 μm stripes.

After the deposition of 5 ML the quantum dots on the flat region and the 15 μm stripe have coalesced and the surface became rough. For the 8 μm and 5 μm mesa stripes, figure 6.4, it can be seen that the first signs of coalescence appeared, between the 5 ML and 6 ML deposition for the 8 μm stripe. For the 5 μm stripes however, the dot density increased until the 6 ML deposition, whereby the size of some QDs increases, suggesting coalescence.

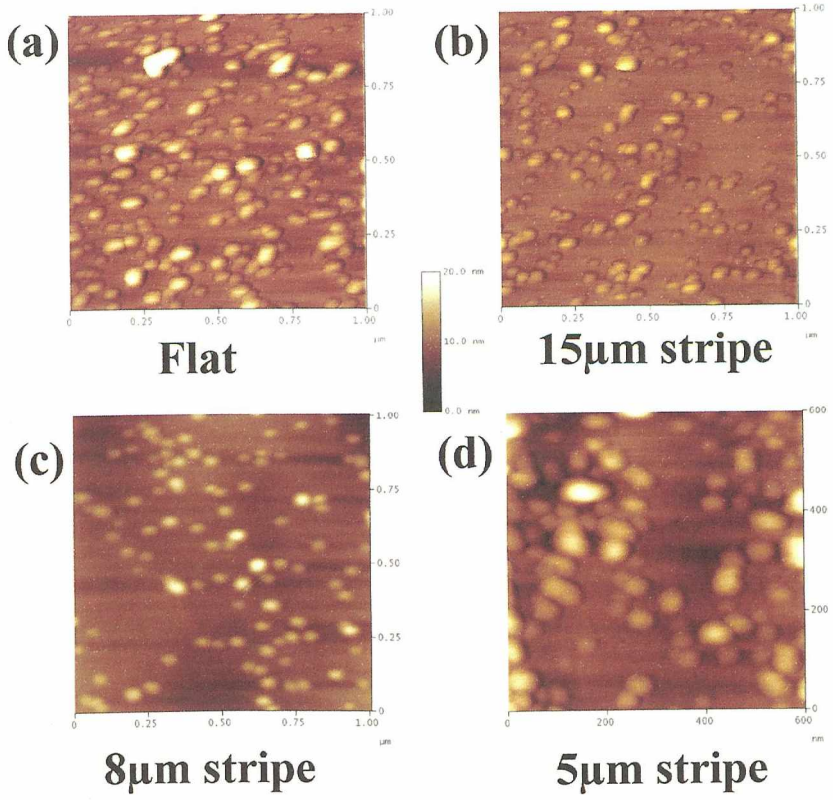


Figure 6.3: AFM images of (a) the flat region, (b) 15 µm stripe, (c) 8 µm stripe and (d), 5 µm stripe after the deposition of 4 ML for a substrate temperature of 480°C.

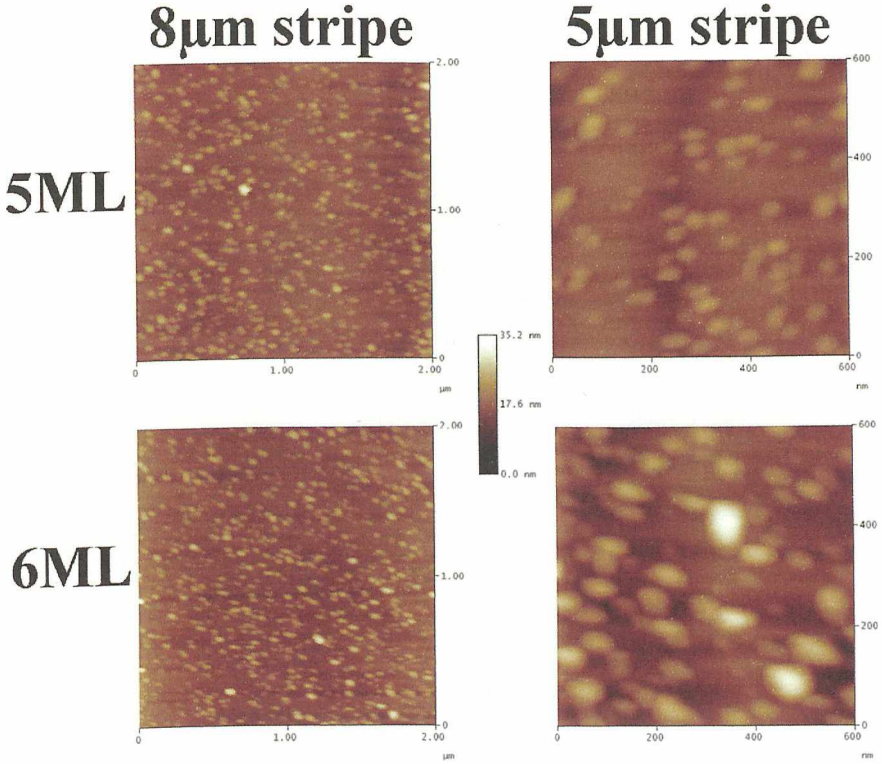


Figure 6.4: AFM images after 5 ML and 6 ML InAs deposition at 480°C for the 8 µm and 5 µm stripes.

6.3.2. Detailed Characterisation of QD Formation on Mesa Stripes.

The 3D island density and size for the experiments performed in this chapter varies with stripe width and a summary is shown in Tables 6.1 and 6.2. The height and width measurements were taken using AFM analysis software, from which the height and width in the *x* and *y* directions were measured.

After deposition of 2 ML InAs, 3D islands appeared on the flat part of the substrate between the patterned features and the 15 μm stripes, but none were observed on the 8 and 5 μm stripes. Figure 6.5 shows how the dot dimensions were measured; in the x direction (l_x) and in the y direction (l_y). The l_y measurement is along [110]. For the 2 ML InAs coverage, the average dot density for the flat region was 0.014×10^{10} cm^{-2} and the average heights and widths were 7.3 nm and (97×88) nm respectively. For the 15 μm wide mesa stripes the average density is lower and the size is smaller (3.6 nm height and 62×47 nm width). For a given InAs deposition, the dot size and density on the flat region of the samples was always larger than that measured for all three mesa widths.

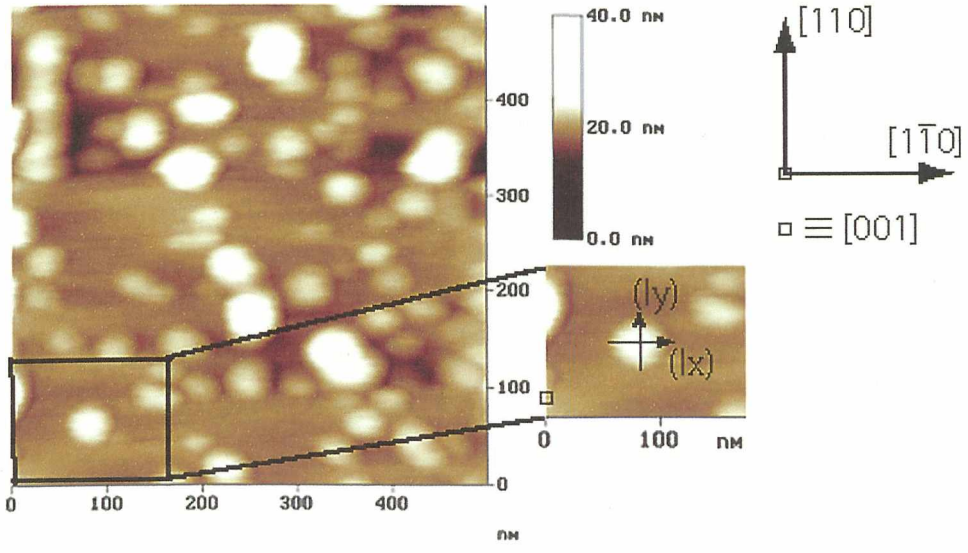


Figure 6.5: AFM image of an enlarged region of a 5 μm stripe where l_x is the length measured in the x direction and l_y is the length measured in the y direction.

	Deposition Quantity/ML					
	2	2.5	3	4	5	6
Flat ($\times 10^{10}cm^{-2}$)	0.014	0.10	0.18	1.90	Coalesced	Coalesced
15 μm stripe ($\times 10^{10}cm^{-2}$)	0.004	0.08	0.17	1.50	Coalesced	Coalesced
8 μm stripe ($\times 10^{10}cm^{-2}$)	–	0.07	0.16	0.90	1.30	1.02
5 μm stripe ($\times 10^{10}cm^{-2}$)	–	–	0.16	1.97	2.30	1.84

Table 6.1: InAs densities for the different stripes and the flat region for the 0.2 μm/h In flux at 480°C at different InAs coverages.

	Deposition Quantity/ML					
	2.0	**2.5**	**3.0**	**4.0**	**5.0**	**6.0**
Flat: ***Height/nm***	7.3	8.6	9.8	8.9	Coalesced	Coalesced
Width (l_x, l_y)***/nm***	l_x= 98	l_x= 101	l_x= 106	l_x= 110		
	l_y= 88	l_y= 82	l_y= 106	l_y= 110		
15 μm: ***Height/nm***	3.6	4.5	5.2	6.0	Coalesced	Coalesced
Width (l_x, l_y)***/nm***	l_x= 62	l_x= 82	l_x= 90	l_x= 85		
	l_y= 47	l_y= 59	l_y= 78	l_y= 80		
8 μm: Height/nm		3.6	4.3	5.4	6.0	7.2
Width (l_x, l_y)***/nm***		l_x= 62	l_x= 43	l_x= 66	l_x= 60	l_x= 67
		l_y= 70	l_y= 35	l_y= 52	l_y= 42	l_y= 55
5 μm: Height/nm		3.3	3.5	4.7	5.0	6.3
Width (l_x, l_y)***/nm***		l_x= 42	l_x= 42	l_x= 55	l_x= 49	l_x= 62
		l_y= 30	l_y= 30	l_y= 31	l_y= 40	l_y= 46

Table 6.2: 3D island height and widths for the different stripes and the flat region for the 0.2 μm/h In flux at 480°C for different InAs coverages.

A plot showing the trends for the variation of the 3D island density with increasing InAs coverage is shown in figure 6.6 and in combination with the results from table 6.2 the following trends can be inferred. For the flat region and the 15 μm mesa stripes; QDs form after ~2 ML deposition and exhibit the first signs of coalescence after the 4 ML deposition. After 5 and 6 ML InAs coverage, coalesce

dominates the whole flat region and the 15 μm mesa stripes causing the increased surface roughness seen in the AFM images. At the same time the dot sizes also increase with InAs coverage, but the average size of the 3D islands on the flat regions is always larger when compared to the 15 μm mesa stripes (see table 6.2). The QD dimensions after 2 ML coverage for the flat and the 15 μm mesa stripes are 7.7 nm (98 nm × 88 nm) and 3.6 nm (62 nm × 47 nm) respectively, whereas after 4 ML, the QD dimensions are 8.9 nm (110 nm×110 nm) and 6.0 nm (85nm × 80 nm) respectively. However, it should be noted that the 3D island density for the central areas of the mesas is considerably lower compared to values obtained from the literature (i.e. ~5×10^{-10} cm^{-2} for planar substrates).

For the 8 μm and 5 μm mesa stripes the 3D island formation begins after 2.5 ML and 3 ML InAs coverage respectively. The QD density for the 8 μm mesa stripes increases up to 5 ML coverage and subsequently decreases, suggesting coalescence has already begun. For the 5 μm mesas, a similar trend was observed but the 3D density appears to be considerably higher compared to the 8 μm mesas, mainly to the scan errors involved as discussed in 6.2. Interestingly, deposition on the 5 μm mesa stripes lead to a density of a 2.30×10^{-10} cm^{-2}, the highest in this growth series, without coalescence occurring.

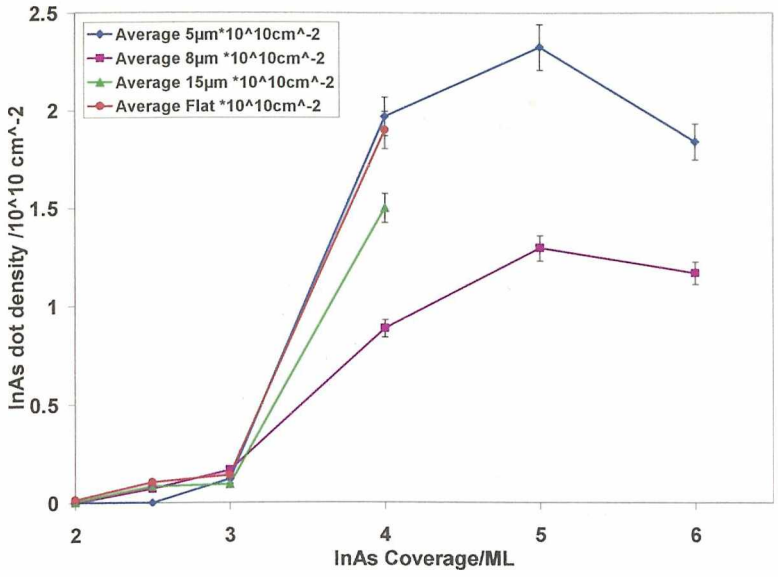


Figure 6.6: Variation of InAs 3D island densities for the three different stripes and the flat region for different InAs coverages for the 0.2 μm/h In flux and at a substrate temperature of 480°C.

High-resolution SEM measurements were also taken of the QD samples to provide supporting information about the spatial position of the QDs on the mesa stripes. An SEM image of the flat region after the deposition of 4 ML InAs is shown in Figure 6.7(a). It can be seen that the dots are distributed evenly throughout the flat area of the sample; however, the size of the dots is not uniform across the entire surface, with some significantly larger islands randomly distributed on the surface, something that is also seen in AFM measurements (figure 6.3 (a)). Similar "mega dots" have been observed when growing InAs dots under an As_4 flux rather than As_2 [137], although the origin of this behaviour is not understood for growth on planar substrates. Figure 6.7(b) shows an SEM image taken from 8 μm mesa stripe from the same sample as the flat region shown in 6.7 (a).

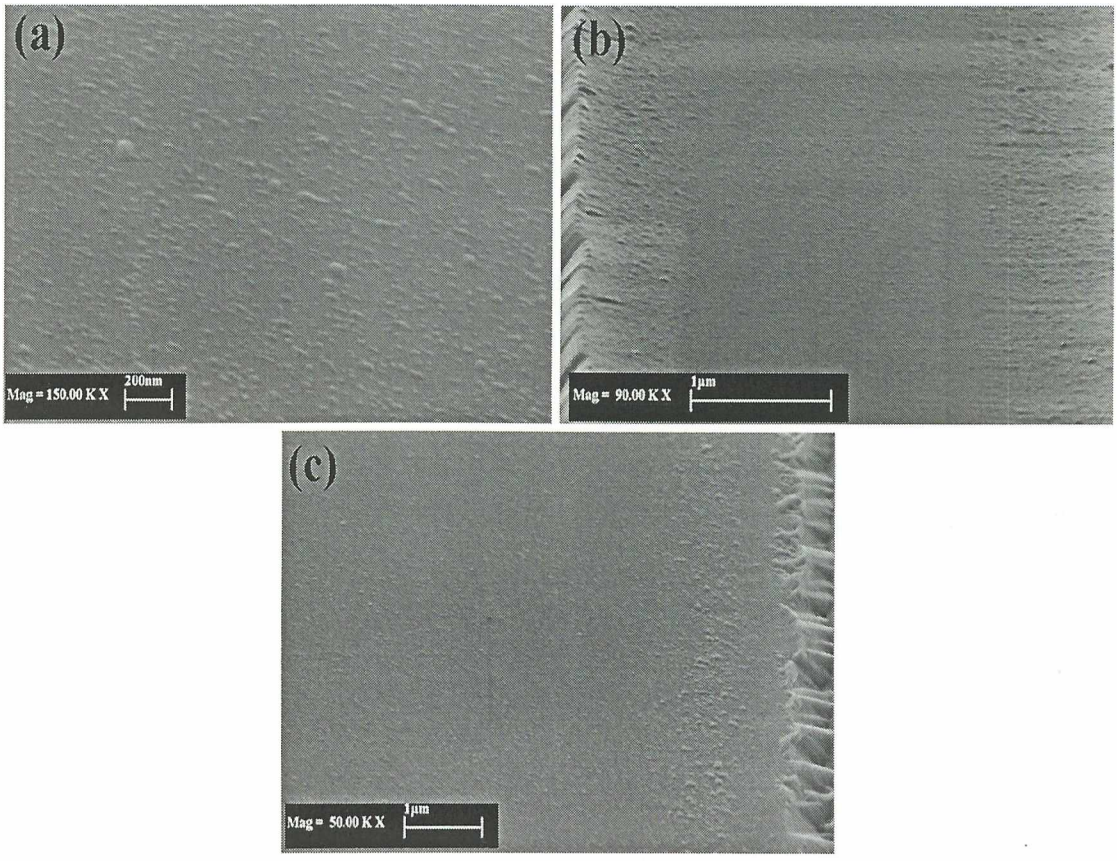


Figure 6.7: SEM images of (a) the flat region, (b) on top of an 8 μm stripe and (c) an area below the 8 μm stripe for 4 ML InAs deposition at 480°C using a 0.2 μm/h In flux.

Dots can be seen across the entire stripe width, but the dots clearly become larger and higher in density at the edges of the mesa. In Figure 6.7(c) the SEM image shows the area surrounding the base of the 8 μm stripe. InAs islands are

formed across the whole planar region but a significantly larger quantity is situated at the base of the trench. In this region, the InAs QD density and size both increase.

In order to study the effects of In adatom diffusion, a technique that measures the relative In concentration in the vicinity of the stripes was required. The one chosen was EDX. Various measurements were performed including line scans across the mesa stripes; area scans, and spot measurements at specific locations on the samples. Due to the very low InAs coverages (< 6 ML) used compared to the detection limit of the EDX system for a reasonably short scan time, In was only measurable in the areas where it appeared most abundantly. Consequently, even though QDs were clearly seen in the AFM and SEM images, the amount of In present was below the detection limit of the EDX, apart from the areas of higher In concentration. All the EDX measurements demonstrated the same basic trend.

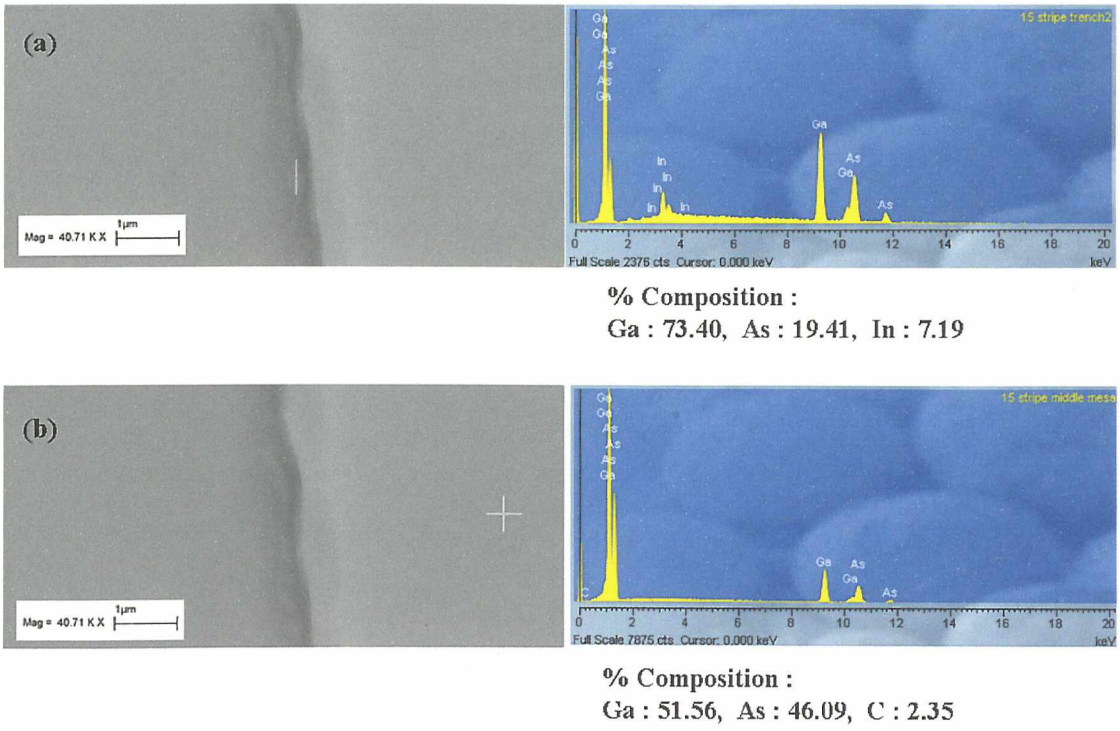


Figure 6.8: (a) SEM image of the trench area where some of the EDX measurements were taken and the corresponding EDX % of the surface composition. (b) SEM image of the area in the middle of the stripe where the EDX was taken and on the right the % surface composition.

Figure 6.8(a) shows an SEM image of the area where the measurement was taken and the EDX spot measurement taken at the position shown, in the trench for

a 15 μm mesa stripe after 3 ML InAs deposition. (The trench is the area between the bottom of the sidewall and the flat region.) Figure 6.8(b) shows an SEM image of the middle of the mesa and the corresponding EDX spectra of the spot measurement taken at the centre of the mesa ridge. The In concentration in the trench next to the stripe is 7.2% compared with no detected In signal in the centre of the 15 μm mesa. This verifies the AFM and SEM results, which show a greater InAs QD density at the base of the mesa stripes. However, there are no conclusive results from the EDX for the edge of the stripe area, which was unfortunately below the detection limit of the system used.

6.4. Discussion.

The key points observed for InAs island formation on patterned substrates at 480°C and 0.2 μm/h In flux are:

(i) The QD densities measured on all samples, on both the stripes and on the flat where considerably lower than those previously reported for similar deposition conditions and planar substrates. Also, the dots were noticeably larger compared to that found on the planar substrates.

(ii) For the varying width mesa stripe investigations, the QD density on the 15 μm stripes was slightly less than that observed on the flat, but for the 8 and the 5 μm stripes, the change in QD density was greater than that for the planar region.

(iii) The dot density and size increased with increasing deposition. For both the flat region and the 15 μm stripes, the islands started coalescing after 4 ML InAs deposition. For the 8 and the 5 μm stripes the density and size continued increasing until 5 ML.

(iv) For the range of stripe widths investigated, there is an increased InAs density of InAs islands at the edge and the base of the mesa stripes.

The lower dot density for the patterned samples compared to planar deposition (for an In flux of 0.13 μm/h, a temperature of 500°C and 2.2 ML deposition, the dot density on planar substrates is ~$5x10^{10}cm^{-2}$ [137]), suggests either that In is being lost through desorption from the substrate surface, or that the enhanced surface roughness on the mesas leads to the formation of fewer, but larger dots. Significant In desorption is unlikely, since the growth temperatures used are relatively low [138]. However, the size of the InAs islands observed, is significantly larger than those reported by other groups for growth on planar substrates [64,67,69,70], which could partly explain the lower dot densities observed. This implies that In adatoms preferentially incorporate at the edges of existing InAs islands or at steps at the edges of the mesas, rather than nucleating new ones, even at low InAs coverages. In addition, there is a possibility that some of the In incorporates onto the 2D InAs wetting layer which because of the lower strain relieved by mesa widths, can become thicker [58,63].

It was observed that the dot density decreases from the flat region to the mesa stripes and also decreases with decreasing mesa width for the 480°C substrate temperature and 0.20 μm/h In flux series. At 2 ML deposition, the flat and the 15 μm mesa stripe show a similar QD formation. This suggests that the migration length of the In behaves similarly in both cases and is of the order of 6-12.7 μm (post-etch mesa width). Since there were no dots forming on the 8 and 5 μm mesa stripes, a lower boundary for the In migration length can be set at ~3-6 μm.

Figure 6.8 shows the QD development for an 8 μm stripe through the whole range of deposition quantities. It can be seen that for 5 ML and 6 ML coverage, the difference in dot density is not clear and after detailed analysis the QD density for the 5 ML coverage was in fact greater. This suggests that the QDs present on both the 8 μm and 5 μm stripe have begun to coalesce at this point.

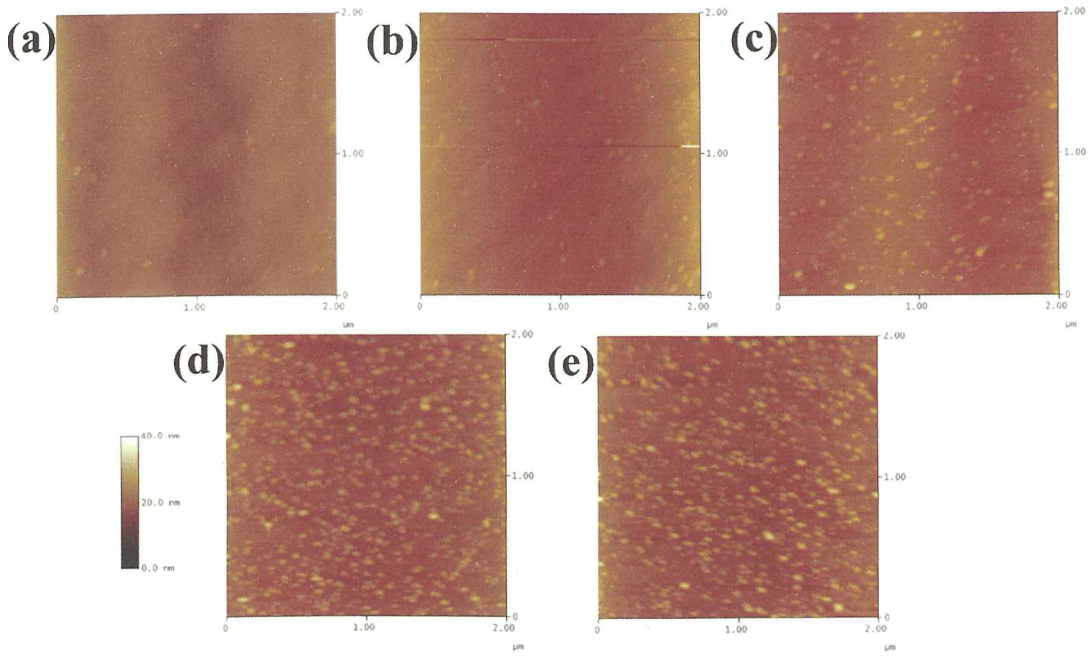


Figure 6.9. AFM images of an 8 μm mesa stripe after the deposition of (a) 2.5 ML, (b) 3 ML, (c) 4 ML, (d) 5 ML, and (e) 6 ML at 480°C.

As previously suggested, there is the possibility of preferential In incorporation at existing InAs islands. This decrease in QD density and increase in size is most likely due to the coalescing of 3D islands. As defined earlier, coalescence occurs with the combination of two or more InAs islands to form a

larger island. This is the first stage, which leads to a decrease in dot density shown in figure 6.9 (d→e). However, for the areas with high dot density (the flat region and 15 μm stripes), when coalescence occurs, the dots become considerably larger and multi-peaked making the surface appear exceptionally rough and the dot density very difficult to measure. An example of this behaviour is shown in the AFM image in figure 6.10. The AFM images of the coalesced samples show that the surface was very rough and that the dots merge between them and have multiple peaks, with one peak higher that the rest. In addition, there was a comparable behaviour of the flat region and the 15 μm stripes since both reached coalescence at the same time although the dots on the 15 μm stripes were considerably smaller in size.

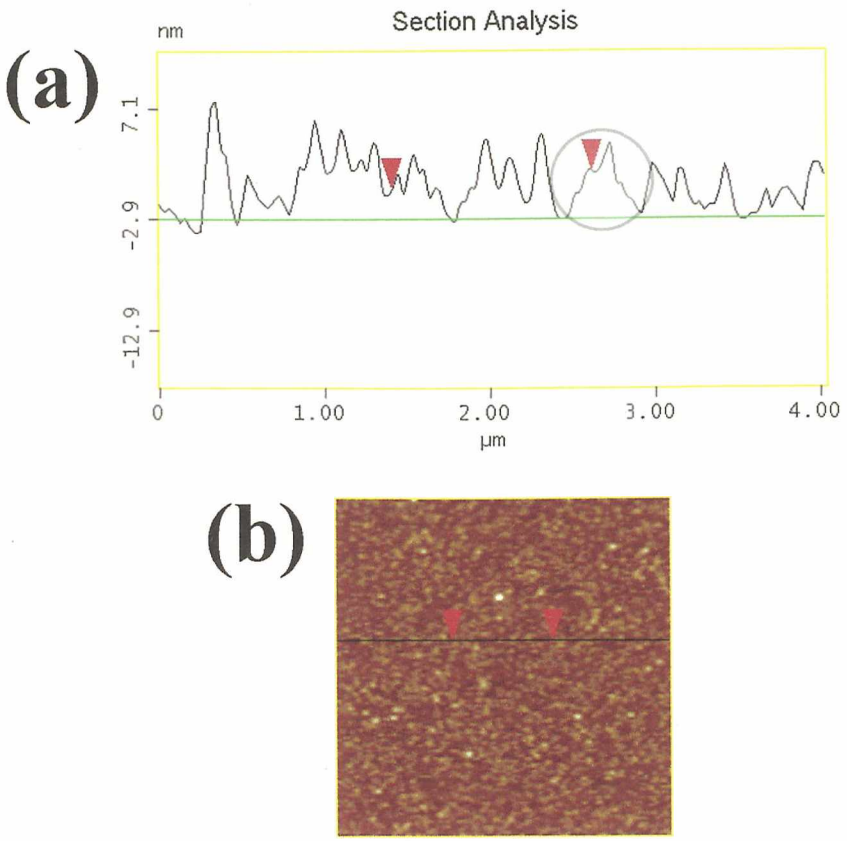


Figure 6.10: AFM section analysis on a flat 4μm region after the deposition of 5 ML of InAs at 480°C. An example of a multi-peaked QD is encircled.

Previous results on planar substrates reported in the literature give mixed information. Some groups suggest that coalescence usually occurs after ~3 ML [58], while others find that coalescence started after 4 ML at 492°C [70]. However,

coalescence at higher coverage is expected in the case of patterned substrate growth, due to the generally lower dot density on the samples. There is also another explanation for the dramatic increase in some QDs. In all AFM scans, the values for the QD dots are averaged and for all the samples there were QDs present with a regular size. At high coverages, the density of larger InAs islands dramatically increased and this suggests that the dots follow a *bimodal* growth behaviour. This means that there are two types of InAs islands forming. The first, is the regular InAs QDs, with a relatively narrow size distribution, and the second the much larger InAs islands, so called "mega dots", that started to form at coverages >3 ML and increase significantly in size, acting as sinks for the additional InAs deposited. Leonard *et al.*[68] and Joyce *et al.* [66] have also observed this phenomenon on planar substrates.

A rough estimation of the QD volume was made assuming the dot volume can be calculated from: $\frac{h \times A}{2}$ where h is the height of a dot and A is the area [65].

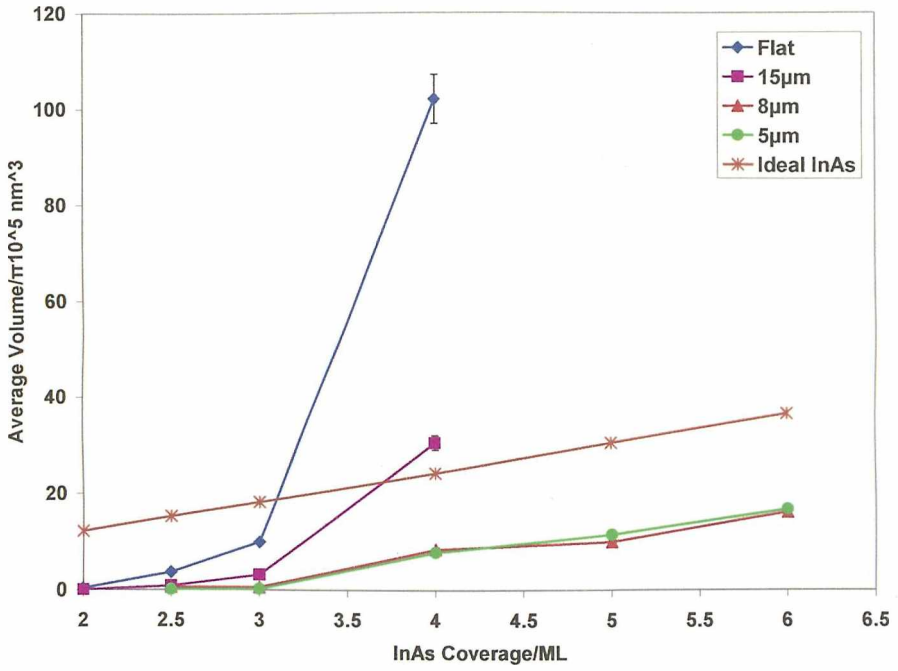


Figure 6.11: The average QD volume determined by AFM as a function of InAs coverage for the three different mesa stripe widths (15, 8 and 5 μm) and the flat region.

The plot of the QD volume for all the mesa stripes and the flat with increasing InAs coverage (figure 6.11) shows that for the flat region and the 15 μm

mesas, the average QD volume after 3 and 4 ML coverages appears to be higher than the "ideal InAs" volume for layer 2D growth expected for the amount of In provided. This is a normal characteristic on the growth on planar substrates, suggesting that either In–Ga intermixing is taking place or material form the wetting layer is being transferred. The In-Ga intermixing has been seen previously in the literature for growth on planar substrates and the QDs are thought to be InGaAs rather than pure InAs [59,65]. Another possible reason for the above "ideal" QD is that a small fraction of material is transferred form the substrate-wetting layer to the 3D islands. This was seen before on planar substrates [58,63]. For the 8 μm and 5 μm mesa stripes, although the trend is expected, the loss of In is noticeable since the InAs volume is considerably less than the amount deposited. A possible reason for this is the tendency of In adatoms to preferentially migrate to the edges and the base of the mesas which act as "traps" for In. (figure 6.7 (b and c)).

It is clear from all the results presented in this chapter that more dots are present at the edges and the base of the stripes. These areas were examined in greater detail although it should be mentioned that this is an exceptionally difficult task due to tip limitations in AFM. The results obtained show that for all stripe widths, the In adatoms diffuse to the mesa edges where the high concentration of atomic steps, results in the enhanced nucleation of quantum dots. These dots frequently fill the mesa edges in chains which can be as long as the patterned features, shown in the AFM and SEM figure 6.12. The dot size at this inter-planar point was greater than for the central area of the mesa stripes.

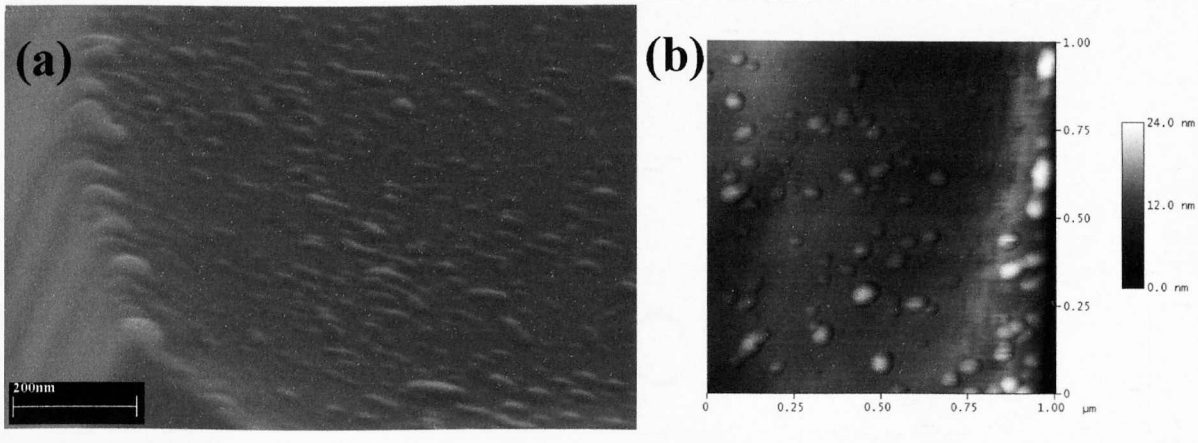


Figure 6.12: (a) SEM image and (b) AFM image taken at the edge of 8 μm mesa stripe after 4 ML InAs deposition at 480°C.

An alternative reason for the In gathering around the mesa base and edge could be the fact that there was no significant In incorporation on the {110} facets and therefore the In adatoms migrate to the closest more favourable sites i.e. stepped region at the mesa edges and mesa base.

Figure 6.13 shows a schematic of the In diffusion process on the mesa stripes. It can be seen that the highest In concentration is either at the top edge of the mesa or the mesa base. An In adatom landing on the {110} facets or the vertical sidewalls, since they are non-growth planes, diffuse either to the top or bottom of the mesa stripes.

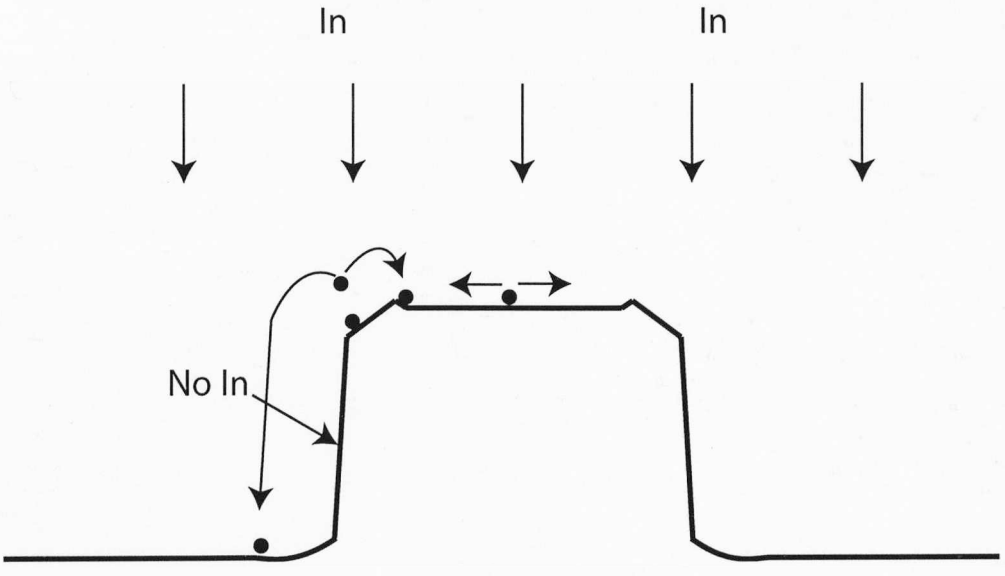


Figure 6.13: Schematic illustration of the possible In adatom diffusion paths across a mesa stripe.

In conclusion, after 2 ML deposition, InAs QDs were formed on the planar region and the 15 μm mesas, suggesting a migration length comparable with the size of the mesa width *i.e.* ~6-12 μm. The QDs are larger than those normally seen during planar QD growth, and the density lower perhaps due to some degree of surface roughness caused by the initial substrate etching process. There is some indication of *bimodal* QD growth since both small and large islands were observed for the higher coverages. The QD volume measurements suggest there is probably some Ga-In intermixing. The dots on the mesas were observed to coalesce at

different ML coverages, according to the mesa width, suggesting coalescence can be controlled. Moreover, the size and density of the QDs changes according to the mesa width. This implies that controlling the mesa width under optimum growth conditions provides a potential method for controlling the QD density and size distribution. This has important implications for producing very low densities of more uniform QDs for applications such as single photon sources.

CHAPTER 7.

Effect of Growth Temperature and Rate on InAs Quantum Dot Formation.

7.1. Introduction.

In the previous chapter, the effect of the different sized mesa stripes on the growth of InAs on GaAs was investigated. In this chapter, an attempt was made to further understand the In diffusion and dot formation by altering the growth conditions.

For planar substrates, it is well known that decreasing the substrate temperature leads to a higher density of smaller 3D islands [57,61,63,64] and also that lowering the growth rate (i.e. increasing the V/III ratio) results in a larger density dots [67].

These experiments were performed in order to investigate the effect of the In migration across the surface. Therefore, two different temperatures and growth rates (V/III ratios) were employed; 450°C and 0.2 μm/h In flux, and 480°C and 0.02 μm/h In flux.

7.2. Experimental Details.

The experimental procedure was identical to the one outlined in chapter 6, with the only significant alteration being the growth conditions. The first set of experiments used a substrate temperature of 450°C and 2-6 ML of InAs deposited at 0.20 μm/h. For the second set of experiments, the temperature was reduced to 480°C and 2-6 ML of InAs was deposited at 0.02 μm/h. Again, the RHEED pattern was checked after InAs deposition, and chevrons were observed, confirming 3-D growth. During deposition, all the samples were rotated at speed of 12 rpm. The samples were characterised using AFM and SEM after removal from the MBE

apparatus. All the AFM images had the background subtracted, but were otherwise unprocessed.

7.3. *Effect of Temperature.*

Growth at 450°C and with a 0.20 μm/h In flux, generally causes a higher number of In nucleation sites and smaller dots compared to the higher temperature growth. After deposition of 2 ML InAs, dots were formed on the flat region, the 15 and 8 μm stripe widths, but not on the 5 μm stripes. For the planar region, the average dot density was $7x10^8$ cm^{-2} and the dot height and width are 5.6 nm and (98×86) nm respectively. For the 15 μm stripes, the average density was 6×10^8 cm^{-2} and the height and lateral dimensions were 4.3 nm and (58×50) nm respectively. These figures show that the average dot density is higher and the average size similar, or slightly smaller than the dots grown at the higher substrate temperatures of 480°C.

Figure 7.1 shows AFM images of (a) the flat, and the (b) 15 μm, (c) 8 μm and (d) 5 μm stripes, after 3 ML InAs deposition. At this coverage, the dot size and density decreases with decreasing mesa width as observed for the 480°C substrate temperature growth. In addition, the quantity of dots for all the mesas and on the planar region is significantly larger than for higher temperature deposition series. The QD dimensions are significantly smaller, especially the lateral directions. For a point of reference, the density of the 3D islands formed on the 15 μm stripes at substrate temperatures of 480°C and 450°C was 0.17×10^{10} cm^{-2} and 1.57×10^{10} cm^{-2} respectively. These QDs had lateral sizes of 101.5 nm and 60 nm at 480°C and 450°C respectively. Furthermore, the 3D islands on the 5 μm stripes (figure 7.1 (d)) show a broad size distribution with the presence of some larger dots similarly to the results shown in Chapter 6 for the higher growth temperature. This behaviour could indicate a bimodal behaviour, and the beginning of coalescence, as once these "mega" dots form, they start to increase rapidly in size consuming the smaller dots at their expense.

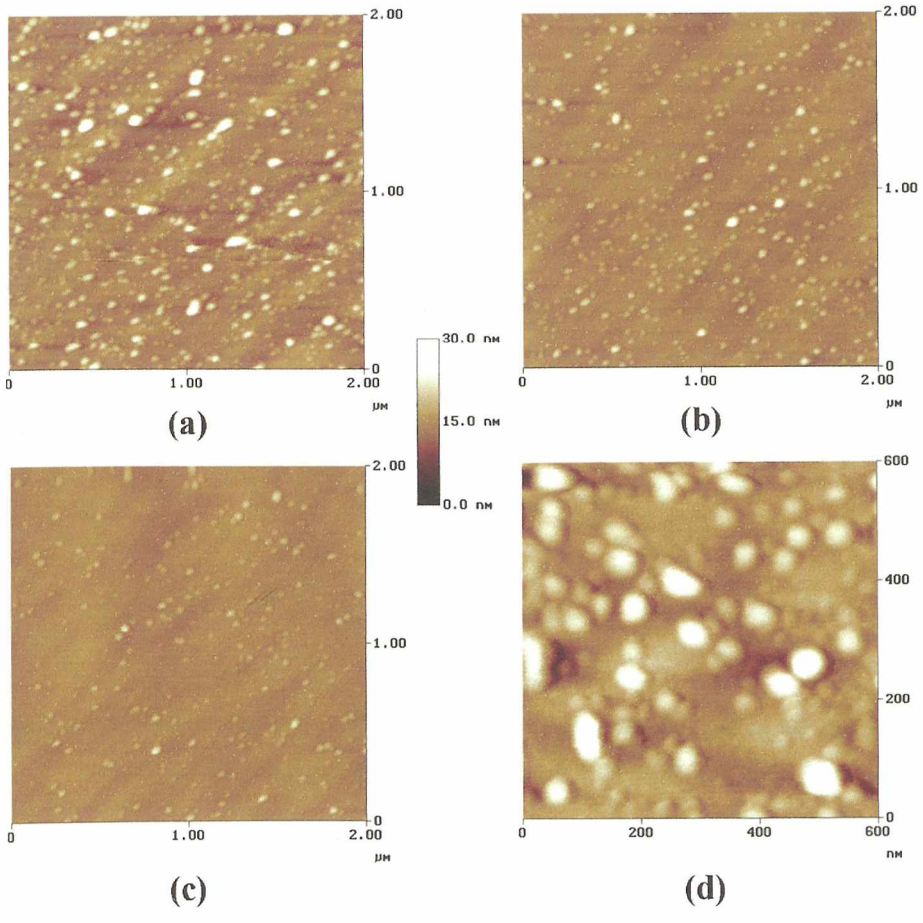


Figure 7.1: AFM images of (a) the flat region, and the (b) 15 μm, (c) 8 μm, and (d) 5 μm stripes after 3 ML deposition at 450°C and a 0.20 μm/h In flux. Note the scale change in (d).

Figure 7.2 shows a plot of the 3D island density as a function of InAs coverage for the two different growth temperatures. It is interesting to observe that both the planar regions and the 15 μm stripes behave similarly for these deposition temperatures. The density for all InAs coverages at the lower substrate temperature is always larger than that for the higher temperature series. In addition, it can be seen clearly that the islands begin to coalesce after 3 ML coverage, whereas for the higher temperature, coalescence occurs after the InAs coverage of ~4 ML. The islands on the 8 μm and 5 μm stripes follow a similar behaviour, but with lower densities. It should be noted that the increase in density for the planar regions and the 15 μm stripes occurs at an earlier stage for the lower temperature sample series. After 3 ML InAs coverage, the dot density is 15 times higher for the 480°C series than the 450°C series. The AFM measurements demonstrate that the QD density for the 8 μm and 5 μm mesa stripes decreases after 4 ML InAs deposition, whereas for the 480°C growth series, this occurs after 5 ML deposition.

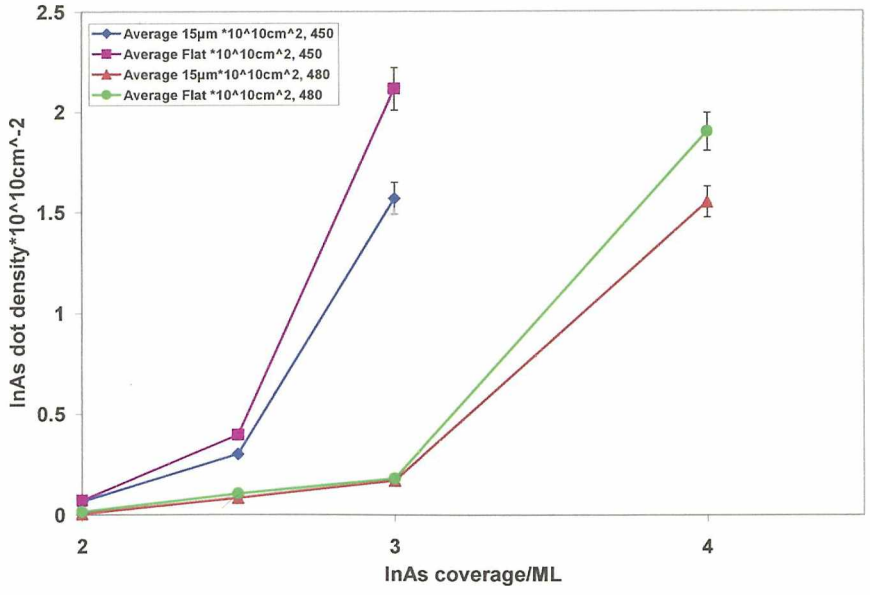


Figure 7.2: Plot of the comparison of the 15 µm stripes and the flat region for the two different temperatures (480°C, 450°C) with a 0.20 µm/h In flux.

Figure 7.3 shows the corresponding SEM images of (a) the 15 µm stripe and (b) the flat region after the deposition of 3 ML InAs. The images shows that 3D island dots appear on the stripes and "mega" dots are more apparent at the edge of the stripes. The quantum dots on the flat region are more developed and the dot density and size are larger. In addition, a few "mega dots" are apparent on the planar regions of the mesa stripe. However, a slightly larger size distribution is observed compared with the higher growth temperature samples.

These observations suggest that the In adatoms diffuse towards the stripe edge. Figure 7.3 (c) shows an AFM image of the edge of a 15 µm mesa stripe after 3 ML InAs deposition. It can be seen that the QDs form a chain along the length of the stripe and in this region their size is considerably larger than for the remaining area of the stripe. These larger QDs are possibly formed by the coalescence of smaller dots on that area or the preferential appearance of large 3D islands there. The size of the islands range from a height of 15-26 nm and lateral dimensions of 80-120 nm, considerably larger than the typical dimensions of InAs/GaAs QDS.

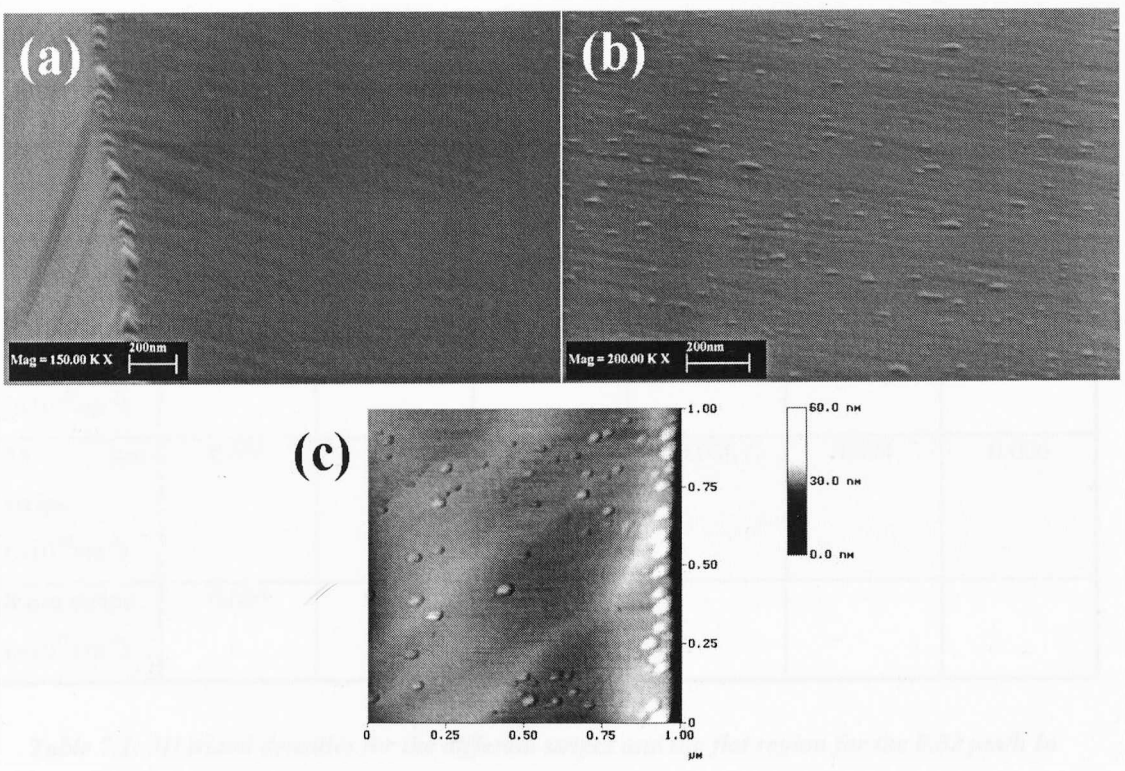


Figure 7.3: SEM images of (a) the edge of a 15 μm stripe ,and (b) the flat region. (c) AFM image of the edge of a 15 μm stripe after the deposition of 3 ML InAs at 450°C and with a 0.20 μm/h In flux.

7.4. Effects of InAs Growth Rate.

To further investigate the In adatom nucleation process, studies were carried out at much lower In fluxes so as to modify the In diffusion.

Previous work published on the effects of the In flux on the formation of the 3D islands demonstrated that as the QD growth rate is decreased, the QD size increases and the density decreases. Bennet *et al.* investigated the nucleation and growth of seeded InAs QDs [67]. The QDs were grown at 495° C and at In flux of 0.01ML/s. The QDs were 45 nm in width and 7 nm in height with a density of $5x10^{10}$ cm^{-2}. The QD size was larger and the density was considerably lower, when compared to samples grown at 0.20 μm/h. Also, Joyce *et al.*, reported a drop in the number density by an order of magnitude from 6×10^{10} to 5×10^{9} cm^{-2} as the growth rate lowered for 0.13 to 0.003 ML/s [66].

After depositing 3 ML of InAs, at an InAs flux of 0.02 μm/h, 3D islands were observed on both the planar regions and the 15 μm mesa stripes, with only a very

small number appearing on the 8 μm mesa stripes. Table 7.1 summarises the densities for all InAs coverages as well as the sizes measured for an In flux of 0.02 μm/h and a substrate temperature of 480°C.

	Deposition Quantity/ML					
	2.0	**2.5**	**3.0**	**4.0**	**5.0**	**6.0**
Flat ($\times 10^{10} cm^{-2}$)	0.02	0.08	0.14	0.16	0.16	0.15
15 μm stripe ($\times 10^{10} cm^{-2}$)	0.008	0.01	0.02	0.005	0.004	0.006
8 μm stripe ($\times 10^{10} cm^{-2}$)	0.005	0.006	0.017	-	-	-

Table 7.1: 3D island densities for the different stripes and the flat region for the 0.02 μm/h In flux at 480°C at different InAs coverages.

For 2 ML coverage island density on the flat regions was 0.02×10^{10} cm^{-2}, with the height and lateral dimensions measured at ~9 nm and 70×70 nm respectively. For the 15 μm stripes the dot density was significantly reduced to 0.008×10^{10} cm^{-2}, and the height and lateral dimensions were 2.8 nm and 60×60 nm respectively. With increasing coverage, the dot density generally increased on the flat regions and the 15 μm mesas until 4 ML had been deposited, after which, the dot density fell for the 15 μm stripes. This can be attributed to the islands becoming larger therefore reducing in density, but increasing in size. For example, the sizes on the flat were initially 6.7 nm high and (49×50) nm wide after 2 ML deposition, increasing to 19.1 nm high and (157x129) nm wide for the 6 ML deposition. It should be mentioned that the QDs on the flat regions and the 15 μm mesa stripes appear to have not coalesced, for this low growth rate, and the densities are considerably lower than seen in all the other growth series. However, the 3D island size distribution appears large for the flat region and the islands are larger than the values observed for the higher flux series, which generally tends to lead to coalescence. For the low growth rate, there are no dots present on the 5 μm stripes for all deposition quantities used.

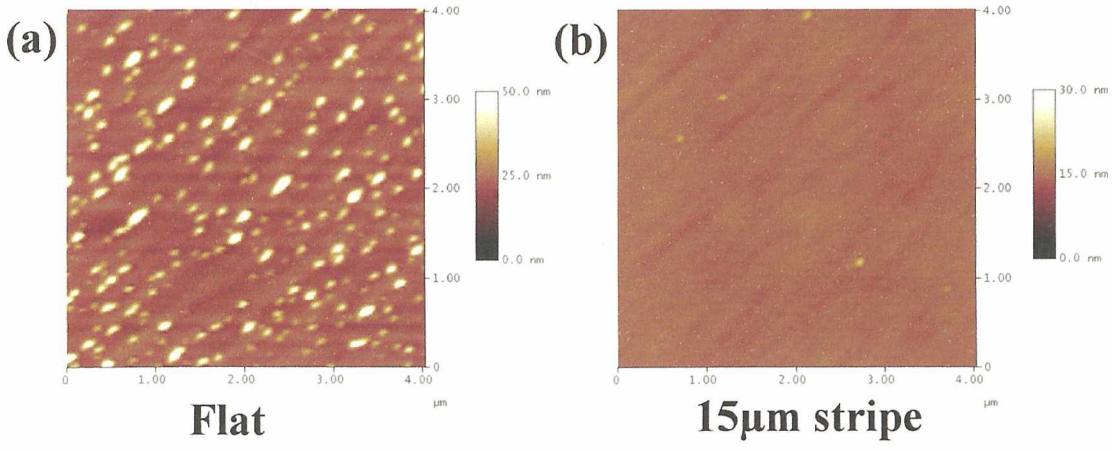


Figure 7.4: AFM images of (a) the flat region and (b) the 15 µm stripe after deposition of 6 ML InAs at 480°C and an In flux of 0.02 µm/h.

Figure 7.4 shows two AFM images of (a) the flat region and (b) a 15 µm stripe after 6 ML InAs deposition at the low growth rate. The QDs on the planar region show a significant increase in size, but a decrease in density compared to the 0.20 µm/h In flux series and the 450°C growth series. The QDs heights range from ~11 to 30 nm. However, in some cases, the dots are so large that they undergo coalescence, even though the inter-island distance is quite large. It appears that the In is preferentially incorporated into pre-formed islands at the low In flux, to a much greater degree than observed for the other growth conditions. For the 15 µm stripes (figure 7.4(b)), the QD density is remarkably low compared with the results obtained for the higher flux, to undergo coalescence. The average QD height and width dimensions are 4.8 nm and (55×39) nm respectively.

The plots presented in figure 7.5 compare the QD densities for the two different fluxes for both the flat region and the 15 µm stripes. For the 0.02 µm/h In flux the QD densities are very low, especially on the 15 µm stripes. The dots on the flat region do not show a rapid increase in density and size with increasing coverage as seen for the higher flux or lower temperature ones. The 15 µm stripes appear to exhibit similar behaviour to the 8 µm and 5 µm mesa stripes rather than the flat regions, which is opposite to the behaviour observed for the 0.20 µm/h flux and 450°C experiments.

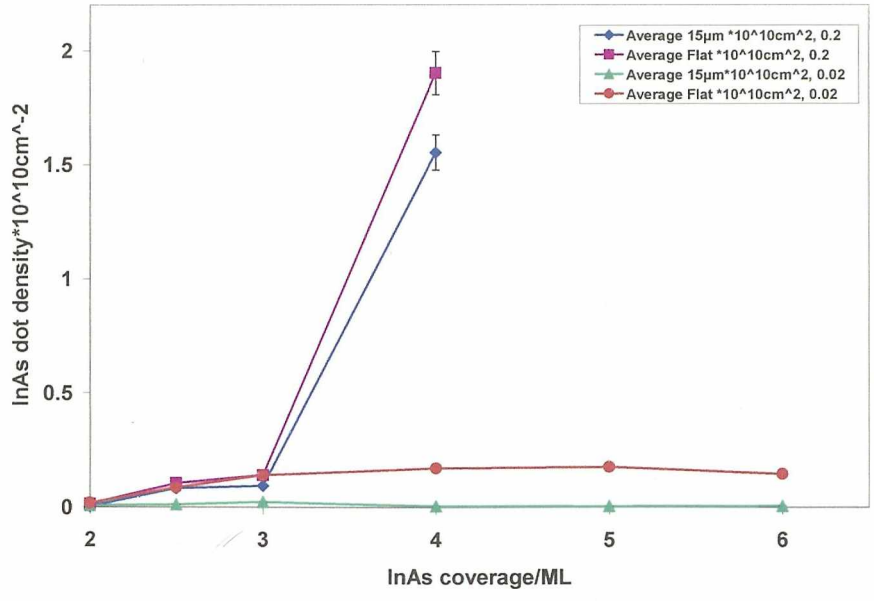


Figure 7.5: Plot of the variation of the 3D island densities for the flat region and the 15 µm stripes as a function of InAs coverage for deposition at 480°C and for both In fluxes.

The QD coverage with respect to the In flux was shown up by very high resolution SEM imaging. These are shown in figure 7.6. It can be seen that the QDs for the 0.02 µm/h In flux (figure 7.6 (a)) are distinctly larger and far fewer than those for the 0.2 µm/h flux (figure 7.6 (c)). For the 0.02 µm/h In flux, the SEM image shows a larger size distribution with the larger dots being dominant. Figure 7.6(b) shows the mesa edge, sidewall and the base area of a 15 µm mesa. The trench is clear in this image. Almost no dots can be seen on the top of the stripe, with the exception of the row of dots that form along the edge of the intersection with the {110} facet in a chain-like formation. Some large dots are formed near the base of the mesa stripe similar to those seen for the 0.2 µm/h In flux experiments. However, for the 0.2 µm/h In flux series, on the 15 µm mesas (figure 7.6(d)), the QDs are present at both the mesa top and surrounding the base of the 15 µm stripe. This is an interesting point that suggests that In adatoms prefer to add to existing islands, rather than initiating new islands because it appears to be a lower energy process. It is apparent, that decreasing the In flux by a factor of 10 has a large effect on the size and density of the QDs. The dots are hardly present on the stripes, even the 15 µm width which suggests that a lower boundary for In migration length could be of the order of ~6-12 µm.

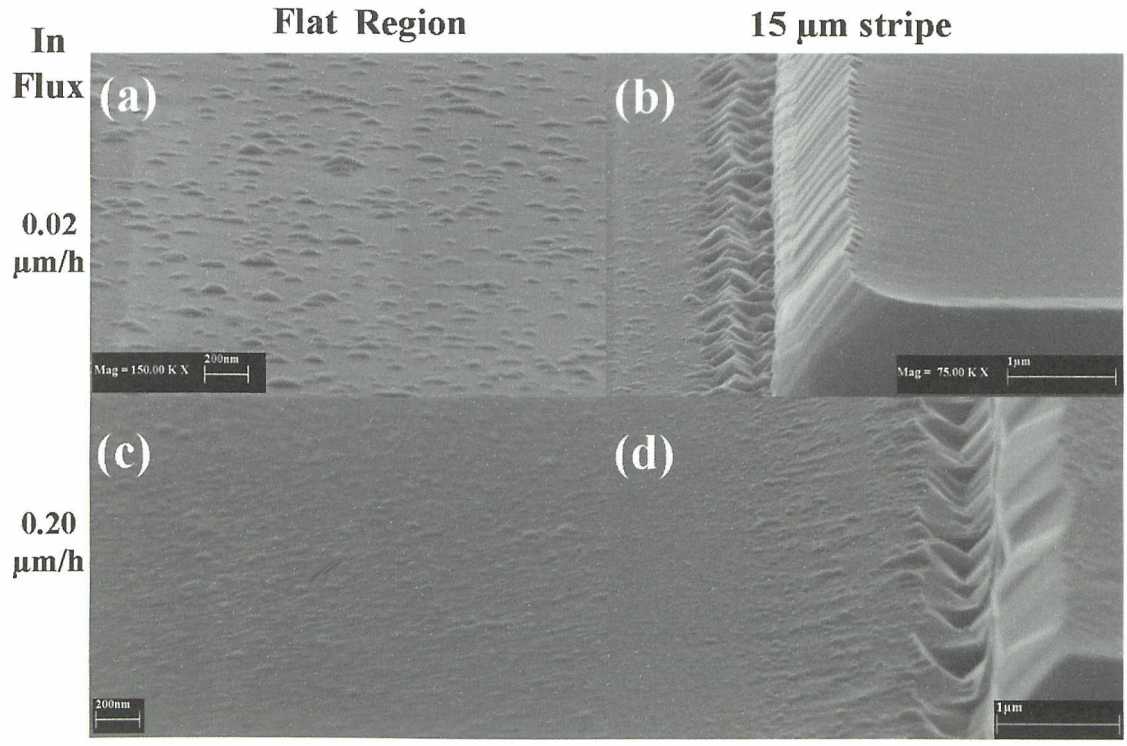
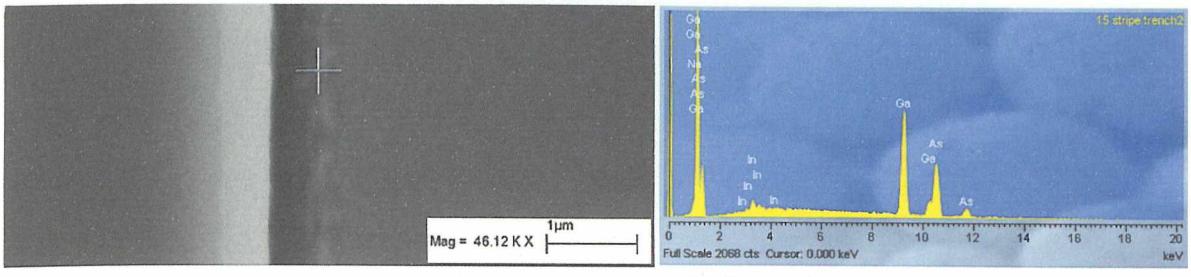


Figure 7.6: SEM images of (a) the flat region, and (b) the edge and the bottom trench of a 15 µm stripe after the deposition of 6 ML of InAs at 480°C under a 0.02 µm/h In flux and; (c) the flat region, and (d) the edge and the bottom trench of a 15 µm stripe after the deposition of 6 ML at 480°C under a 0.2 µm/h In flux.

EDX measurements performed on these samples showed an In excess compared to the other mesa areas, which verified the preferred direction of In migration to the bottom trench of the stripes. Figure 7.7 shows the SEM and corresponding EDX spectrum for a spot measurement taken at the bottom of a 15 µm stripe after 3 ML deposition.



% Composition:
Ga : 81.53, As : 15.78, In : 2.70

Figure 7.7: SEM image of the trench where the EDX was taken and on the right is the EDX results of the % surface composition.

As expected, the In concentration is lower for the 0.02 μm/h In flux series, than for the 0.2 μm/h In flux (which was 7.2%). However, the same trend is observed, with the In appearing at the edge of the mesa and mainly near the mesa base and in the trench. This suggests that In adatoms can also migrate from the flat region towards the trench which acts as a sink for In adatoms.

7.5. Discussion and Conclusions.

Comparing the results of our experiments, the key points are:

- The dot densities for all stripe widths and especially for the flat regions of the samples, during the 450°C substrate temperature and the 0.02 μm/h In flux experiments, were considerably lower and the dot size larger than those found by other groups on planar substrates using similar growth conditions.
- The island density increases with a reduction in substrate temperature, although the QDs formed were smaller for both the flat regions and all mesa stripe widths.
- Decreasing the In flux, cause a dramatic decrease in the dot density and an increase in the size of the dots.
- For all stripe widths and growth conditions investigated, a large number of InAs islands were concentrated at the mesa edges and the base areas surrounding the mesa stripes.

7.5.1. Comparison of the Effect of the Two Different Temperatures on QD Formation.

As seen in the plot in figure 7.2, the dot density on the flat region and the 15 μm stripes for the 450°C series is greater than for the 480°C growth series. However, the dot size is smaller, which can be expected as seen previously in literature [71,72]. Shiramine *et al.* investigated growth temperature effects on adatom migration during quantum dot formation [61]. The dots were grown on

planar GaAs(001) substrates under an As_4 flux, an In growth rate of 0.18 ML/s and with an InAs coverage of 2 ML. The 3D islands produced at 450°C were 16-50 nm in diameter and 1-7 nm in height- considerably smaller than those observed in this work. The experiments were repeated at 480, 510 and 530° C. They found that the dot size increased and the dot density decreased with increasing substrate temperature. This was attributed to an increase in the In diffusion length with increasing temperature. Kamiya *et al.* investigated methods to control the density and size of InAs dots on GaAs(001) planar substrates[64]. Their growth was performed under an As_4 flux and at various substrate temperatures and InAs coverages. At 455°C and 1.8ML coverage, the QD size and density were ~16-22 nm and $6x10^{10}$ cm^{-2} respectively. When the temperature was increased to 500° C, the QD size increased to 28-35 nm and the density decreased. Madhukar *et al.* published similar results, with comparable experiments and InAs coverage of 1.74 ML, the dot density is seen to reduce with increasing substrate temperature [63].

No dots formed on the 8 μm and 5 μm stripes when growth was carried out at 480°C and after 2 ML InAs deposition, whereas for the 450°C temperature series, 3D islands appeared on the 8 μm stripes immediately after the deposition of 2 ML InAs. The dot density for the flat regions and the 15 μm mesa stripes during the 480°C series, after 3 ML InAs deposition, was lower than that seen for the 450°C series, which demonstrates that for the lower temperature series, the dots form significantly earlier. Also, at 450°C coalescence occurs after deposition of 3 ML on the flat regions and the 15 μm stripes, and after 4 ML for the 8 μm and the 5 μm stripes. For the 480°C growth series, coalescence occurred after 4 ML and 5 ML respectively, also seen by Solomon *et al.,* who found that isolated island growth was maintained until 3 ML coverage at 457°C [70]. Figure 7.8 shows two AFM images of the flat regions after the deposition of 4 ML of InAs at (a) 480°C and (b) 450°C respectively. It is clear that the dot density is greater for the lower deposition temperature and the dot size smaller. There is evidence of small regular and large irregular islands and the latter increases considerably with depositions quantity. The appearance of large dots increases, which maybe evidence of coalescence or the increase in bimodal behaviour, which will ultimately lead to coalescence. After 5 ML InAs deposition, the dots are completely coalesced. As the

islands coalesce, more adatoms reach the islands, simply as a result of their increased surface area, and the island growth rate changes.

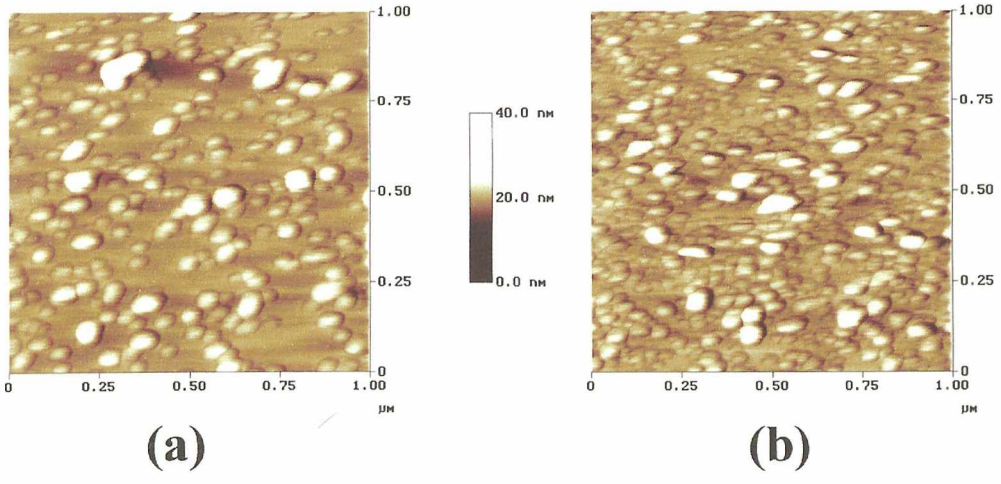


Figure 7.8: AFM images of the flat region after the deposition of 4 ML of InAs at (a) 480°C and (b) 450°C.

When the average dot area was calculated it demonstrated some interesting results. Figure 7.9 shows a plot of the variation of average island area with monolayer coverage for the 15 μm stripes at both growth temperatures. The island area is calculated as the area of a circle. It can be seen that as the temperature decreases, the island area decreases. This was seen previously by Solomon *et al.*[70], in similar experiments, conducted with an As_2 flux at 457°C and 492°C where the average dot diameter was 15 nm and 32 nm respectively. As previously described, coalescence occurs at lower InAs coverages for lower temperatures. The average QD width and height, increases with temperature. When the temperature is increased, the average diameter and height increases. Since the raised substrate temperature increases the vertical surface diffusion and therefore the height, this permits the in-plane diameter to grow larger before coalescing [70]. In addition, increased surface migration due to the increase in substrate temperature extends the spatial distance between coherent dots and the coalescence is relatively suppressed. For these reasons, coalescence started earlier for the lower temperature growths.

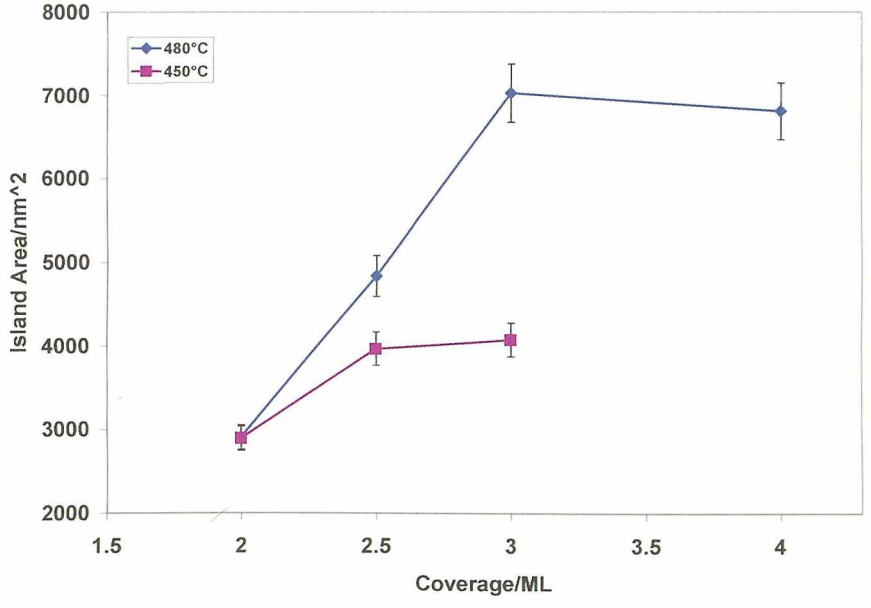


Figure 7.9: Variation of the InAs QD area with monolayer coverage for the 15 μm stripe at 450°C and 480°C.

The same trend for the preferential generation of large InAs islands at mesa top edges and near the base of the stripes observed for the 480°C 0.20 μm/h In flux experiments, is also seen for the 450°C substrate temperature series. For instance for the 450°C and at 3 ML InAs coverage, the average height and width of the dots at the edges of the 15 μm stripe are 22.7 nm and 147×129 nm respectively. For the 8 μm stripes, the height and width are 13 nm and 63×92 nm respectively. These values are significantly higher that the ones obtained for the QDs on the middle of the mesas, or on the flat regions for these growth conditions. The same trend was observed for the low flux experiments. This finding was most likely due to the increased number of atomic steps present that provide a seed for InAs nucleation.

7.5.2. Comparison of the effect of the two different In fluxes on QD formation.

When comparing the two different fluxes, there is a huge difference in the dot density, significantly greater than that conventionally observed for growth on

planar substrates; however, it is quite comparable with the trends observed from our other studies. Several groups have reported that low As flux, produces fewer quantum dots, which are bigger in size [71,72]. After 2 ML deposition, the 3D islands for the 0.02 μm/h In flux are smaller than those for the higher flux, but after 3 ML deposition, the dots for the lower In flux start increasing in size, and at 6 ML they reach a height and width of 19.1 nm and (157x129) nm. Interestingly, the dot density shows a decrease after the deposition of 3 ML for the 0.20 μm/h In flux and 5 ML for the 0.02 μm/h In flux, for all the sizes of stripes and on the flat areas of the substrate. This can be partly explained by the sudden large increase in the dot size, with the larger dots growing at the expense of the smaller ones, indicating the beginning of coalescence. However, this does not account for all of the incoming In adatoms. For all samples grown, the density of the quantum dots formed on the stripes is significantly less than the total amount of In provided.

Figure 7.10 shows a plot of the 3D island volume on the flat region as a function of the volume of material supplied, for both high and low In flux experiments at 480°C and the "ideal InAs" volume.

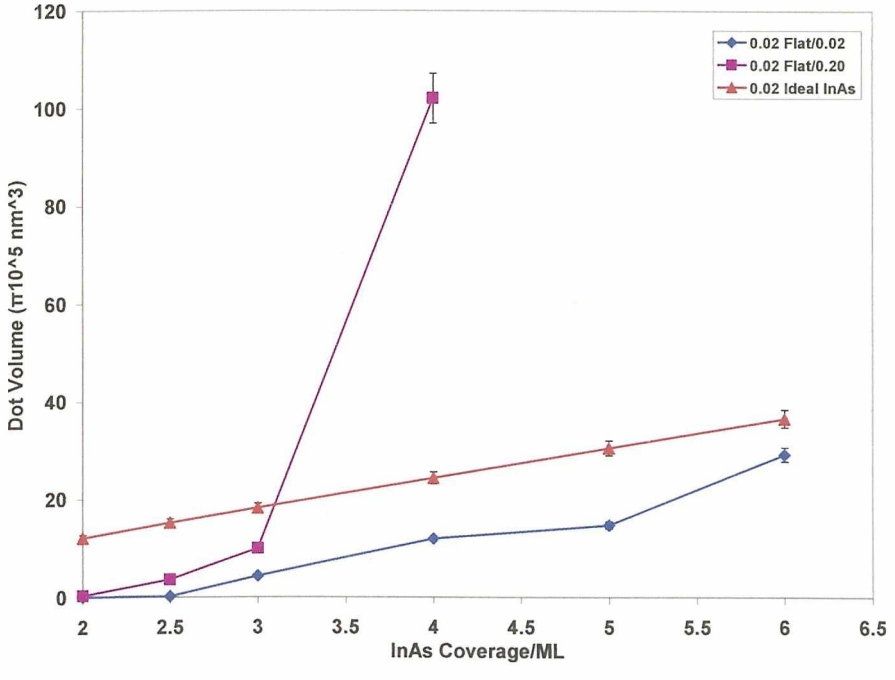


Figure 7.10: Variation of the total deposited In volume with the measured dot volume for the 3D islands on the flat region of the 0.20 μm/h and 0.02 μm/h In flux experiments at 480°C.

During the initial stages of the growth, the average dot volume for both In fluxes is similar. However, after 3 ML InAs deposition, the dot volume increases

rapidly for the high In flux series and the QDs rapidly coalesce. For the 0.02 μm/h In flux series, the dot volume continues to increase at the same rate, until the final InAs deposition. It can be seen that the volume for the low flux series is lower than for the "Ideal InAs" volume for all depositions. This implies In loss which could be attributed either to the large In concentration at the edge of the mesa top or at the base of the mesa stripes or to an increase in the 2D wetting layer thickness. For the 15 μm stripes, the number of 3D islands formed is very small and in the case of the 8 μm and the 5 μm stripes almost non-existent. This is partly explained by the larger islands forming at the mesa edges, due to migration effects. The QDs also form near the mesa bases, possibly because the incoming In preferentially migrates to that area or to pre-existing islands, causing their enlargement. If the increase in the vertical diffusion is also taken into account, the islands are permitted to grow larger before coalescing. However, the In volume measured seems to be less than the incoming In provided suggesting a thicker 2D InAs wetting layer in order to adjust for the reduction in In volume measured or, that there is sufficient In-Ga intermixing as discussed in Chapter 6.

7.5.3. Conclusions

In conclusion, when the substrate temperature is decreased, the dots were smaller and the density was increased when compared with the higher temperature experiments. Dot formation occurred in earlier stages of growth in comparison with the 480°C and consequently, coalescence occurred earlier. Reducing the In flux (increasing the V/III ratio) led to a significant QD density reduction and increase in QD size. The volume of the QDs is significantly less than the "ideal" suggesting In incorporation to the 2D wetting layer or increased In adatom incorporation at the edges of the top and base of the mesa stripes.

It is possible therefore, to control the size and densities of the QDs by varying the growth conditions and or the mesa width and optimise these conditions for different applications.

CHAPTER 8

Conclusions and Future Work.

8.1. Introduction.

In order to achieve high quality growth on patterned substrates, precise control over several key aspects is required. The substrates must be contaminant free with well-defined mesa structures. This requires accurate control of the etching and the subsequent cleaning procedures; *i.e.* using high purity chemicals for the etching and solvent cleaning, and also oxygen ashing, outgassing and AH cleaning prior to growth. Results showed that high quality surfaces were obtained only after each of these stages were undertaken.

These investigations were concentrated in two main fields. The first examined the homoepitaxial growth of GaAs on GaAs(001) patterned mesa stripes. These stripes were oriented along the <001> directions, had sidewall angles of 73°, and were of various widths. For the second segment of research, InAs was deposited on GaAs mesa stripes with 90° sidewalls, oriented along the <001> directions under various growth conditions. Quantum dot formation under various growth parameters was also investigated.

8.2. Work on Patterned Substrates.

In all experiments, the formation of {110} facets was observed and the 5 μm mesa ridges closed-off after depositing 1.00 μm of GaAs. Growth series at different temperatures, Ga flux (altering the effective V/III ratio) and type of As species (As_2 and As_4) was undertaken. Higher Ga fluxes produced rougher {110} surfaces and a more pronounced bottom {310} facet, which led to facet overgrowth of the mesa. Lower substrate temperatures resulted in an overall smoother growth and considerably less overgrowth partly due to growth on the {110} facets leading to an outward extension of the ridge structures. When As_2 was employed, the growth was smoother, with long {110} facets formed with the ridge extending

slightly outwards and less overgrowth of the ridge bases. It would appear that the best ridges were produced with high V/III ratios, low substrate temperatures and using an As_2 as opposed to an As_4 flux.

This work concentrated on the trends observed during growth under different conditions. An extension of the GaAs deposition quantity investigations could be useful in order to observe if it is possible to completely overgrow the stripes. It would also be useful in the case of the 15 μm stripes to see whether they close off or become overgrown from the base area first. In addition, in order to look more closely at the diffusion processes, smaller deposition gaps would need to be used and possibly a wider range of temperature and V/III ratios. Additionally, a further investigation including the *square* mesas oriented along the <100> directions could be undertaken. This would involve a more complex facet-facet interaction process since Ga adatoms can migrate around the whole structure and also the corners of the squares, which could provide extra facets for growth. Thus, for optimum conditions, when the squares mesas would close off, they would produce perfect pyramidal structures. These can be used for pyramidal based cube-corner reflectors [49,50]. Figure 8.1 shows an example of a possible pyramid microcavity structure.

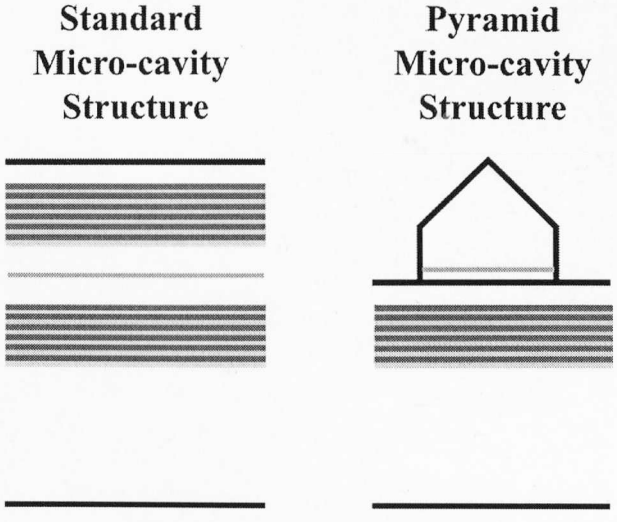


Figure 8.1: Schematic illustration of (a) standard, and (b) pyramid micro-cavity structure.

A normal micro-cavity structure consists of two mirror-type reflectors and an emitter layer positioned between them. The emitter layer is usually formed by QWs or QDs, placed precisely between the two highly reflective surfaces, which

are usually Distributed Bragg Reflectors (DBRs). For the pyramid micro-cavity, the upper DBR is substituted by a pyramidal structure, which acts as the top reflector of the cavity structure. The advantage of using re–growth of the pyramidal structures is that less positional precision is required for the placement of the upper reflector, which is a technically demanding issue with standard DBR reflectors. For example, deposition of an InGaAs QW or InAs/InGaAs QD's, can induce defects in the surrounding metal [54]. Another advantage is that the reflectivity appears to be higher due to the total internal reflection.

AFM measurements proved to be difficult due to the nature of the samples investigated. An improved AFM instrument model could provide better resolution and up to a 10× faster scan rate which would further increase the quality and reduce the time taken for each scan.

8.3. InAs/GaAs Growth on Patterned Substrates.

In these investigations, the 3D island formation on patterned mesa stripes with various widths and under various growth conditions was investigated. The QDs formed were larger and fewer than those reported in the literature for comparable growth conditions on planar GaAs substrates. There are some indications of bimodal growth *i.e.* formation of two types of islands; both small regular ones and large irregular ones. The density and size of the dots decreases with decreasing mesa width and island coalescence appears to be controlled by mesa width. In addition, preliminary measurements suggest there is either some In-Ga intermixing, or that material has transferred from the 2D wetting layer to the 3D islands. A large concentration of dots was found to be located at the edges of the mesas and near the bases suggesting preferential In adatom migration in these areas.

When varying the growth conditions, an increase in density and a decrease in size was observed for the lower temperature growths; this again demonstrated that it is possible to reduce the density and size by lowering the mesa width. The QDs coalesced earlier for the lower temperature than for the higher temperature growths. When the In growth rate was reduced from 0.2 μm/h to 0.02 μm/h, a

dramatic decrease in the dot density and increase in dot size was observed. Again most of the 3D islands appear to be concentrated at the mesa edges and the base of the mesa stripes.

Extension of these growth series could include InAs deposition of less than 2 ML in order to investigate the initial stages of QD formation. Also, smaller deposition gaps near the point of coalescence would provide a better insight into how the phenomenon evolves. The use of As_2 as opposed to As_4 could provide additional useful information since there are recent reports that the change in As species has direct effects on the QD formation [137]. Furthermore, investigations of some of the other mesa widths *i.e.* the 3, 4 and 10 μm mesa widths would provide essential information related to the dot volume measurements and coalescence point. Investigation of the square mesas along the <001> directions could also prove useful; especially for possible future uses as an active layer within a microcavity structure. Once the condition for controlling the QD density and size are optimised, mesa stripes with a single dot array or squares with a single dot can be constructed, the latter forming a single photon emitter.

The AFM measurements, especially for these series of investigations, proved to be extremely difficult. The reason for this was the relatively small scan size and the fact that the tip had to be very precisely positioned on the top of each mesa stripe to scan the area required. Better contact tips, along with the improvements suggested above could reduce the difficulty and improve these measurements. In addition TEM may provide useful topographical and morphological information.

Through these investigations, some progress was made into further understanding the Ga adatom diffusion on patterned substrates to facilitate the optimisation of the growth conditions. Growth of InAs on GaAs patterned substrates also highlighted the mechanisms of In adatom diffusion on patterned substrates and provided the initial steps into a more thorough investigation with the ultimate goal of producing controllable QDs and possibly even single QDs on patterned substrates.

8.4. Modelling Patterned Substrates.

The work presented in this thesis is based on measurements obtained from structures grown under different growth conditions. In principle, a theoretical model based on this information could be constructed for the diffusion of the Ga adatoms in an attempt to accurately portray the final shape of the grown structure. To date, only a limited number of attempts have been made to construct a working model to predict growth on non-planar substrates. The main reason for the limited amount of work is the increased complexity of Ga adatom diffusion when more that one plane is available.

One of the first attempts to model epitaxial growth was for planar substrates [139] followed by some work on two-facet diffusion. Yamashiki *et al.* [32] investigated Ga adatom diffusion for the {110}-(001) system and Kishimoto [140] and Ogura *et al.* [31] derived simple models of the (111)B-(001) system. These are all relatively simple models for calculation of the diffusion length, and only involve a two-facet interaction. They do not take into account new facet formation as the structure is grown.

Ohtsuka *et al.* [129] made attempts to model MBE growth on a surface that consisted of multifaceted crystal structures. The growth model used was based on three phases and modelled MBE growth. Firstly, the vacuum phase, which consists of incident atoms, secondly, the ~1ML thick adatom phase in which adatoms are migrating, and thirdly, the crystal phase where adatoms have their own finite size. As a result, the processes involved on these phases are:

(i) The incoming flux of atoms from the vacuum phase to adatom phase and *vice versa*,
(ii) The surface migrations of adatoms,
(iii) The incorporation of adatoms into the crystal phase and *vice versa*.

The number of atoms moving directly between the vacuum and the crystal phase was thought to be minimal and therefore neglected. The growing surface at time t was considered to be represented by a function $z\ (x,t)$ in a Cartesian coordinate system (x,y,z) where z is the axis of the incident flux. From the kinetic view of

growth, four basic quantities were introduced: the current density of incident adatoms (flux *f*), the surface migration coefficient (*D*), the average adatom lifetime until desorption (τ_v), the average adatom incorporation lifetime (τ_c) and finally the number of adatoms per unit surface area. *D*, τ_v, τ_c, are orientation dependent quantities but *D* and τ_v were regarded as constant values. The model described the growth behaviour for the two-facet interaction and the development of sharp edge.

A very basic model for patterned growth which provide a prediction of the diffusion length was proposed by Ogura *et al.* [31]. This model was based on predicting the diffusion length by measuring the structure at a point using μ-RHEED. The spatial distribution of the growth rate ($R_p(x)$) was said to be comprised by $R_L(x)$ the growth rate by the lateral flux, and R_V the growth rate by a direct flux from the K-cell:

$$R_p(x) = R_V + R_L(x) \qquad (6)$$

where x is the distance on the (001) surface from the edge. In the model, τ is the Ga adatom lifetime until incorporation and the parameters on the (001) planar surface and the sidewall are symbolised as "p" and "s" in the suffix of each variable, respectively. The equations from the surface diffusion theory given are:

$$D_p \frac{d^2 N_p}{dx^2} - \frac{N_P}{\tau_P} + J_{Ga} = 0 \qquad (7)$$

$$D_s \frac{d^2 N_s}{dx^2} - \frac{N_s}{\tau_s} + J'_{Ga} = 0 \qquad (8)$$

where N, τ, D, x and y are defined as the surface density of Ga adatoms, the lifetime of Ga adatoms until incorporation, the surface diffusion coefficient, and the distance from the edge between the (001) and the sidewall on each surface. $J'_{Ga} = J_{Ga}\cos\theta$, where θ is the angle between the (001) and the sidewall surface and J_{Ga} the flux form the K-cell. Taking into account the boundary conditions that the surface densities of Ga adatoms on the (001) and the sidewall are equal where the facets meet and that the lateral Ga flux at the edge is continuous, the growth rate $R_p(x)$ on the (001) surface and near the edge can be obtained as:

$$R_p(x) = \frac{N_p(x)}{\tau_p} = J_{Ga} + \frac{J_{Ga} D_s \lambda_p (\tau_s \cos\theta - \tau_p)}{(D_s \lambda_p + D_p \lambda_s)\tau_p} \exp(-\frac{x}{\lambda_p}) \qquad (9)$$

Ozdemir *et al.* [125,126] , also studied the epitaxial growth on non-planar substrates using phenomenological equations of motion. The model was extended to include the driving force for migration and attempted to predict the facets formed during growth. The kinetic processes of adatom deposition, desorption, inter-facet migration, adatom exchange between terraces and kink sites and capillary driven mass transfer was included. They discussed homoepitaxial growth but stated that it could be used for heteroepitaxial growth also. However, the nucleation and the growth of new facets were not considered.

In order to model the growth described in this thesis, the above requirements need to be taken into account as a bare minimum. Firstly, because Ohtsuka *et al.* model is a model of a diffusion front it cannot be used to predict the facets formed and it only measures the diffusion length at a point, not as growth progresses. The Ozdemir *et al.* model on the other hand, although more extensive, it only deals with a two facet interaction system, whereas in this thesis there is a minimum of three facet interaction processes as shown in the diagram in figure 8.

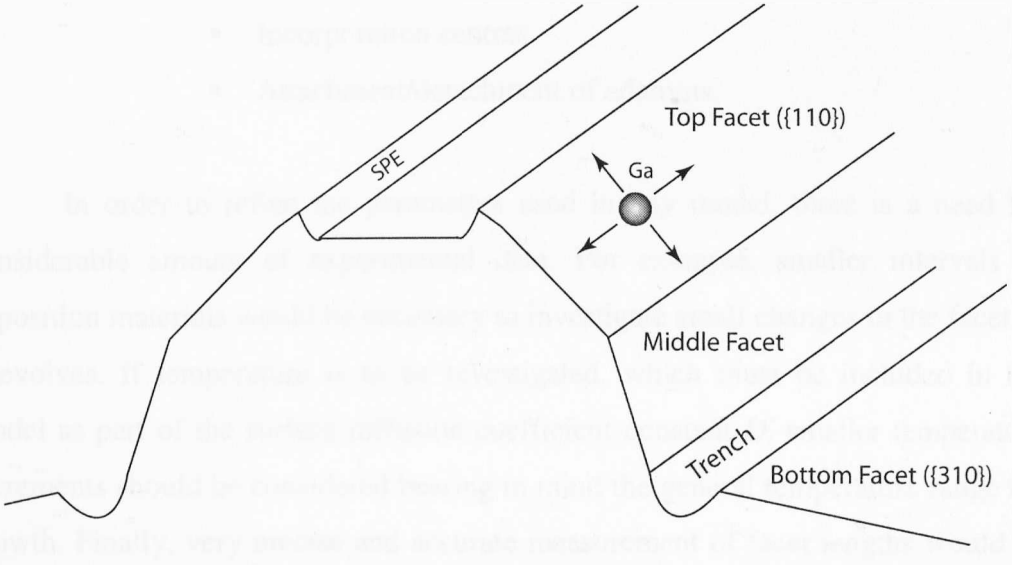


Figure 8. : Schematic illustration of facets that can be accessed by Ga adatom migration. The arrows indicate the direction of migration of a Ga adatom.

In addition, the Ozdemir *et al.* model assumes that there is no new facet formation whereas in this case a minimum number of two facets are clearly visible (the {110} and the {310}). The SPE effect also causes a complication since at this area there is more than one plane present which would alter the local growth conditions; causing an extra degree of difficulty to define and to model.

Therefore, if a more detailed model were to derived for this work, it should ideally include terms:

- Definition of the surface in question
    - Define the mesa structure (two or three facet interaction)
    - 2D or 3D
    - Surface reconstructions locally (this could be complex)
- Atoms arriving on the surface
    - Ga Flux
    - Angle of incidence of the flux
    - Desorption of Ga adatoms
    - V/III ratio
- Surface Interactions
    - Binding potentials (Ga desorption/incorporation)
    - Nucleation centres (Ga preferential diffusion on surface kinks)
    - Incorporation centres
    - Attachment/detachment of adatoms.

In order to refine the parameters used in any model, there is a need for considerable amount of experimental data. For example, smaller intervals of deposition materials would be necessary to investigate small changes in the facet as it evolves. If temperature is to be investigated, which must be included in the model as part of the surface diffusion coefficient constant D, smaller temperature increments should be considered bearing in mind the general temperature range for growth. Finally, very precise and accurate measurement of facet lengths would be required for the prediction of the final shape of the structure. On the whole, this would amount to very lengthy procedure, which would definitely provide a better understanding of Ga diffusion, and furthermore a way of predicting the shape of the final structure on growth on patterned substrates.

In conclusion, although modelling is very useful tool for obtaining diffusion lengths and predicting the shape for simpler systems, where there are three interacting facets any model would require careful and extensive development. To check the applicability of any model, detailed further growth studies are likely to be required.

Acknowledgements

Firstly, I would like to acknowledge my supervisor Prof. Tim Jones for his thorough guidance during the course of my PhD study.

I am very grateful to Mark Ashwin, Richard Williams and Jim Neave for very exciting discussions, useful advice and considerable help regarding my project.

I would also like to thank Christine Roberts for her technical support on the Wet Chemical Etching.

Special thanks to Barbara Shollock for help in EDX measurements, and Steve Cassell for his technical support.

I would like to acknowledge, Helen Parry, Rob Price, Azadeh Khatiri, Adam Bone, Patrick Howe, Sandrine Heutz, James Levitt, and all the members of "the basement", for providing a pleasant working environment.

I would also like to thank "the flatmates" and friends, Athina Milona, Laure Gayet, Nisha Sohal, for putting up with my mood swings; also my friends, Lia Koufopoulou, Irini Proiou and Manos Topoglidis for being there. I apologise to anyone not on this list. I assure you it was not intentional.

I would finally like to thank both my parents for all the support they have given me during the course of my study.

List Of Publications

"Interplay of growing facets during self-assembled growth on GaAs patterned substrates."

C.Chandrinou, M.J.Ashwin, J.H.Neave and T.S.Jones,

Semiconductor Science and Technology, **18**, 950, (2003)

"Effect of growth parameters on inter-facet Ga adatom migration."

C.Chandrinou, M.J.Ashwin, J.H.Neave and T.S.Jones,

To be submitted.

"Low density controlled QD formation on GaAs(001) patterned substrates."

C.Chandrinou, M.J.Ashwin, J.H.Neave and T.S.Jones,

To be submitted.

References

[1] L. Daweritz, *Superlattices Microstruct.*, **9,** 141 (1991).

[2] D. W. Pashley, "*Growth and Characterisation of Semiconductors*", (Adam Hilger, 1990).

[3] F. C. Frank and J. H. van der Merwe, *Proc. Roy. Soc.*, **A198,** 205 (1949).

[4] F. C. Frank and J. H. van der Merwe, *Proc. Roy. Soc.*, **A198,** 216 (1949).

[5] C. T. Foxon and B. A.Joyce, *Surf. Sci.*, **50,** 434 (1975).

[6] C. T. Foxon and B. A. Joyce, *Surf. Sci.*, **64,** 293 (1977).

[7] E. S. Tok, J. H. Neave, J. Zhang, B. A. Joyce, and T. S. Jones, *Surf. Sci.*, **374,** 397 (1997).

[8] E. S. Tok, "*Kinetic Studies of GaAs Growth and Doping by Molecular Beam Epitaxy*", PhD Thesis, Imperial College, London, 1997.

[9] L. T. P. Allen, E. R. Weber, J. Washburn, Y. C. Pao, and A. G. Elliot, *J. Cryst. Growth*, **87,** 193 (1988).

[10] L. T. P. Allen, E. R. Weber, J. Washburn, and Y. C. Pao, *Appl. Phys. Lett.*, **51,** 670 (1987).

[11] J. H. Neave, J. Zhang, X. M. Zhang, P. N. Fawcett, and B. A. Joyce, *Appl. Phys. Lett.*, **62,** 753 (1993).

[12] P. N. Fawcett, J. H. Neave, J. Zhang, and B. A. Joyce, *J. Vac. Sci. Technol. A-Vac. Surf. Films*, **12,** 1201 (1994).

[13] D. M. Holmes, J. G. Belk, J. L. Sudijono, J. H. Neave, T. S. Jones, and B. A. Joyce, *Appl. Phys. Lett.*, **67,** 2848 (1995).

[14] D. M. Holmes, E. S. Tok, J. L. Sudijono, T. S. Jones, and B. A. Joyce, *J. Cryst. Growth*, **192,** 33 (1998).

[15] E. S. Tok, J. H. Neave, M. J. Ashwin, B. A. Joyce, and T. S. Jones, *Journal of Applied Physics*, **83,** 4160 (1998).

[16] M. R. Fahy, K. Sato, and B. A. Joyce, *Appl. Phys. Lett.*, **64,** 190 (1994).

[17] E. S. Tok, T. S. Jones, J. H. Neave, J. Zhang, and B. A. Joyce, *Appl. Phys. Lett.*, **71,** 3278 (1997).

[18] D. A. Woolf, D. I. Westwood, and R. H. Williams, *Appl. Phys. Lett.*, **62,** 1370 (1993).

[19] J. S. Smith, P. L. Derry, S. Margalit, and A. Yariv, *Appl. Phys. Lett.*, **47,** 712 (1985).

[20] M. Mannoh, T. Yuasa, S. Naritsuka, K. Shinozaki, and M. Ishii, *Appl. Phys. Lett.*, **47,** 728 (1985).

[21] A. Y. Cho and W. C. Ballarmy, *Journal of Applied Physics*, **46,** 783 (1975).

[22] W. T. Tsang and A. Y. Cho, *Appl. Phys. Lett.*, **30,** 293 (1977).

[23] M. Hata, T. Isu, A. Watanabe, and Y. Katayama, *Appl. Phys. Lett.*, **56,** 2542 (1990).

[24] J. H. Neave, P. J. Dobson, B. A. Joyce, and J. Zhang, *Appl. Phys. Lett.*, **47,** 100 (1985).

[25] M. Hata, T. Isu, A. Watanabe, and Y. Katayama, *J. Vac. Sci. Technol. B*, **8,** 692 (1990).

[26] T. Nishinaga, A. Yamashiki, and X. Q. Shen, *Thin Solid Films*, **306,** 187 (1997).

[27] X. Q. Shen, D. Kishimoto, and T. Nishinaga, *Jpn. J. Appl. Phys. Part 1 - Regul. Pap. Short Notes Rev. Pap.*, **33,** 11 (1994).

[28] T. Nishinaga, X. Q. Shen, and D. Kishimoto, *J. Cryst. Growth*, **163,** 60 (1996).

[29] S. Koshiba, Y. Nakamura, M. Tsuchiya, H. Noge, H. Kano, Y. Nagamune, T. Noda, and H. Sakaki, *Journal of Applied Physics*, **76,** 4138 (1994).

[30] Y. Nomura, Y. Morishita, S. Goto, Y. Katayama, and T. Isu, *Appl. Phys. Lett.*, **64,** 1123 (1994).

[31] T. Ogura, D. Kishimoto, and T. Nishinaga, *J. Cryst. Growth*, **226,** 179 (2001).

[32] A. Yamashiki and T. Nishinaga, *J. Cryst. Growth*, **199,** 1125 (1999).

[33] M. Lopez and Y. Nomura, *J. Cryst. Growth*, **150,** 68 (1995).

[34] H. Temkin, G. J. Dolan, M. B. Panish, and S. N. G. Chu, *Appl. Phys. Lett*, **50,** 413 (1987).

[35] M. Lopez, T. Ishikawa, and Y. Nomura, *Jpn. J. Appl. Phys. Part 2 - Lett.*, **32,** L1051 (1993).

[36] M. Lopez, N. Tanaka, I. Matsuyama, and T. Ishikawa, *Appl. Phys. Lett.*, **68,** 658 (1996).

[37] Y. Kadoya, T. Yoshida, Y. Nagamune, H. Noge, and H. Sakaki, *J. Cryst. Growth*, **150,** 317 (1995).

[38] S. Koshiba, H. Noge, H. Akiyama, T. Inoshita, Y. Nakamura, A. Shimizu, Y. Nagamune, M. Tsuchiya, H. Kano, H. Sakaki, and K. Wada, *Appl. Phys. Lett.*, **64,** 363 (1994).

[39] S. Ando and T. Fukui, *J. Cryst. Growth*, **98,** 646 (1989).

[40] E. Kapon, M. C. Tamargo, and D. M. Hwang, *Appl. Phys. Lett.*, **50,** 347 (1987).

[41] E. Kapon, D. M. Hwang, and R. Bhat, *Phys. Rev. Lett.*, **63,** 430 (1989).

[42] Y. Liu, S. Shimomura, N. Sano, K. Gamo, A. Adachi, and S. Hiyamizu, *Semicond. Sci. Technol.*, **8,** 2197 (1993).

[43] T. Takebe, M. Fujii, T. Yamamoto, K. Fujita, and T. Watanabe, *J. Vac. Sci. Technol. B*, **14,** 2731 (1996).

[44] A. Konkar, K. C. Rajkumar, Q. Xie, P. Chen, A. Madhukar, H. T. Lin, and D. H. Rich, *J. Cryst. Growth*, **150,** 311 (1995).

[45] J. Kasai, S. Tanaka, K. Higuchi, and Y. Katayama, *J. Vac. Sci. Technol. B*, **15,** 862 (1997).

[46] J. Kasai, S. Tanaka, K. Higuchi, and Y. Katayama, *Phys. Rev. B*, **60,** 13727 (1999).

[47] R. S. Williams, M. J. Ashwin, J. H. Neave, and T. S. Jones, *J. Cryst. Growth*, **227,** 56 (2001).

[48] R. S. Williams, M. J. Ashwin, J. H. Neave, and T. S. Jones, *Journal of Applied Physics*, **95,** 6112 (2004).

[49] R. M. F. Oulton, P. N. Stavrinou, R. S. Williams, M. J. Ashwin, O. McCarthy, J. Tucker, C. Roberts, T. S. Jones, and G. Parry, in *Optical properties of novel semiconductor microstructures.*, CLEO/QELS 2000 Conf, Tech. Digest, 2000, p. 55.

[50] R. E. Pritchard, R. F. Oulton, P. N. Stavrinou, G. Parry, R. S. Williams, M. J. Ashwin, J. H. Neave, and T. S. Jones, *Journal of Applied Physics*, **90,** 475 (2001).

[51] Y. Liu, N. Yamamoto, Y. Nishimoto, N. Kamikubo, S. Shimomura, K. Gamo, K. Murase, N. Sano, A. Adachi, K. Fujita, T. Watanabe, and S. Hiyamizu, *J. Cryst. Growth*, **150,** 299 (1995).

[52] B. A. Joyce, D. D. Vvedensky, A. R. Avery, J. G. Belk, H. T. Dobbs, and T. S. Jones, *Appl. Surf. Sci.*, **132,** 357 (1998).

[53] P. B. Joyce, T. J. Krzyzewski, P. H. Steans, G. R. Bell, J. H. Neave, and T. S. Jones, *Surf. Sci.*, **492,** 345 (2001).

[54] S. Guha, A. Madhukar, and K. C. Rajkumar, *Appl. Phys. Lett.*, **57,** 2110 (1990).

[55] C. W. Snyder, D. Barlett, B. G. Orr, P. Bhattacharya, and J. Singh, *J. Vac. Sci. Technol. B*, **9,** 2189 (1991).

[56] D. Leonard, M. Kishnamuthy, S. Fafard, J. L. Merz, and P. M. Petroff, *J. Vac. Sci. Technol. B*, **12,** 1063 (1994).

[57] A. Madhukar, Q. Xie, P. Chen, and A. Konkar, *Appl. Phys. Lett*, **64,** 2727 (1994).

[58] J. M. Moison, F. Houzay, F. Barthe, and L. Leprince, *Appl. Phys. Lett*, **64,** 196 (1994).

[59] A. Rosenauer, U. Fischer, D. Gerthsen, and A. Forster, *Appl. Phys. Lett*, **71,** 3868 (1997).

[60] F. Lin, J. Wu, W. Jiang, H. Cui, and Z. Wang, *J. Cryst. Growth*, **223,** 55 (2001).

[61] K. Shiramine, T. Itoh, S. Muto, T. Kozaki, and S. Sato, *J. Cryst. Growth*, **242,** 332 (2002).

[62] K. Tillmann, D. Gerthsen, P. Pfundstein, A. Foster, and K. Urban, *Journal of Applied Physics*, **78,** 3824 (1995).

[63] A. Madhukar, T. R. Ramachandran, A. Konkar, I. Mukhametzanov, W. Yu, and P. Chen, *Appl. Surf. Sci.*, **123,** 266 (1998).

[64] I. Kamiya, I. Tanaka, and H. Sakaki, *J. Cryst. Growth*, **201,** 1146 (1999).

[65] P. B. Joyce, T. J. Krzyzewski, G. R. Bell, B. A. Joyce, and T. S. Jones, *Phys. Rev. B*, **58,** R15981 (1998).

[66] P. B. Joyce, T. J. Krzyzewski, G. R. Bell, and T. S. Jones, *Phys. Rev. B.*, **64,** 235317 (2001).

[67] A. J. Bennett and R. Murray, *J. Cryst. Growth*, **240,** 439 (2002).

[68] D. Leonard, K. Pond, and P. M. Petroff, *Phys. Rev. B.*, **50,** 11687 (1994).

[69] G. S. Solomon, J. A. Trezza, and J. S. Harris, *Appl. Phys. Lett*, **66,** 3161 (1995).

[70] G. S. Solomon, J. A. Trezza, and J. S. Harris, *Appl. Phys. Lett*, **66,** 991 (1995).

[71] B. J. Riel, K. Hinzer, S. Moisa, J. Fraser, P. Finnie, P. Piercy, S. Fafard, and Z. R. Wasilewski, *J. Cryst. Growth*, **236,** 145 (2002).

[72] K. Yamaguchi, K. Yujobo, and T. Kaizu, *Jpn. J. Appl. Phys.*, **39,** L1245 (2000).

[73] H. Kitabayashi and T. Waho, *J. Cryst. Growth*, **150,** 152 (1995).

[74] S. Fafard, D. Leon, D. Leonard, J. L. Merz, and P. M. Petroff, *Phys. Rev. B.*, **50,** 8086 (1994).

[75] E. C. LeRu, P. Howe, T. S. Jones, and R. Murray, *Phys. Rev. B.*, **67,** 165303 (2003).

[76] D. S. L. Mui, D. Leonard, L. A. Colden, and P. M. Petroff, *Appl. Phys. Lett*, **66,** 1620 (1995).

[77] M. Kitamura, M. Nishioka, J. Oshinowo, and Y. Arakawa, *Appl. Phys. Lett*, **66,** 3663 (1995).

[78] N. Ikoma and S. Ohkouchi, *Jpn. J. Appl. Phys.*, **34,** L724 (1995).

[79] T. Mano, R. Notzel, G. J. Hamhuis, T. J. Eijkemans, and J. H. Walter, *Journal of Applied Physics*, **92,** 4043 (2002).

[80] R. Leon, T. J. Senden, Y. Kim, C. Jagadish, and A. Clark, *Phys. Rev. Lett.*, **78,** 4942 (1997).

[81] T. Ishikawa, T. Nishimura, S. Kohmoto, and K. Asakawa, *Appl. Phys. Lett*, **76,** 167 (2000).

[82] T. Ishikawa, S. Kohmoto, T. Nishimura, and K. Asakawa, *Thin Solid Films*, **373,** 170 (2000).

[83] Q. Xie, A. Madhukar, P. Chen, and N. Kobayashi, *Phys. Rev. Lett.*, **75,** 2542 (1995).

[84] Q. Xie, J. L. Brown, and J. E. Van Nostrand, *Appl. Phys. Lett*, **78,** 2491 (2001).

[85] S. Jeppesen, M. S. Miller, D. Hessman, B. Kowalski, I. Maximov, and L. Samuelson, *Appl. Phys. Lett*, **68,** 2228 (1996).

[86] C. Lobo and R. Leon, *Journal of Applied Physics*, **83,** 4168 (1998).

[87] Y. Nakamura, O. G. Schmidt, N. Y. Jin-Phillipp, S. Kiravittaya, C. Muller, K. Eberl, H. Grabeldinger, and H. Schweizer, *J. Cryst. Growth*, **242,** 339 (2002).

[88] R. Tsui, R. Zhang, K. Shiralagi, and H. Goronkin, *Appl. Phys. Lett.*, **71,** 3254 (1997).

[89] R. Zhang, R. Tsui, K. Shiralagi, D. Convey, and H. Goronkin, *Appl. Phys. Lett.*, **73,** 505 (1998).

[90] K. Shiralagi, R. Zhang, and R. Tsui, *J. Cryst. Growth*, **202,** 1209 (1999).

[91] A. Y. Cho, *J. Cryst. Growth*, **150,** 1 (1995).

[92] B. A. Joyce, *Rep. Prog. Phys.*, **48,** 1637 (1985).

[93] H. Hasegawa and H. Fujikura, *Microelectron. J.*, **28,** 887 (1997).

[94] C. A. Mullan, D. A. Thompson, and G. C. Weatherly, *J. Cryst. Growth*, **182,** 266 (1997).

[95] S. M. Sze, "*Semiconductor Devices. Physics and Technology*", (John Wiley and Sons, New York, 1985).

[96] S. Gonda, Y. Matsushima, Y. Makita, and S. Mukai, *Jpn. J. Appl. Phys.*, **14,** 935 (1975).

[97] H. Sakaki, T. Noda, K. Hirakawa, M. Tanaka, and T. Matsusue, *Appl. Phys. Lett*, **51,** 1934 (1987).

[98] R. A. Stradling and P. C. Klipstein, in "*Growth and Characterisation of Semiconductors.*" (1990).

[99] B. A. Joyce, *Thin Film Growth of Semiconductors lecture notes*, (2000).

[100] *EPI Product Guide*.

[101] D. P. Woodruff and T. A. Delchar, *Modern Techniques of Surface Science*, (1994).

[102] J. H. Neave, B. A. Joyce, P. J. Dobson, and N. Norton, *Appl. Phys. A-Mater. Sci. Process.*, **31,** 1 (1983).

[103] J. H. Neave, B. A. Joyce, and P. J. Dobson, *Appl. Phys. A-Mater. Sci. Process.*, **34,** 179 (1984).

[104] M. A. Herman and H. Sitter, "*Molecular Beam Epitaxy. Fundementals and Current Status*", Second, Revised and Udated ed., (Springer, Berlin, New York, London, 1996).

[105] G. R. Bell, N. S. Kaijaks, R. J. Dixon, and C. F. McConville, *Surf. Sci.*, **401,** 125 (1998).

[106] J. I. Goldstein, D. E. Newbury, P. Echlin, D. C. Joy, C. Fiori, and E. Lifshin, "*Scanning Electron Microscopy and X-ray Microanalysis*", (Plenum Press, New York, 1981).

[107] J. W. Niemantsverdriet, *Spectroscopy in Catalysis*, (1995).

[108] F. Meldrum, *Techniques in Microscopy (lecture notes)*, (1998).

[109] L. Reimer, "*Scanning Electron Microscopy. Physics of Image Formation and Microanalysis*", (Springer-Verlag, Berlin, 1985).

[110] G. Binnig, C. F. Quate, and C. Gerber, *Phys. Rev. Lett.*, **56,** 930 (1986).

[111] D. Instruments, *AFM Instruction Manual*, (Santa Barbara, 1998).

[112] P. W. Atkins, "*Physical Chemistry*", 6th ed., (Oxford University Press, 1998).

[113] N. Elsner, *PhD Seminar*, (2003).

[114] Private Communication, O. McCarthy, "*Progress Report on GaAs Mesa Fabrication by Wet Etching*", 1999.

[115] Y. Mori and N. Watanabe, *J. Electrochem. Soc.*, **125,** 1510 (1978).

[116] X. Q. Shen, M. Tanaka, and T. Nishinaga, *J. Cryst. Growth*, **127,** 932 (1993).

[117] A. Adachi and K. Oe, *J. Electoch. Soc- Sol. State Sc. and Techn.*, **130,** 2427 (1983).

[118] J. J. Harris, *Private Communication*, (2001).

[119] A. Gustafsson, F. Reinhardt, G. Biasiol, and E. Kapon, *Appl. Phys. Lett.*, **67,** 3673 (1995).

[120] K. C. Rajkumar, A. Madhukar, K. Rammohan, D. H. Rich, P. Chen, and L. Chen, *Appl. Phys. Lett.*, **63,** 2905 (1993).

[121] R. E. Pritchard, R. F. Oulton, P. N. Stavrinou, G. Parry, R. S. Williams, M. J. Ashwin, J. H. Neave, and T. S. Jones, *To be published*, (2002).

[122] M. Tanaka, T. Suzuki, and T. Nishinaga, *J. Cryst. Growth*, **111,** 168 (1991).

[123] T. Shitara, E. Kondo, and T. Nishinaga, *J. Cryst. Growth*, **99,** 530 (1990).

[124] H. Yamaguchi and Y. Homma, *Appl. Phys. Lett*, **73,** 21 (1998).

[125] M. Ozdemir, *Appl. Surf. Sci.*, **152,** 200 (1999).

[126] M. Ozdemir and A. Zangwill, *J. Vac. Sci. Technol. A-Vac. Surf. Films*, **10,** 684 (1992).

[127] M. Ohtsuka and A. Suzuki, *Journal of Applied Physics*, **73,** 7358 (1993).

[128] R. C. Sangster, in "*Compound Semiconductors*"; *Vol. 1*, edited by R. K. Williardson and H. L. Goering (Reinhold, London, 1962), p. 241.

[129] M. Ohtsuka, *J. Cryst. Growth*, **205,** 112 (1999).

[130] R. S. Williams, M. J. Ashwin, J. H. Neave, and T. S. Jones, *J. Appl. Phys.(submitted)*, (2004).

[131] D. K. Choi, T. Takai, S. Erkoc, T. Halicioglu, and W. A. Tiller, *J. Cryst. Growth*, **85,** 9 (1987).

[132] R. S. Williams, "*M.B.E. Growth on GaAs (001) Patterned Substrates*", PhD Thesis, Imperial College, London, 2002.

[133] T. Ogura and T. Nishinaga, *J. Cryst. Growth*, **211,** 416 (2000).

[134] M. Pelton, J. Vuckovic, G. Solomon, C. Santori, B. Zhang, J. Plant, and Y. Yamamoto, *Physica E*, **17,** 564 (2003).

[135] M. Pelton, C. Santori, G. S. Solomon, O. Benson, and Y. Yamamoto, *Eur. Phys. J. D*, **18,** 179 (2002).

[136] C. Santori, M. Pelton, G. Solomon, Y. Dale, and Y. Yamamoto, *Phys. Rev. Lett.*, **86,** 1502 (2001).

[137] P. Howe and A. Khatiri, *Private Communication*, (2003).

[138] K. Pak, M. R. Fahy, X. M. Zhang, and B. A. Joyce, *J. Cryst. Growth*, **186,** 21 (1998).

[139] C. Heyn, T. Franke, and R. Anton, *J. Cryst. Growth*, **201,** 67 (1999).

[140] D. Kishimoto, T. Ogura, A. Yamashiki, T. Nishinaga, S. Naritsuka, and H. Sakaki, *J. Cryst. Growth*, **216,** 1 (2000).